POLITECNICO
MILANO 1863

SCUOLA DI INGEGNERIA INDUSTRIALE
E DELL'INFORMAZIONE

von KARMAN INSTITUTE
FOR FLUID DYNAMICS

Inter refrigerated compression through stator cooling

Tesi di Laurea Magistrale in
Mechanical Engineering - Ingegneria Meccanica

Author: **Stefano Platini**

Student ID: 969363
Advisor: Prof. Paolo Gaetani
Co-advisors: Prof Fabrizio Fontaneto,Bogdan Cernat
Academic Year: 2021-22

Abstract

Hydrogen is considered the fuel for future engine: its application in an aeroengine is more problematic due to the issue in storing it in on-board, of keeping it at liquid state, of injecting it in the combustor. The optimal state to put it inside a fuel tank is the liquid state but to keep it at atmospheric temperature a huge pressure is required, a pressure higher than the optimal combustion chamber one. The pressure gradient between fuel and oxidizer can be exploit with an expansion process of fuel. This process produce an heat sink that can be exploit to cool down the air inside the compressor. The inter refrigerated compression is already exploit in some land application to increase the thermodynamic cycle efficiency. This thesis analyses with a numerical code the advantages of a real Joule Brayton cycle with a refrigerated compression respect the adiabatic case, two real engine (CFM and GENX) are studied at both cruise and takeoff condition. The optimal cooling position to maximise cycle efficiency obtained is in the booster: the low pressure compressor. The ideal increase of efficiency is higher than 1%. To keep the same weight the heat exchange process is perform with a stator blade. The heat transfer coefficient is estimated through *CFD* simulation: the solver used is *NUMECA* and the airfoil analysed is the DREAM compressor, a booster in the Von Karman institute facility. The analysis of the real capacity of a stator blade to cool down the flow estimate an heat transfer coefficient value of $80\frac{KW}{m^2K}$ for a booster stator blade at design condition. The real heat transfer capacity of a blade does not allow the ideal cooling but still gives an advantages in efficiency. The coupling in the same fluid of fuel and refrigerant allow to perform inter refrigeration and preheating simultaneously giving a further cycle optimisation.
This thesis work is a principle analysis of a technology that could be an huge transition in the civil aircraft market. The deadline imposed by European project(Zero Emission Aviation) is 2050 and the improvement in cycle efficiency are very relevant, coupling it with the environmental one give no more reason to not push lot of effort in the developing of hydrogen engine.

Keywords: Higher efficiency aeroengine, zero emission fuel, thermodynamic cycle analysis, CFD

Abstract in lingua italiana

L'idrogeno è da molti considerato il combustibile del futuro. La sua applicazione nel mondo aeronautuico è molto complessa a causa dei limiti di peso, spazio e delle condizioni operative del motore di aereo. Per conservarne a bordo una quantità sufficiente a volare, l'idrogeno deve essere mantenuto allo stato liquido: a temperatura ambiente ciò è possibile solo a pressioni molto elevate, maggiori della pressione operativa del propulsore. Il processo di espansione necessario tra serbatoio e propulsore genera un pozzo di calore, sfruttabile per raffreddare l'aria nel compressore. Questa tesi analizza tramite codici numerici un ciclo Joule Brayton reale con una compressione interrefrigerata, confrontandolo con il caso adiabatico. I parametri di due motori attualmente in commercio (CFM e il GENX) sono stati considerati come riferimento. Il risultato di questa analisi è un incremento di efficienza maggiore dell'1% con una refrigerazione nel compressore di bassa pressione (booster). Per mantenere costante il peso macchina, il processo di scambio termico è eseguito tramite una pala di statore. L'analisi *CFD*, eseguita con *NUMECA* su uno stadio del compressore *DREAM* ha restituito un coefficeicnte di scambio termicopari a $80\frac{KW}{m^2K}$ alla condizione di design. La quantità ottimale di calore estratto trovata nell'analisi termodinamica del ciclo non può essere ottenuta tramite un singolo statore: nonostante ciò, una refrigerazione parziale ha comunque effetti favorevoli sull'efficienza di ciclo. Con questa nuova concezione di ciclo l'idrogeno assumerebbe il ruolo sia di combustibile che di liquido refrigerante, realizzando oltre alla refrigerazione dell'aria un pre-riscaldamento del combustibile con ulteriori incrementi di efficienza del ciclo.
Questo lavoro è un'analisi di principio di una tecnologia che rivoluzionerebbe completamente il mercato aeronautico. Il progetto della Commissione Europea (Zero Emission Aviation) ha l'obbiettivo di azzerrare le emissioni areonautiche entro il 2050. I vantaggi ecologici sono evidenti; questo lavoro mostra i possibili vantaggi in termini di efficienza, e quindi economici, dell'applicazione dell'idrogeno come combustibile fornendo una spinta ulteriore alla ricerca in questo settore.

Parole chiave: Aumento di efficienza, idrogeno, analisi del ciclo Joule Brayton, CFD

Contents

Introduction

European and global aeroengine market is thinking of using the hydrogen like fuel for linear plane. This idea is based on two reason: the lack of fossil fuel that will be expected in the next 30 years and the reduction of carbon dioxide emission.To store a sufficient amount of hydrogen on board it can be only boarded at liquid state with a very high density and so low specific volume.

The possibility of using hydrogen as fuel for aeroengine is nowadays taken into account also by some company as GE (General Electric) [14] and Safran [31] both as individual energy carrier or coupled with another fuel.

Hydrogen behaviour is very close to a perfect gas one with a low molar mass ($2.0158 \left[\frac{Kg}{Kmol}\right]$) and so a high gas constant R ($4.1243 \left[\frac{KJ}{kg \cdot K}\right]$). The hydrogen reach a sufficient density condition only at very high pressure (something about 1000 bar) or in a cryogenic state (around 40 K). In both cases a heat sink is available: in a cryogenic state we have already a very low temperature while with high pressure liquid an expansion process causes a strong reduction in temperature too.

The expansion process is required by the state of art of burners: pressure ratio in the combustion chamber is around 60 bar and we can not directly inject hydrogen with such an high pressure: an expansion between the storage tank and the burner is necessary.

The heat sink can not be used in the turbine: the film cooling technologies can not be exploit with the fuel because it is downstream the burners and an internal cooling of blade is not sufficient. The heat sink can be exploit in the compressor to develop an inter refrigerate compression process, cooling the fluid, the work needed to reach the same pressure ratio decrease and so thermodynamic cycle efficiency increase. This technology is already present in the derivative based aeroengine, in land application to produce energy and the cooling is perform through an heat exchanger. The addition on the plane of another component increases the weight of the machine and should be avoid: for this reason the idea of this project is to use stator blade as heat exchanger to both decrease the hydrogen pressure and cool the flow.

Stator blades are not designed to perform an heat exchange process and it will probably be not efficient but gradient of temperature and the Reynold number are very high and help increasing the heat flux.

This thesis work would like to figure out if a inter cooling compression through the stator blade could have a positive effect on the cycle. Next steps will understand how to perform this heat exchange: at casing, at hub and how to consider the losses. Finally the trade off between the thermodynamic advantages and the complexity of system require would lead to the conclusion on the real possibility in exploiting this technology in real engines.

Literary survey

In this chapter are reported the state of the art and the scientific literature on heat exchange process in a compressor.

0.1. Advantages of inter cooling in turbomachine

The heat exchange effect in the turbomachinery performance is a recent research topic. In literature there are not similar studies on the possibility of applying an inter refrigeration compression through the blades of a real machine as a civil aircraft engine. Turbomachinery are traditionally studied as adiabatic machine being the amount of work extracted much higher than the heat exchange between flow and metal. Instead of the positive effects of cooling are several [36] [28].

1. Increase of overall pressure ratio due to a reduction of total pressure lost
2. Increase of maximum mass flow capability, due to a reduction of annulus boundary layer thickness [28]
3. Increase of efficiency (η)
4. Higher stability respect choking
5. Reduction of the deviation angle with some correlation available [36]

P.N.Shan and C.S.Tan studied in 2007 the effect of blade cooling on some airfoils using 2D and 3D CFD calculation with *Fluens* [28]. Their result shows an increase of performance in the compression process applying cooling in an axial multistage compressor and the advantages are more considerable with a cooling in the downstream stage.

Maccalum and Grant [24] report that a positive heat flux reduces the stability region of compressor map because it increases the rate at which the layer develops, by the influence of local density reduction on the momentum integral equation. From a negative heat flux, an heat sink, it is reasonable to expect an opposite behaviour with an increase of stability region.

Lot of authors describe the effect of heat exchange on the compressor stability during a transient: acceleration and deceleration. The constant corrected speed on a compressor map raises with cooling respect an adiabatic line as reported in Equation 1,

$$N_c = \frac{N}{\sqrt{\frac{T_{t,in}}{T_{ref}}}} \tag{1}$$

The variation of N to keep the same Nc parameter is due to the work and the pressure ratio required by the stage. The Nc parameter should remain constant and an increase (or decrease) of the gas temperature should lead to and increase (or decrease) of the velocity of rotation to keep the same work done by the stage and so the same compression ratio. A change of gas temperature due to the variation of metal temperature changes the velocity triangle and the similarity is no more respected, this leads to stall condition[30] due to the variation of incidence angle in the blade row.

A quantification of the advantages in terms of a decrease in the total pressure losses is reported in articles [28] and [12].

0.2. Models of heat transfer in a compression

In literature lot of models for heat exchange process are available for liquid metals with a Prandtl number close to "1" [35] [19] due to their high capability of heat transfer. In a turbulent gaseous flow, as is air inside a compressor there are not unique and most validate approach. To establish the amount of cooling power, in literature are described different techniques:

1. Fourier and Newton law approach
2. The definition of a non-dimensional heat transfer parameter ($q*$) [28]
3. The variation of total enthalpy [17]
4. The Stanton number definition [15]
5. A mean line lumped capacitance mode [1].

The calculation of the convective heat transfer coefficient downstream the rotor is assumed linear by some authors [22]. This decision is an approximation due to the high variability that this coefficient has along the blade chord. In this work it is calculated and estimated as a singular value by a post procession of the CFD results in chapter 2. Stanton number correlation is modelled for a supersonic flow (Mach=2.44) and it is not appropriate for a

civil aircraft engine compressor which works in subsonic range [15]. In the thermodynamic analysis of the cycle the non-dimensional parameter $q*$ is taken in this work to quantify the optimal amount of cooling.

0.3. Model of heat transfer in the CFD simulation

CFD studies on heat transfer flux between liquids and solid surface are largely performed on liquid metal because of their Prandtl number in the range from 0.01 to 0.001. This characteristic gives to this metal an high capability to store energy [35] [19]. The comparison of *DNS* simulation with *RANS* model shows that *RANS* models are not able to predict correctly the heat transfer in a ribbed channel with turbulence flows [21]. The turbulence flow considered in this article (~ 4000) is not comparable with the values of turbulence in an aeroengine (~ 400000) , this leads the choice of the $k-\omega SST$ instead of the $\overline{v^2}-f$ model (suggested in some articles [21]) to simulate properly the kinematic turbulent boundary layer.

In literature no suggestion on high turbulent flow model or condition for thermal boundary layer are reported. This is probably due to the lack of measurement that avoid a comparison with *RANS* results and a validation of turbulent model. There are no articles related to *DNS* with a thermal boundary layer too. A high contribution in this research field comes from the work of N.J. Kormanik III published in December 2021. In this dissertation [17] experimental and numerical results are comparable: the behaviour of the facility is far from adiabatic and from his results, the best model to simulate this behaviour is a conjugate heat transfer model on the blade (green line),couple with an adiabatic condition on the external casing (red contour). The results and the condition are visible in Figure 1.

(a) Boundary condition applied

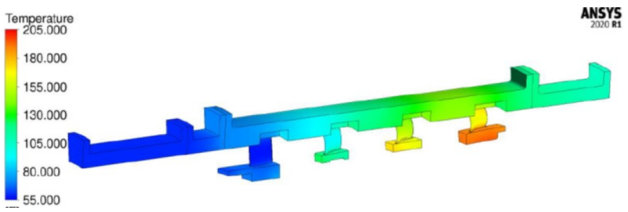

(b) Solid temperature results

Figure 1: More reliable results and boundary condition

Kormanik results open a new possible research field on the thermal effect inside a turbomachine cascade. In this thesis work, due to the lack of experimental results and the due to the research of the effect of a metal temperature on the flow compared to the adiabatic one, only adiabatic and isothermal simulation will be run.

0.4. Optimal cooling position

The optimal cooling condition is a trade off between the thermodynamic efficiency, for which it is better to cool at the beginning to reduce the work require by following stage and the higher temperature gradient available in the rear stage of the compressor. The ∇T is a necessary condition to extract heat from a hot fluid and in the last stage of compressor the gradient of gases temperature is higher: this allows an higher heat transfer efficiency. Another parameter that affects the position of optimal cooling is the blade surface: due to flaring the surface of the stage diminishing through the machine so the heat transfer is higher in the first stage while the heat transfer per unit of area is higher in the smaller blade near the rear of HP compressor [30] [36]. The decreasing of surface available for heat flux is enhanced also by the casing: heat flux doesn't flow only through the blade but also in the other solid surface as disc, casing, seals. A common assumption used also in this thesis is that the majority of heat will go in the blade [30].

0.4.1. ASME paper GT2022-82744

In the *ASME Turbo Expo 2022* held in Rotterdam from 13-17 of June, a paper regarding the possibility of using heat transfer in an aeroengine is presented [23]. In this paper the authors apply an heat transfer for partial inter cooling and thrust augmentation. This effect is obtained passing the heat from the HPC (high pressure compressor) to the bypass flow and the thrust increase due to an higher energy of the exhaust gases out of the nozzle. In this work the heat is removed completely by the air flow and is added to the fuel. The paper conclusion are done without a thermodynamic analysis of the cycle, the heat transfer is obtained with an heat exchanger and with an effectiveness (ϵ) of 0.2. The real case, compared to the ideal one with ϵ=1, shows that the advantages of thrust augmentation in the bypass slightly decrease and compressor work saving is not as high. The advantages in the SFC (specific fuel consumption) obtained is around 4.3%. A thermodynamic simulation of the cycle reported in this article is performed to understand if the optimal inter-cooling position that maximizes thrust is also the one with the best effect on efficiency. The efficiencies matrix, function of amount of heat extracted q^* and the compression ratio after which inter cooling happen, are reported changing the ϵ of

the heat exchanger. ϵ parameter is define as the ratio between $\frac{Q_{inbypassflow}}{Q_{extracted}}$ and moving far the ideal case ($\epsilon = 1$) the optimal cooling position moves from the HP compressor to the booster: Figure 2.

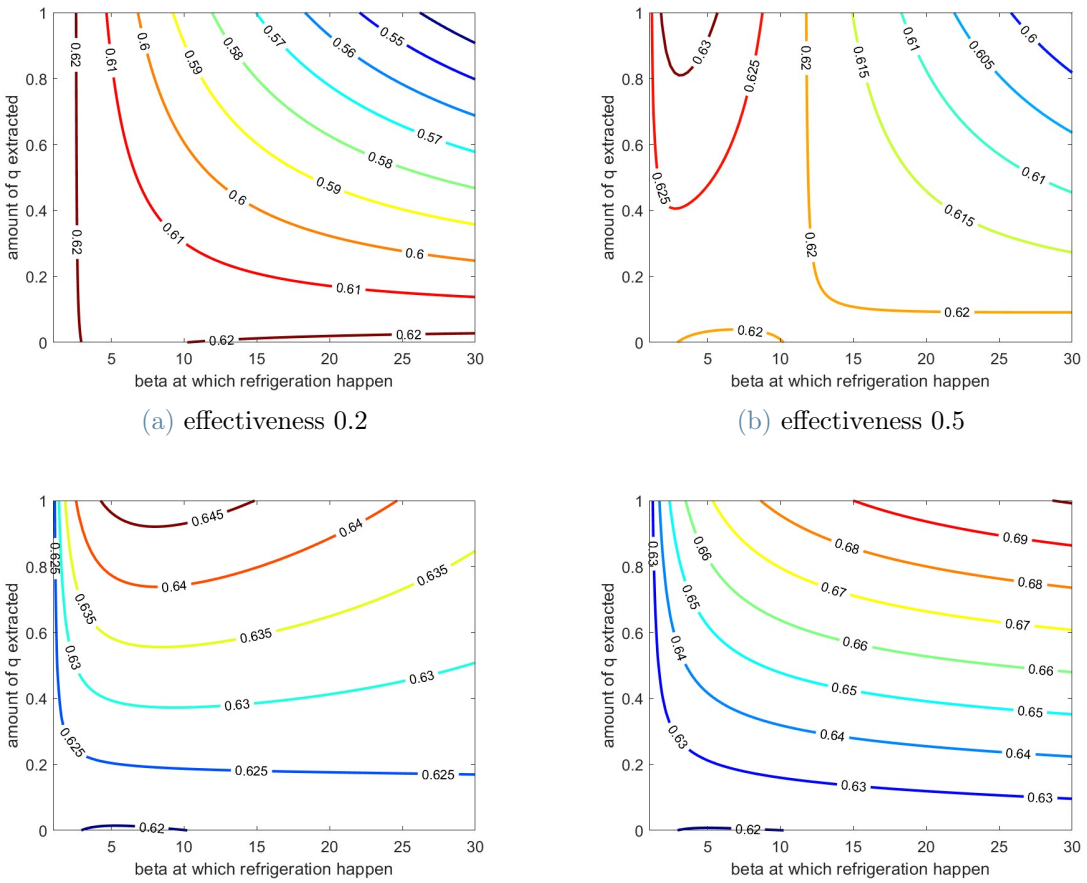

(a) effectiveness 0.2

(b) effectiveness 0.5

(c) effectiveness 0.7

(d) effectiveness 1

Figure 2: Efficiency map of Joule Brayton cycle with heat exchange between the flow inside the core and bypass one: different heat exchanger effectiveness

The results show that with an effectiveness below 0.5 it is more convenient to remove a lower quantity of heat in the booster and decreasing the work required by the HPC despite of removing a large amount of heat, increasing more the thrust but without decreasing the work require in the compressor.

The cycle analysis is a very complex topic because lot of parameter are chained: a common results with this thesis is the possibility of increasing the engine performance exploiting the heat produced by the compressor.

1 | Analysis of the thermodynamic cycle

In this section the numerical analysis of a Joule Brayton inter refrigerated cycle is described to find the optimal position of a refrigeration in the compression process. The analyses will be parametric in terms of heat power removed and pressure ratio at which cooling happens, to understand which is the optimal cooling position which maximise efficiency in a multistage compression. The analysis is performed with *Matlab 2022*, the numerical code is validate with some exercise of the *Politecnico di Milano* course of *Macchine* [10], [29] and with a comparison to the result obtained in the thesis written by a previous VKI short training student [4].

The code analyses a mean line cycle for both fan and the booster. This approach is theoretically not applicable to the real machine in which the pressure ratio produced by the fan affects only the by-pass flow and not the core one. The mid fan analysis is used being this thesis work a principal analysis of a machine that doesn't exist yet. Some future application presents a mid-fan engine design that could be apply in civil aviation [6].

The fluid is considered pure air with an adiabatic coefficient(γ) of 1.4 and the entropy reference quantity is estimated with an average mean of oxygen and nitrogen entropy of formation weighted with their mass weight (22% and 78%) [3]. The molecular mass is estimated as $28.88 \frac{Kg}{Kmol}$, the specific heat capacity c_p as $1.007 \frac{kJ}{kg \cdot K}$, the entropy of formation results $6.7348 \frac{kJ}{kg \cdot K}$. This value is the starting point for the cycle, even if entropy is never considered like absolute value but as variation between two different conditions; on the entropy-temperature diagram it affects a lot the amount of divergence of different isobaric line. The amount of cooling estimation technique follows the approach used by Shah and Tan [28]. The amount of heat removed is a q^* parameter defined as the ratio between the heat removed and the total enthalpy increase due to the previous compression stage. This parameter is discretized between "*0*" and "*1*": a "*0*" means that no cooling is applied to the cycle while "*1*" simulate an inter-refrigeration that remove all the enthalpy generated

by previous stage. This parameter is considered the most reasonable since the real final application will be the aircraft engine, a machine that works in an environment that remains at a thermodynamic condition equal to the inlet flow condition. This external boundary condition limits the maximum amount of cooling applicable: the flow inside the compressor can not be colder than environment or it will be heat up by the flow in the bypass. The parameter q^* allows the code to simulate an inter refrigeration that cooled the flow without over passing the environment temperature threshold. To study the most effective cooling position from the thermodynamic cycle point of view the effectiveness of heat exchange process is considered unitary. In a future development of this project a trade off between thermodynamic advantages and a global heat exchange effectiveness, that increase with the amount of heat removed, will give the optimal point of inter-cooling. The cycle analysis could be affected by lots of parameters: the choice of single value cannot be done freely because some parameter are correlated and connected to the optimal cycle efficiency value. To do it an overall knowledge on the behaviour of all the components (compressor, burners, turbine, auxiliaries) is required but it is not the focus on this thesis.

1.1. Inter refrigerated compression

The first analysis focuses on the compression process only that is simplified in two consecutive compressions, between them the inter refrigeration happens. The cycle is reported in the figure Figure 1.1:

- "0" is the inlet condition at which air flow in the compressor
- "1" is after the first compression
- "1c" is on the same isobaric line of point "1" but with a lower amount of total temperature due to inter cooling
- "2" is the condition at the end of the compression process

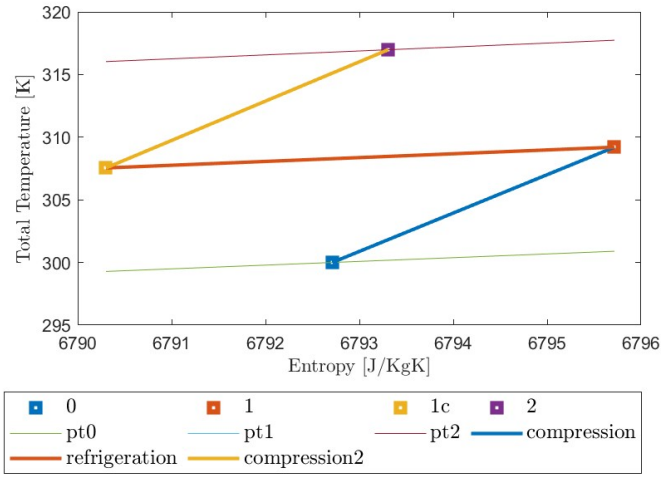

Figure 1.1: Inter-refrigerated compression process

Efficiency is the key parameter of this study. To estimate the inter refrigerated compression efficiency, a definition based on the ratio between isentropic and real work is used. The real work can be estimated as the difference between the total enthalpy of final state h_{T2} and the total enthalpy of initial state h_{T1} plus the removed heat Q how reported in Equation 1.1 . The heat extracted has to been considered to avoid an efficiency value higher than "1". The inter refrigeration manages to reduce the work required by second compression decreasing the entropy and the enthalpy generate by the first one. This energy is part of the work done by upstream compressor stage and so it must be considered in the computation of the work done by machine. A similar expression is reported also by Shan and Than in [28].

$$\eta = \frac{c_p \cdot T_{T0} \cdot ((\beta_1 \cdot \beta_2)^{\frac{\gamma-1}{\gamma}} - 1)}{h_{T2} - h_{T1} + Q} \tag{1.1}$$

Numerical results show an increase of efficiency with the amount of dimensionless heat removed parameter q^*, while no variation is associated to the boundary condition: the total temperature and pressure at the inlet of compressor do not affect the final compression process efficiency. Efficiency maps are visible in Figure 1.2.

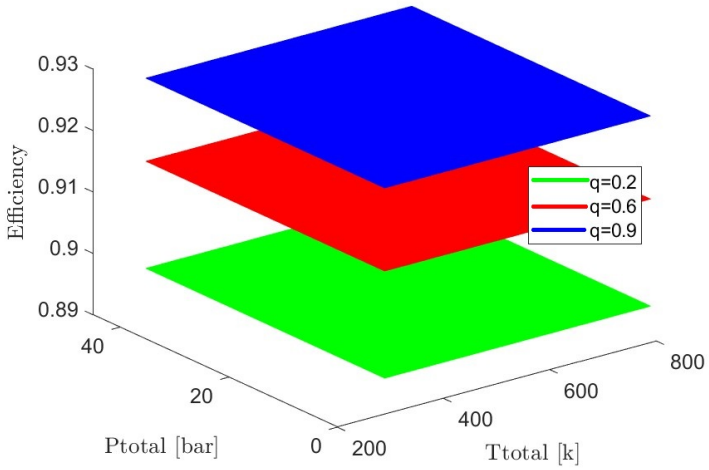

Figure 1.2: Effect of total inlet condition in the stage efficiency

These result can be explained looking at the compression process on the T-S diagram and at the cycle efficiency definition used. Fixing the efficiency and the compression ratio of the single stage, the entropy generation remain the same percentage of the total enthalpy increase. That value of work provided to the fluid, so the increase of enthalpy is fixed being the compression ratio and the process efficiency imposed. The analytical explanation is reported in Appendix A. The final efficiency expression is Equation 1.2:

$$\eta = \frac{(\beta_1 \cdot \beta_2)^{\frac{\gamma-1}{\gamma}} - 1}{(a \cdot b - 1) + (\beta_1^{\frac{\gamma-1}{\gamma}} - 1) \cdot q^*} \tag{1.2}$$

In which the two parameters a and b are:

$$a = \frac{1}{c_p \cdot \eta} c_p \cdot [(\beta_2^{\frac{\gamma-1}{\gamma}} - 1) - c_p + \eta] \tag{1.3}$$

$$b = 1 + \left(\frac{1}{c_p \cdot \eta} + q\right) \cdot \left(\beta_1^{\frac{\gamma-1}{\gamma}} - 1\right) \tag{1.4}$$

This expression explains the results of Figure 1.2. The numerator is fixed with the total compression ratio require and the denominator doesn't depend on initial condition: the compression efficiency is only function of: single compression ratio, heat extracted and efficiency of compression ratio as shown in Equation 1.5.

$$\eta_{compression} = f(\beta_1, \beta_2, q, \eta_{stadio}) \tag{1.5}$$

The inlet conditions describe the operative point of the engine: during the take off phase they will be almost atmospheric while during cruise the temperature and pressure of air diminish significantly. The results obtained in this section are due to the analysis of the compression process only, in the complete cycle they affect the efficiency and their effect is analyzed and described in section 1.2

1.2. Full Joule-Brayton cycle

In this section the full Joule Brayton is simulated to estimate the advantages of inter refrigeration in the compression process and the optimal position to maximize the efficiency. In scientific literature, as already report in subsection 0.4.1 some authors suggest applying the inter refrigeration in the high pressure compression to exploit the higher thermal gradient available. This section presents an efficiency study based purely on the numerical simulation of Joule Brayton cycle with an inter-cooling compression. The feasibility analysis of this process is reported in chapter 2 and chapter 3.

To be more realistic, inlet condition, compression ratio, mass flow and amount of fuel are taken from two real engines; the CFM56-7824 and GENX-1864,in the takeoff and at cruise [4] . The input parameters are reported in Table 1.1

Parameter	CFM		GENX	
	Cruise	Takeoff	Cruise	Takeoff
Mass flow of air [kg/s]	136	327	435.521	1109.07
Total temperature inlet [K]	246.9	288.15	248.095	288.15
Total pressure inlet[Pa]	36356.86	101325	31005.97	101325
Mass flow of fuel [Kg/s]	0.42	1.025	0.8247	1.8735
LHV fuel [kJ/Kg]	43200	43200	43200	43200
HP turbine expansion ratio	3.367	3.357	4,451	4.451
LP turbine expansion ratio	4.067	4.053	5.4617	5.467
Fan compression ratio	1.6	1.54	1.45	1.36
Fan efficiency	0.89	0.94	0.925	0.95
Efficiency LPC	0.9	0.91	0.925	0.936
Efficicency HPC	0.91	0.9125	0.925	0.936
Efficiency HPT	0.91	0.9108	0.93	0.93
Efficiency LPT	0.91	0.91104	0.93	0.9312
Bypass Ratio	5.3	5.55	8.53	9.2
Global compression ratio	40	35.11	52.3	41.4

Table 1.1: Real engine parameter

The results obtained with this input parameter in the *Matlab* code used are comparable to the results from *the EcosimPro* model developed in another VKI project [4] and perform a further validation of the code. The inter-cooling stage is added to the adiabatic cycle changing the position of the refrigeration through the parameter β_1 and the severity of cooling with the parameter q^*.

This code simulates a principle analysis of a technology that doesn't exist yet; this condition allows some freedom in the parameters selection. To simulate a more general and recent engine, the following parameter are set manually:

- The global compression ratio is imposed equal to *60* at cruise and *45* at take off [2].
- The expansion ratio of the LPT is adapted to the new global value of pressure ratio to obtain the same thrust at the core exit. This change allows also an increase of the work extracted by turbine and available for the compression
- The efficiency value of compressors and turbine is equalized to more general value: *0.88* for the compression process and *0.91* for the expansion one. Real value cannot be find in any website, paper or manual because it is covered by industrial secret;

the value used comes from a common knowledge of this technology.

- The bypass ratio is imposed constant end equal to *5.75* for CFM and *9.75* for the GENX to decrease the number of variables in this first cycle analysis.

Their new values, input of the code, are reported in Table 1.2.

Parameter	CFM		GENX	
	Cruise	Takeoff	Cruise	Takeoff
LP turbine expansion ratio	6.101	5.195	6.2659	5.942
Fan efficiency	0.88	0.88	0.88	0.88
Efficiency LPC	0.88	0.88	0.88	0.88
Efficicency HPC	0.88	0.88	0.88	0.88
Efficiency HPT	0.91	0.91	0.91	0.91
Efficiency LPT	0.91	0.91	0.91	0.91
Bypass Ratio	5.75	5.75	9.5	9.5
Global compression ratio	60	45	60	45

Table 1.2: Engine parameter used in numerical code

Even if there are no applications to compare the results with, some constrains to the numerical code have to be imposed. The work extracted by the turbine should be always higher than the work required by compressor and fan, to allow a positive energy balance at crankshaft. This result is not obvious since a cooling in the compression moves, in case of fixing amount of fuel injected subsection 1.2.1 all the cycle to lower value of enthalpy. The maximum temperature point of the cycle decrease and the turbine outlet point is moved to the left, this change reduces the advantages of the combustion. The combustion is performed after compression to increase the temperature of gases moving the operative point of turbine at an higher level of entropy, where the divergence of isobaric line is higher and so the enthalpy drop available increase too. This difference can be seen in the following graph (Figure 1.3) where, due to cooling, with a fixed amount of fuel injection the total temperature passes from 4513 K to 4086 K. The consequence of this variation will be described in the next subsection subsection 1.2.1.

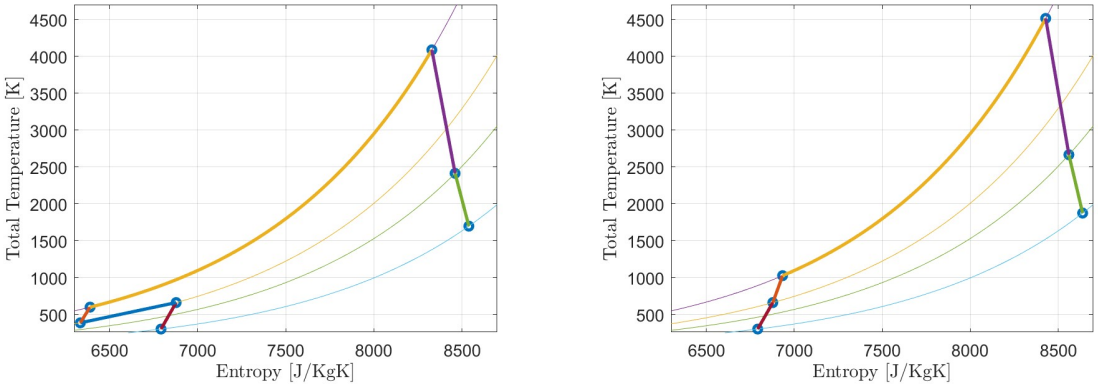

(a) Cooling: $q^*= 0.9$ (b) No cooling: $q^*= 0$

Figure 1.3: Joule Brayton cycle with and without cooling: T_t variation at inlet turbine

The turbine section is kept constant in all the simulation since the focus of this work is on the compressor. The inlet turbine condition changes only in temperature in case of fixed amount of fuel injection subsection 1.2.1, while there is no pressure variation (the global pressure ratio is steady).The expansion ratio and the exit temperature are kept constant to try to maintain the thrust of the core constant.

1.2.1. Fixed amount of fuel injected

A primitive analysis of the inter refrigerated cycle is performed by keeping the amount of fuel injected constant. This choice would like to maintain the equivalent ratio of combustion process invariable, equal to the reference adiabatic case and keep constant the power injected in the cycle. The constant amount of fuel injected will affect the turbine entry temperature and so the overall pressure ratio required by the compressor. The turbine entry temperature is maximise for a specific global pressure ratio to obtain the maximum efficiency of the real Joule Brayton cycle: the results always refer to an adiabatic case. In this analysis the results show that a cooled cycle could obtain a similar power (since the global efficiency and the heat injected does not change) with a lower turbine entry temperature. This could have a greatest technology advantages since with a lower temperature the amount of film cooling required is less and the mass flow of the core could be increased. For all the 4 machine conditions analysed (CFM cruise, CFM takeoff, GENX cruise and GENX take off) two cases are taken into account changing the efficiency of compression process between two reference values of *0.88* and *0.84*.

For all the machines the combination of pressure ratio and amount of heat that maximise efficiency is:

- Maximum amount of heat removed: $q^* = 1$
- Pressure ratio below 2 that means performing the inter-refrigeration in the booster compressor.

The results reported in this thesis are obtained with an efficiency $\eta = 0.88$ because it is considered more realistic for modern application: the same conclusions are true for the $\eta = 0.84$. The result can be seen also in the best thermodynamic cycle compute for all the application. The Figure 1.4 shows the four different application:

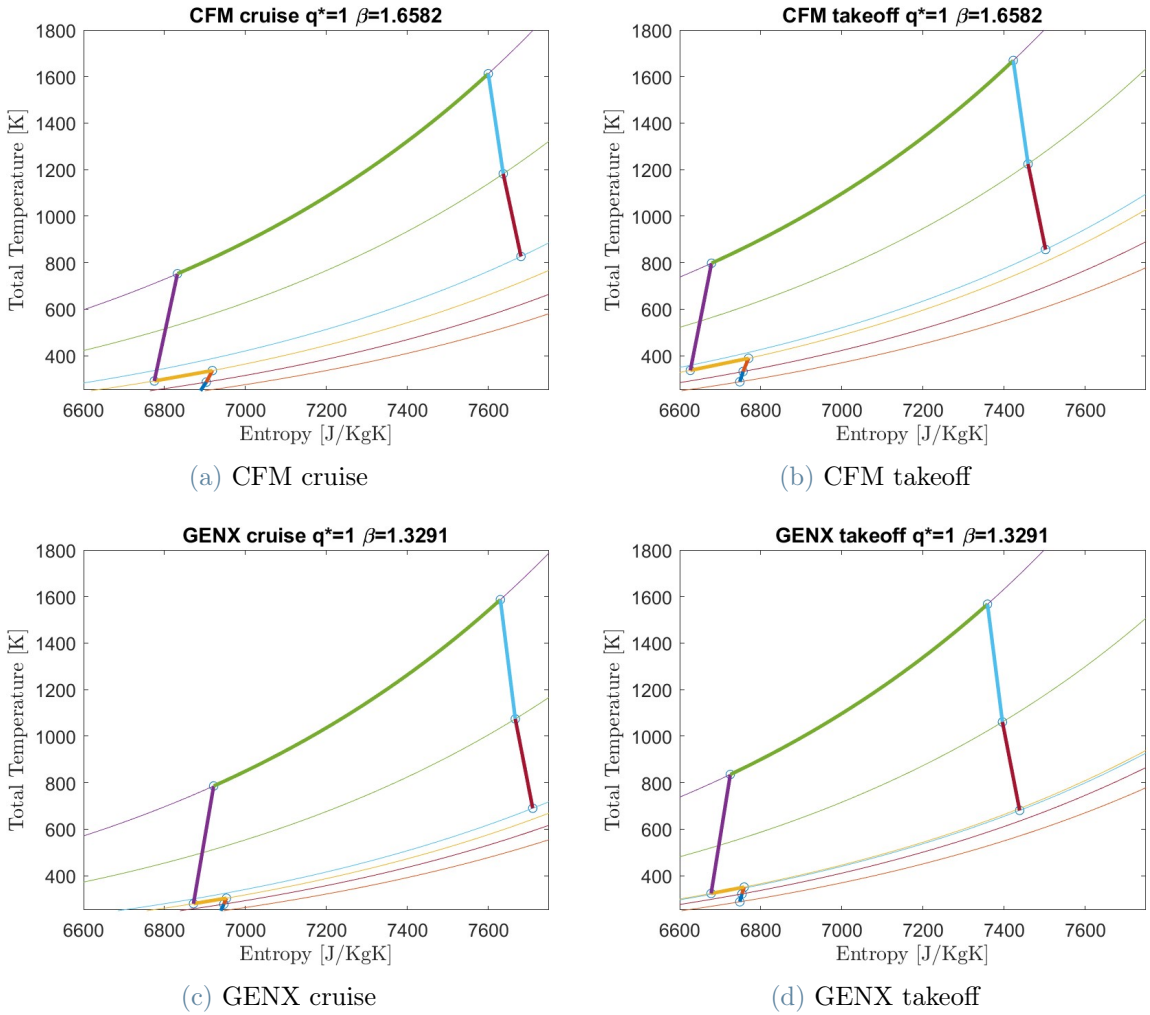

(a) CFM cruise

(b) CFM takeoff

(c) GENX cruise

(d) GENX takeoff

Figure 1.4: Optimal inter-refrigerate Joule Brayton cycle for the four machine

The advantages of an inter-refrigerated cycle over the adiabatic one are visible in the increase of the cycle area.

The area enclosed by the cycle is the work done by the process: with a refrigeration during compression it is possible to increase it in the lower left part. There are some constrains

that should be always respected like the power balance at the engine crankshaft. The cycle could not be applicable to a real engine if a severe cooling is applied: in case of fixing the amount of fuel, removing energy from the compression moves all the cycle in the lower-left region where the isobaric lines are less divergent. The decrease of the total enthalpy at turbine inlet reduces the availability of power that can be extracted during expansion until it will not be sufficient to balance the power required during compression. The analysis of the maximum amount of cooling is visible in Figure 1.5

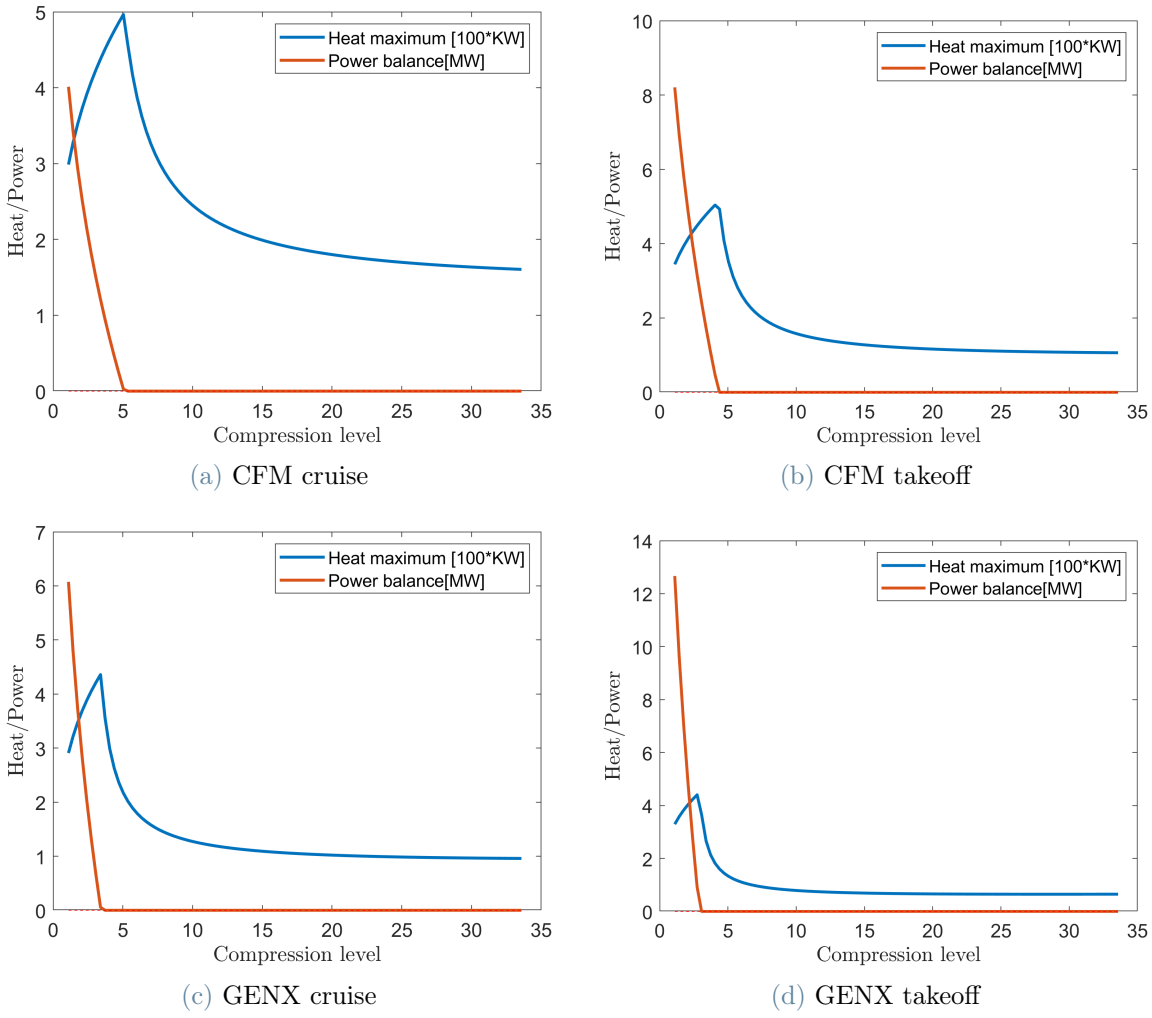

(a) CFM cruise

(b) CFM takeoff

(c) GENX cruise

(d) GENX takeoff

Figure 1.5: Maximum amount of cooling available in the Joule Brayton cycles for the four applications studied

All the machines reach a plateau if the cooling is applied at high pressure level. This results confirm that,if the pressure level increase, the cooling parameter q^* has to be limited due to the decrease of turbine available power.

The work extracted by the different combination of the parameter q^* and β is reported

in the Figure 1.6.

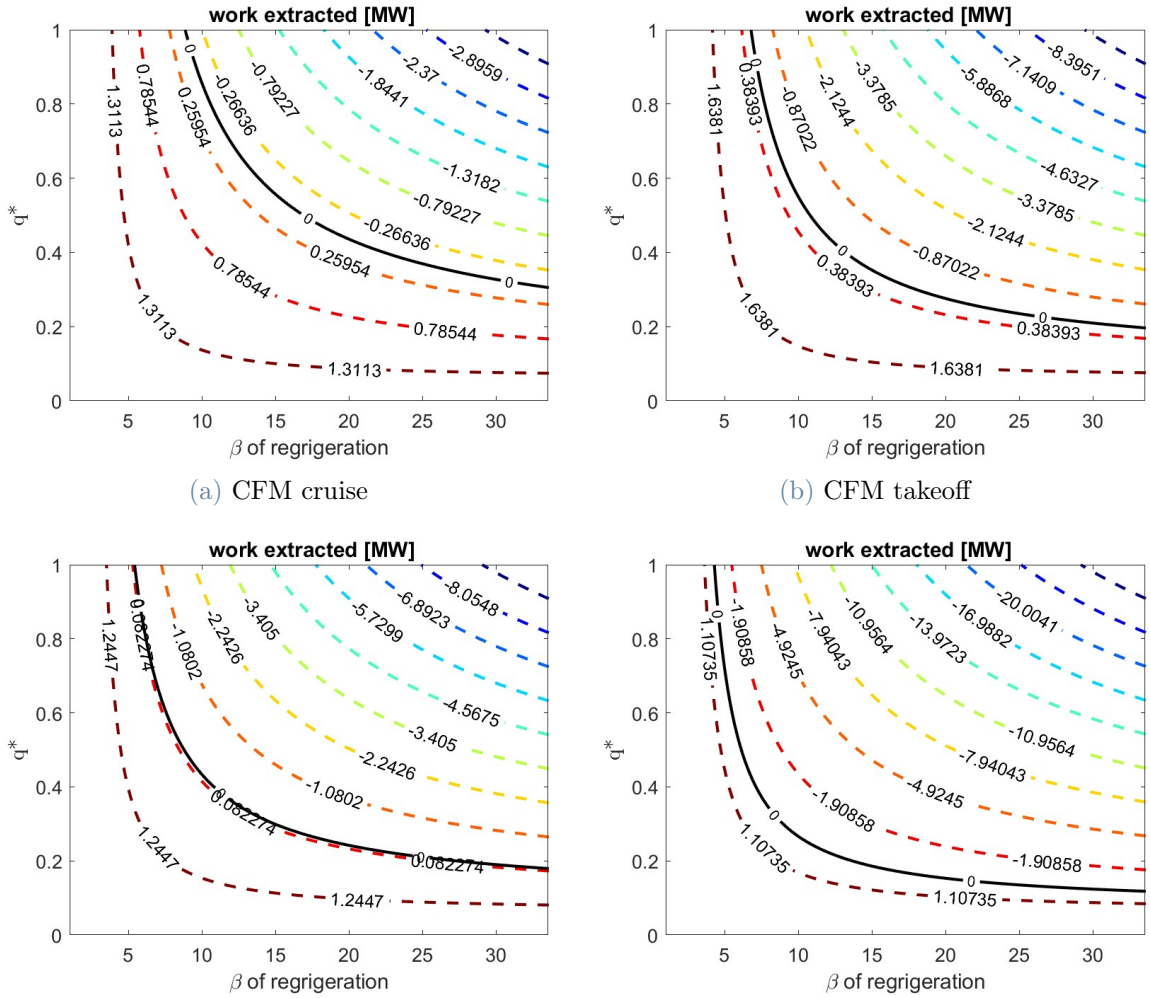

(a) CFM cruise

(b) CFM takeoff

(c) GENX cruise

(d) GENX takeoff

Figure 1.6: Power output of refrigerated Joule Brayton applied to the four applications

The black line is the zero power isoline; only the combination in the lower left region can be considered suitable and applicable to a real machine. The same graphs are obtained for efficiency and its variation from the adiabatic case. Those will be reported later in chapter 3 for a real possible Joule Brayton cycle refrigerated through a compressor blade.

The final results of the code, for both compression efficiency (0.88 and 0.84), are summed up in the Table 1.3:

Machine	$\eta = 0.88$		$\eta = 0.84$	
	Cruise	Takeoff	Cruise	Takeoff
CFM	$\eta_{max} = 0.406$ $\beta = 1.6582$ Q: 997 [KW] W: 1.837 [MW] $\Delta\eta$: 0.0113	$\eta_{max} = 0.38544$ $\beta = 1.6582$ Q: 2.22 [MW] W: 2.89 [MW] $\Delta\eta$: 0.01	$\eta_{max} = 0.390$ $\beta = 1.6582$ Q: 1004.2 [KW] W: 1.2787 [MW] $\Delta\eta$: 0.0133	$\eta_{max} = 0.3685$ $\beta = 1.6582$ Q: 2.22 [MW] W:1.47 [MW] $\Delta\eta$: 0.0118
GENX	$\eta_{max} = 0.457$ $\beta = 1.3291$ Q:1.2 [MW] W: 2.407 [MW] $\Delta\eta$: 0.0076	$\eta_{max} = 0.42637$ $\beta = 1.3291$ Q: 2.86 [MW] W: 4.123 [MW] $\Delta\eta$: 0.0066	$\eta_{max} = 0.4441$ $\beta = 1.3291$ Q: 1.2 [MW] W: 1.19 [MW] $\Delta\eta$: 0.0089	$\eta_{max} = 0.428$ $\beta = 1.3291$ Q: 2.87 [MW] W:1.1454 [MW] $\Delta\eta$: 0.0709

Table 1.3: Results of numerical code

The results shows that the decrease in the efficiency of the compression leads to:

- An higher $\Delta\eta$ due to cooling with respect the adiabatic process in case of lower η_{comp}. This result is reasonable since a lower value of η is related to an higher increase of entropy and so an higher work required by downstream compressor to reach the required overall pressure ratio. The cooling process decrease the entropy generation and mitigate the increase of entropy due to low efficiency values.
- There is no variation of maximum amount of heat extracted since it is calculated as a percentage of total enthalpy variation due to compression
- The useful work decreases since the efficiency of the cycle decreases

The analysis already reported is done also with a fixed turbine temperature in the next section. This second case is considered to compare the results to some authors like Kurtze [20] and to compare the adiabatic and cooled cycle in case of constant work extracted by turbine.

1.2.2. Fixed amount of temperature at turbine inlet

In the thermodynamic cycle the most important relationship to maximise efficiency is the one between pressure and temperature at the turbine entry section. The entry turbine temperature sizes the design of all the machine and there are relationships that couple the compression ratio with a turbine entry temperature to maximise efficiency [20].

This approach is used also by other authors as Thomas Morgan [23] and P.N. Shah [28]. By fixing the global pressure ratio and an optimal temperature, an increase of temperature causes an increase of the pressure ratio required to obtain the same efficiency: in conclusion for a pressure ratio there is just one temperature that maximizes efficiency.

This relationship can be seen in the Figure 1.7 taken by the Von Karman lecture series [20]:

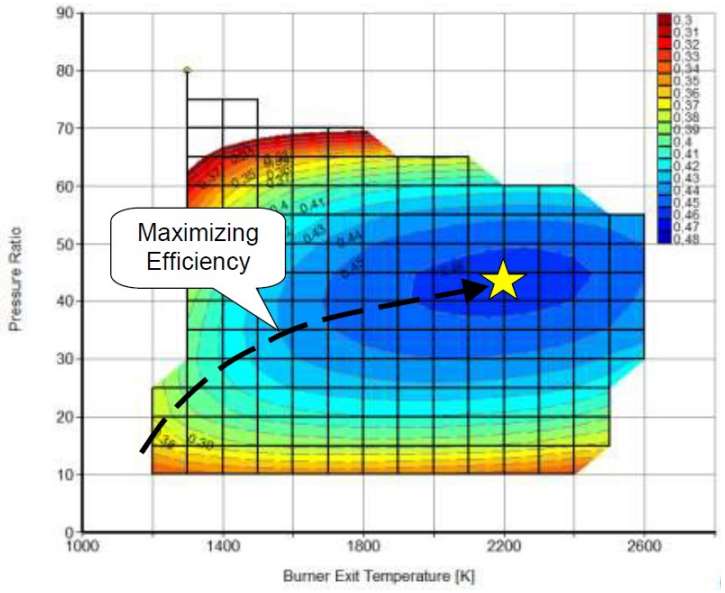

Figure 1.7: Effect of pressure ratio and burner exit temperature combination on efficiency

The lecture series was presented in 2013 when there were no applications with a compression ratio close to 60, The actual efficiency map obtained with *GasTurb* are shifted upstream in the global compression ratio due to different architecture and the performance of machine are improved too. From the graph in Figure 1.7 the optimal combination of pressure and temperature is $T = 2200K$ and $\beta = 45$. This result set the reference temperature at turbine inlet to $2200K$, then the reference results are compared to other cycles with an entry temperature of $1600K, 1800K, 2000K$ and $2400K$. The temperature-overall compression ratio relationship requires an increase of fuel injection (Figure 1.8) and so an increase of the engine power; this allow to fix the amount of work extracted in the turbine.

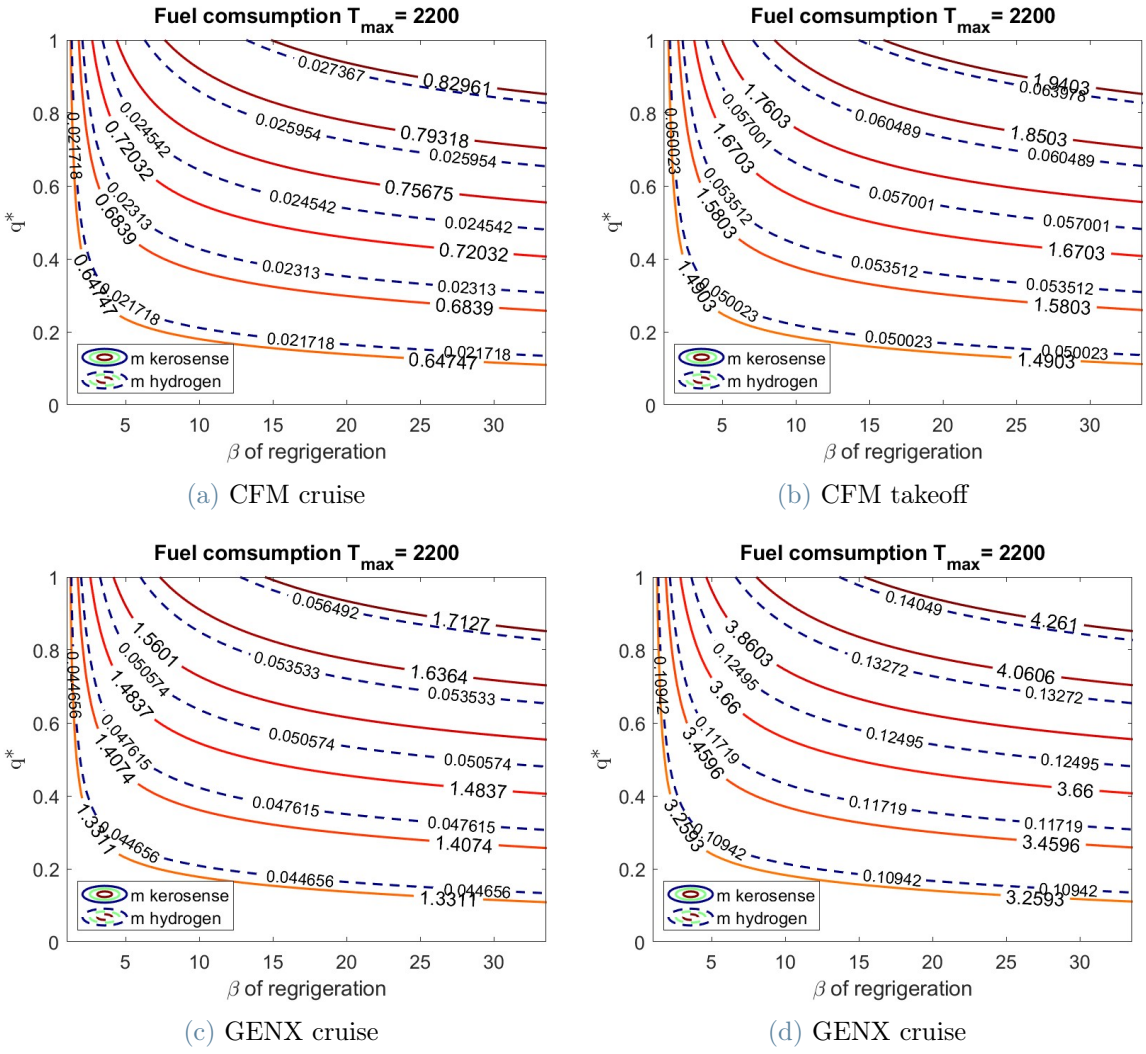

(a) CFM cruise

(b) CFM takeoff

(c) GENX cruise

(d) GENX cruise

Figure 1.8: Fuel consumption with a turbine entry temperature of 2200 K

Those values are higher than the reference one (Table 1.4):

CFM cruise	CFM takeoff	GENX cruise	GENX takeoff
0.42[Kg/s]	1.025 [Kg/s]	0.8247 [Kg/s]	1.8735 [kg/s]

Table 1.4: Reference amount of fuel injected

The increase of mass flow can be compensated changing the fuel LHV from kerosene (continue line) to hydrogen (dotted line). This allows also the reduction of the fuel tank size but the analysis of the interaction between this technology and aircraft system is not part of this work.

The cycle with a burner exit temperature of $1600K$ has a particular behaviour since it

has a lower temperature respect the optimal case found with fixed amount of fuel in Figure 1.4. The adiabatic cycle with this maximum temperature is not able to generate sufficient power to move the fan too and only with cooling it can become applicable in real engine. This characteristic is more relevant during takeoff: without cooling the turbine cannot drives the compressor and the fan, Figure 1.9 shows this relationship and the black line is the threshold to imagine it in a real application.

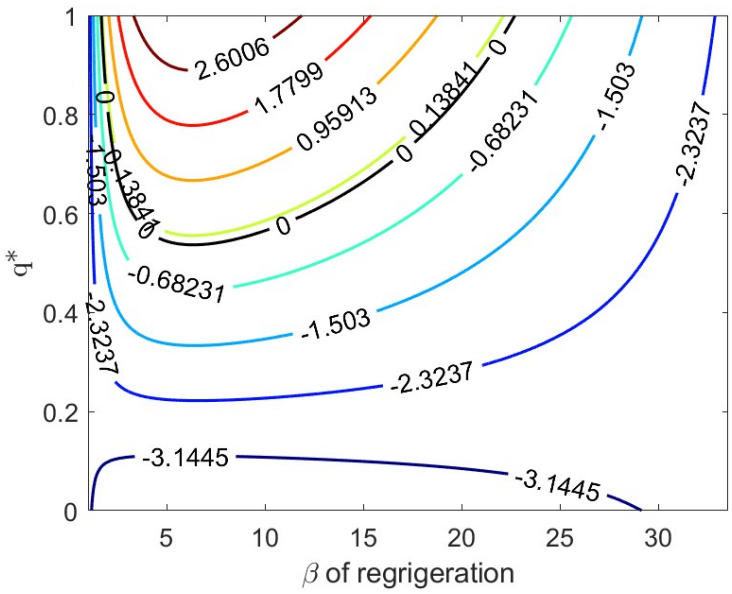

Figure 1.9: Work extracted at CFM takeoff with a turbine entry temperature of 1600 K

The results with a fixed temperature agree with the inter-refrigerated cycle with a fixed amount of fuel injected. In both cases, by fixing power injected in the cycle (subsection 1.2.1) or fixing amount of work extracted (subsection 1.2.2), the efficiency is higher than the adiabatic case.

The increase of both efficiency and the fuel consumption causes an higher power extracted and explains why it is always possible to perform the cycle with a turbine entry temperature higher than the 1800 K. The additional power extracted can be exploited by auxiliary device as an alternator to convert mechanical to electrical energy to charge electric engine [4]. The optimal refrigerated cycles for the 4 applications, with a turbine entry temperature of 2200 K are shown in Figure 1.10:

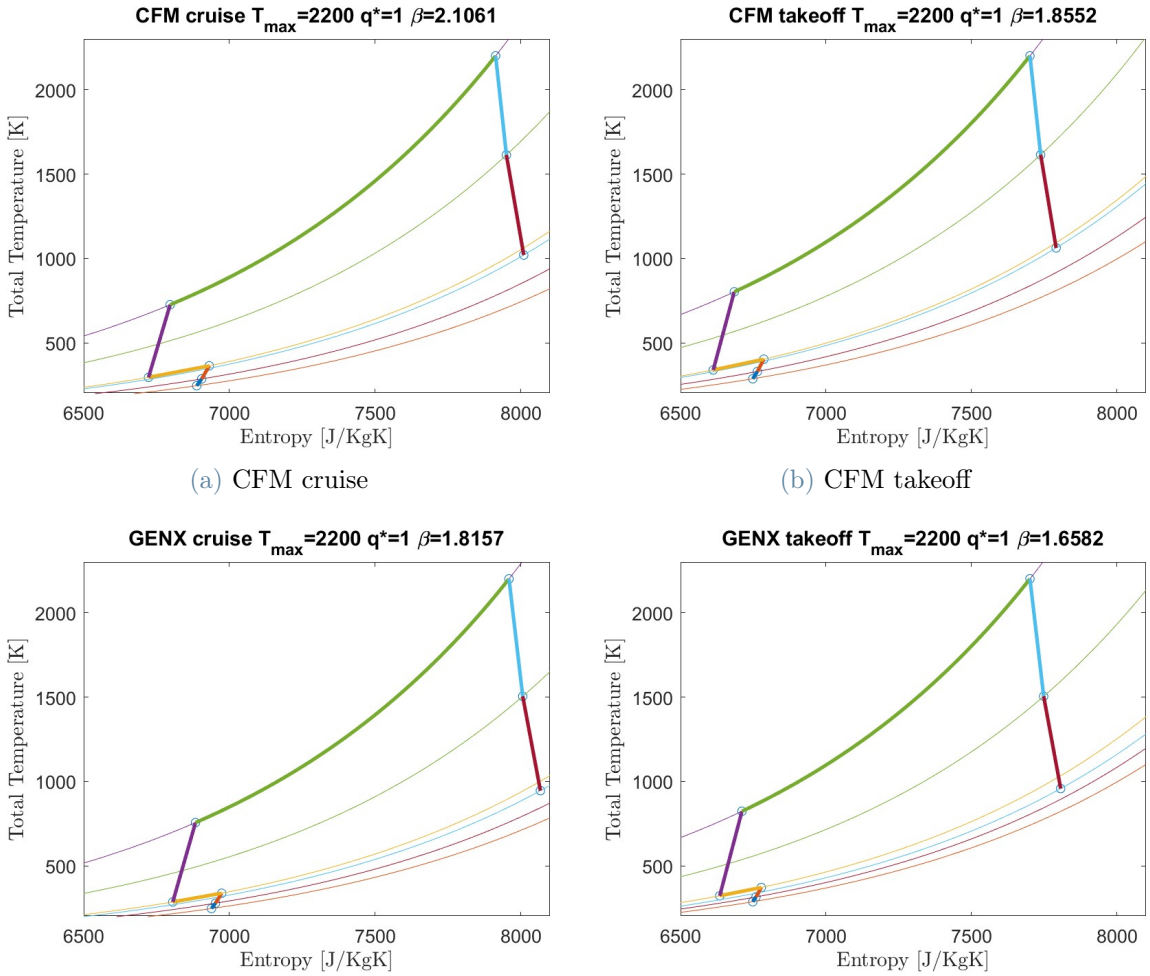

(a) CFM cruise

(b) CFM takeoff

(c) GENX cruise

(d) GENX takeoff

Figure 1.10: Optimal inter-refrigerate Joule Brayton cycle for the four machine

The results with the different temperature analysed are summarised in the table Table 1.5

T_t turbine	CFM		GENX	
	Cruise	Takeoff	Cruise	Takeoff
Constant fuel	$\eta_{max} = 0.406$ $\beta = 1.6582$ Q:997 [KW] W: 1.837 [MW] $\Delta\eta$: 0.0113 $T_{max} = 1583K$	$\eta_{max} = 0.38544$ $\beta = 1.6582$ Q: 2.22 [MW] W:2.89 [MW] $\Delta\eta$: 0.01 $T_{max} = 1681K$	$\eta_{max} = 0.457$ $\beta = 1.3291$ Q: 1.2 [MW] W:2.407 [MW] $\Delta\eta$: 0.0076 $T_{max} = 1636K$	$\eta_{max} = 0.42637$ $\beta = 1.3291$ Q: 2.86 [MW] W:1.123 [MW] $\Delta\eta$: 0.0066 $T_{max} = 1568K$
1800	$\eta_{max} = 0.46827$ $\beta = 2.152$ Q:1.56 [MW] W:4.39 [MW] $\Delta\eta$: 3.15%	$\eta_{max} = 0.41873$ $\beta = 2.3911$ Q:4.10 [MW] W: 6.93[MW] $\Delta\eta$: 3.5%	$\eta_{max} = 0.5005$ $\beta = 1.8477$ Q:2,66[MW] W: 8.45 [MW] $\Delta\eta$: 2.34%	$\eta_{max} = 0.49483$ $\beta = 1.8694$ Q: 20.82 [MW] W:20.82 [MW] $\Delta\eta$: 2.19%
2200	$\eta_{max} = 0.4833$ $\beta = 1.9564$ Q:1.35[MW] W:8.91[MW] $\Delta\eta$: 1.73%	$\eta_{max} = 0.4573$ $\beta = 2.1303$ Q:3.48 [MW] W:17.33 [MW] $\Delta\eta$: 1.82%	$\eta_{max} = 0.53151$ $\beta = 1.6955$ Q:2.27 [MW] W:18.32 [MW] $\Delta\eta$: 1.27%	$\eta_{max} = 0.5269$ $\beta = 1.7173$ Q:5.64 [MW] W:1.45.72 [MW] $\Delta\eta$: 1.12%
2400	$\eta_{max} = 0.4955$ $\beta = 1.9129$ Q:1.3 [MW] W:11.23[MW] $\Delta\eta$: 1.39%	$\eta_{max} = 0.47042$ $\beta = 2.065$ Q: 3.32 [MW] W:22.69[MW] $\Delta\eta$: 1.43%	$\eta_{max} = 0.54241$ $\beta = 1.652$ Q: 2.16 [MW] W: 23.39[MW] $\Delta\eta$: 1.01%	$\eta_{max} = 0.538$ $\beta = 1.652$ Q:5.2 [MW] W:58.35 [MW] $\Delta\eta$: 0.87%

Table 1.5: Results of numerical code

The results with an inlet turbine temperature of 2000 and 1600 are reported in Appendix B. The results of Table B.1 and Table 1.5 may be summed up as follows:

- The inter refrigeration in the compressor has a positive effect on efficiency at both aircraft operative condition (cruise and takeoff).
- The efficiency advantages of cooling decrease with the turbine entry temperature, this happens because the global cycle area increases while the advantages of cooling remain the same. The global efficiency increase too: the effects of different

parameter on efficiency are reported in the section subsection 1.3.2.

- Increasing the turbine entry temperature, the optimum β of cooling decrease.
- At a fixed temperature the efficiency of cruise for both engines remains higher than the takeoff one but the advantages of cooling, in terms of $\Delta\eta$, are higher at take off for CFM and at cruise for GENX. To investigate this behaviour, the effect of single parameter on efficiency and $\beta_{optimal}$ is analysed in section 1.3.

1.3. Effects of different parameters on efficiency and β optimal cooling

In this section the effects of cycle boundary condition (inlet and outlet pressure and temperature) machine characteristic (mass flow at inlet, bypass ratio, compression ratio of the fan,efficiency of compressors) and numerical setup (discretisation level) are analysed singularly. The aim is to understand how they affect the solution of efficiency value and optimal beta condition in a Joule Brayton cycle with a fixed turbine entry temperature ($2200K$). The effect of the single parameter can be explained looking at the entropy-temperature graph; changing one single parameter causes a variation on the global cycle area. The analysed parameters are:

- The effect of the numerical discretisation on the results
- The relationship between optimal $\beta_{cooling}$ and efficiency
- The mass flow through the cycle
- The total temperature at machine inlet
- The total pressure at machine inlet
- The bypass ratio
- The pressure ratio at machine outlet
- The compression ratio imposed by the fan on the all mass flow
- The efficiency of the compression process

The global compression ratio is divided in two main compressions, previous and after the cooling. Three different discretisations are applied to this range: the code runs with 100, 1500 and 2500 steps. The results are comparable in both the optimal cooling position and efficiency value of the cycle. The results for the optimal cooling position are reported in

Table 1.6 and they are similar.

	100 steps	1500 steps	2500 steps
CFM cruise	4%	3%	3%
CFM takeoff	4%	3.6%	3.56%
GENX cruise	3%	2.2%	2.2%
GENX takeoff	3%	2.26%	2.2%

Table 1.6: Optimal percentage for cooling found with different discretisations

The variation on efficiency with discretisation is even more negligible; the optimal results are reported in Table 1.7:

	100 steps	1500 steps	2500 steps
CFM cruise	0.48334	0.48335	0.48335
CFM takeoff	0.45718	0.45729	0.45729
GENX cruise	0.5315	0.5315	0.53151
GENX takeoff	0.5269	0.5269	0.5269

Table 1.7: Efficiency value with different discretisations

In a real multistage compressor the stages are between 10 and 15; this limitation in the real discretisation of compression process makes the 1500 and 2500 discretisations unfeasible. The results with 100 possible cooling pressure ratio are a good compromise between real application and numerical simulation power.

The reference machine to make the comparison is the base condition described in Table 1.2; this choice is made to have a non dimensional variation range respect a known value. The non dimensional variation will describe a linear variation trend and some correlations are found. The correlations allow predicting the machine performance and the optimal cooling position in a faster way and works in a range of $\pm 20\%$ instead of the reference value. The bypass ratio result does not show any effect on both the efficiency and in the optimal beta cooling in all the cases studied. It will affect the power of the cycle, more air enters in the core and more useful power is produced by the cycle. The mass flow inside the cycle does not affects the result to, since the efficiency definition is normalized respect it in its definition consider only specific quantity (Appendix A). Fixing the entry temperature the mass flow appears at both denominator and numerator and it is canceled out. The last free parameter is the total pressure value at inlet. This parameter moves

the cycle point on different isobaric line but, since the compression ratio is fixed, does not affect the area of the cycle. It will affect efficiency and optimal cooling pressure if, instead of a pressure ratio, a maximum pressure level is imposed in the combustion chamber, but this consideration changes completely the cycle analysis. The decision of a fixing pressure ratio is more reliable since the machine geometry, velocity and so the work done by compressor on the fluid is fixed in real application. The other parameter affects both efficiency and optimal pressure of cooling and a correlation is found for each of them. To quantify the linear trend, the Pearson-Bravais correlation coefficient is used [33]; this coefficient (called P-B value in the following table) is calculated as:

$$PB = \frac{\sum (x - \overline{x})(y - \overline{y})}{\sqrt{\sum (x - \overline{x})^2 \sum (y - \overline{y})^2}} \tag{1.6}$$

x and y are the two arrays between which a linear correlation is looked for. In this application they are the correlation and the numerical code results. The Pearson-Bravais parameter remains always between ± 1 and in particular:

- P-B value of 1 indicates a strong positive correlation
- P-B value of-1 indicates a strong negative correlation
- P-B value of 0 indicates no correlation at all

This parameter is estimated for each variable analysed and it confirms a close linear effect of a relative change of input parameter on efficiency and optimum beta cooling.
The final correlations are:

$$\eta = \eta_{ref} + m_{\beta_{fan}} \cdot \left(\frac{\beta_{fannew}}{\beta_{fanref}} - 1\right) + m_{\beta_{out}} \cdot \left(\frac{\beta_{outnew}}{\beta_{outref}} - 1\right) + m_{T_{t_{in}}} \cdot \left(\frac{T_{t_{in}}}{T_{t_{inref}}} - 1\right) + m_{\eta_{cnew}} \cdot \left(\frac{\eta_{cnew}}{\eta_{cref}} - 1\right) \tag{1.7}$$

$$\beta = \beta_{ref} + m_{\beta_{fan}} \cdot \left(\frac{\beta_{fannew}}{\beta_{fanref}} - 1\right) + m_{\beta_{out}} \cdot \left(\frac{\beta_{outnew}}{\beta_{outref}} - 1\right) + m_{T_{t_{in}}} \cdot \left(\frac{T_{t_{in}}}{T_{t_{inref}}} - 1\right) + m_{\eta_{cnew}} \cdot \left(\frac{\eta_{cnew}}{\eta_{cref}} - 1\right) \tag{1.8}$$

The m_x coefficient is the slope of the trend for each x parameter. They are estimated with the *Microsoft Excel* solver and reported separately in the next subsection. The single parameter result will be discussed completely in the dedicated subsections: subsection 1.3.3 and subsection 1.3.2.

1.3.1. Relationship between optimum $\beta_{cooling}$ and efficiency

The first parameter which affect the optimal cycle efficiency is the β at which the inter refrigeration happen. The trend between the compression ratio at which cooling happen and efficiency is reported in Figure 1.11.

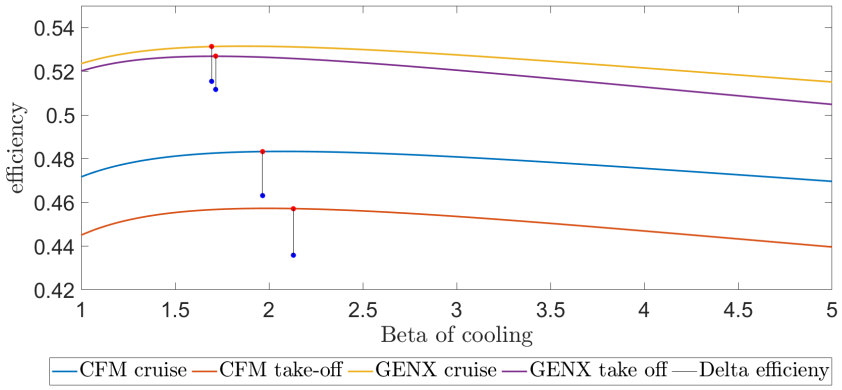

Figure 1.11: Relationship between $\beta_{cooling}$ and η_{cycle}

The red dot is the new optimal efficiency and the blue one is the adiabatic reference case. The relationship between the efficiency and the β at which refrigeration happen shows a single optimal point with a light gradient in the curve. This results means that the variation of the compression ratio at which cooling happen does not affect significantly the efficiency advantage of a inter refrigerated cycle respect the adiabatic one.
The efficiency variation has a different trend: Figure 1.12 shows a parabolic trend in the variation of efficiency respect the reference case.

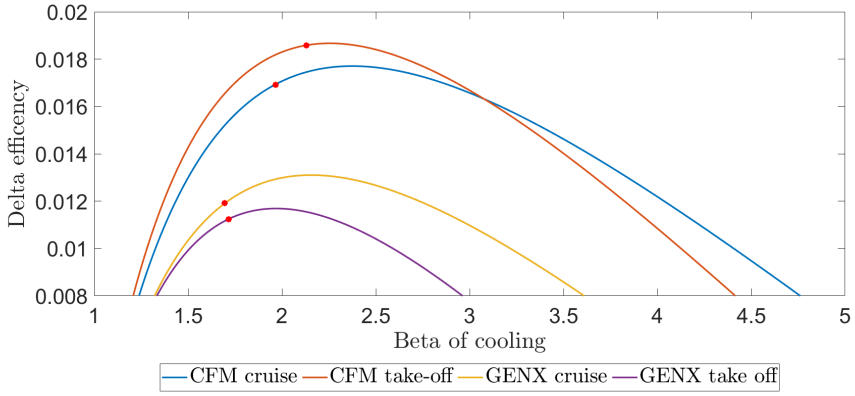

Figure 1.12: Relationship between $\beta_{cooling}$ and $\Delta\eta_{cycle}$

The red point represents the optimal condition and their value is the length of the dark line in Figure 1.11. The difference between the two graphs is the variation also, in the $\Delta\eta$ graph, of the adiabatic efficiency one that decrease splitting the global compression ratio between the two stage: the optimal adiabatic condition is to compress with just a machine to have the minimum total temperature at compressor inlet and so the minimum isentropic work. The interesting results of this trend are:

- In case of a complete refrigeration ($q^* = 1$) in the booster compressor, the exactly value of the compression ratio does not affect significantly the machine efficiency
- The optimal value for efficiency is different from the maximum value of the efficiency variation.

The $\beta_{cooling}$ is selected to optimise the efficiency of the Joule-Brayton cycle with the numerical code. The effects of the other parameters, which define the cycle and are given as input from another thesis work [4], will be describe in the next subsection.

1.3.2. Effect of different parameter on efficiency

The correlations found for the efficiency are summarised in Table 1.8

		CFM cruise	CFM takeoff	GENX cruise	GENX takeoff
β_{fan}	coefficient	0.0432	0.054	0.045	0.0563
	P-B value	0.999	0.999	0.999	0.999
β out turbine	coefficient	-0.176	-0.192	-0.1654	-0.178
	P-B value	-0.999	-0.999	-0.999	-0999
T_t inlet	coefficient	-0.120	-0.134	-0.103	-0.106
	P-B value	-0.998	-0.998	-0.998	-0.998
$\eta_{compression}$	coefficient	0.247	0.276	0.226	0.243
	P-B value	0.9814	0.9814	0.982	0.982

Table 1.8: Correlation between parameter and efficiency value

To explain this trend some hypotheses are made:

- The increases of β_{fan} slightly increase the efficiency. This coefficient is one order of magnitude lower instead of the other parameter and that is reasonable since there is not a easily and intuitive explanation of this results. A further investigation is required but it is not the topic of this job.
- The increased of the pressure ratio after the low pressure turbine, decrease the

efficiency since the flow is ejected with an higher power that is not used to drive the machine.

- The increase of T_t at the inlet of turbine decreases the efficiency too. This can be caused by the upper-right movement of the starting point of the cycle where the compression work required is higher.
- The $\eta_{compression}$ increases the global efficiency. This result is straightforward from the losses, and so the entropy generation decreases with the efficiency of the machine.

In Figure 1.13 it is possible to graphically see the match between the result obtained with the code and the correlation found. In the graph a single parameter is changed and it affects linearly the results in the limited range of ± 20.

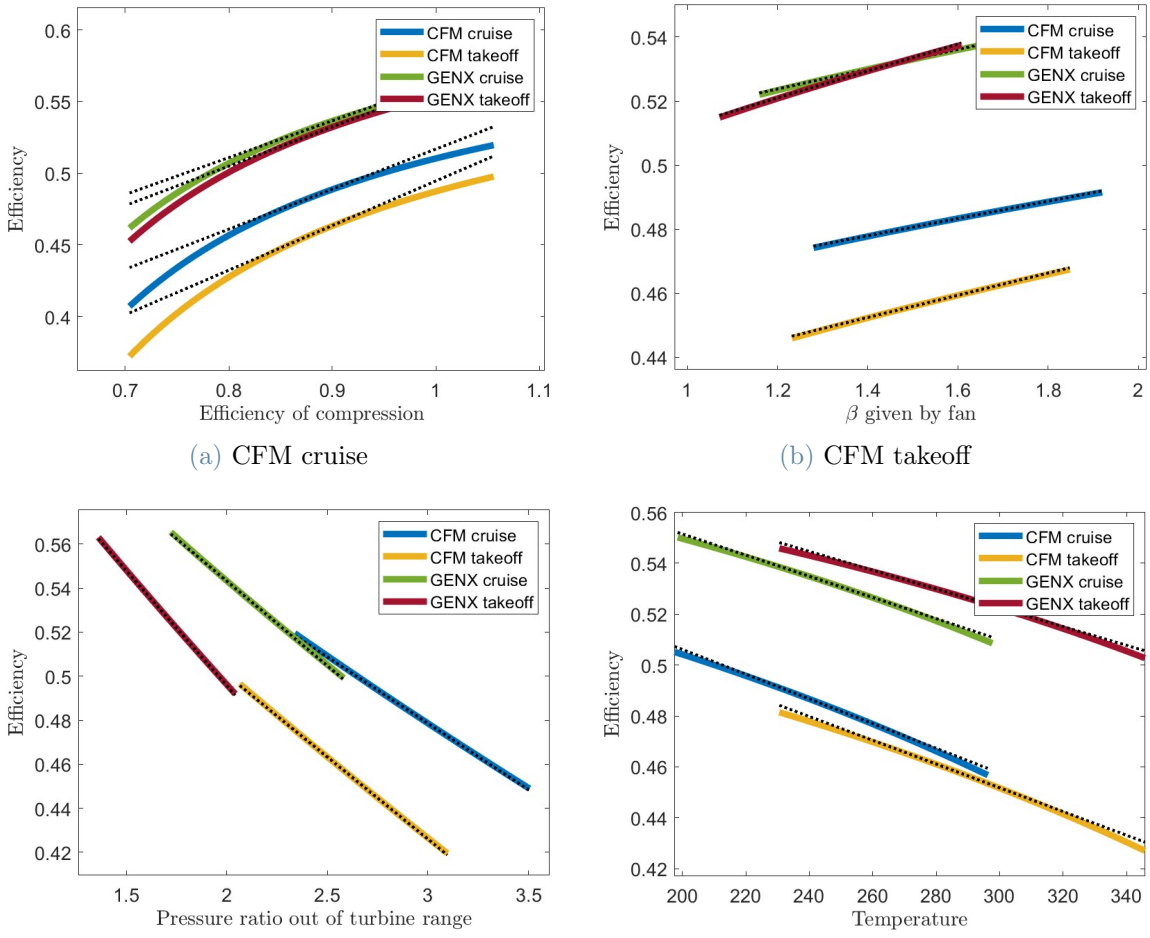

(a) CFM cruise

(b) CFM takeoff

(c) GENX cruise

(d) GENX takeoff

Figure 1.13: Comparison between numerical results and correlation

A quantitative estimation of the matches is represented by the absolute error between the

two results in Figure 1.14. The estimation error is confined in the analysed range in the order of 10^{-3} with some inconsistency in the relationship with the efficiency of compression. The parabola shape is due to the approximation technique used, the linear trend is customised compared to the reference case (zero variation) and the slope is estimated to better fit the results. The further the value changes, the more the approximation becomes unreliable.

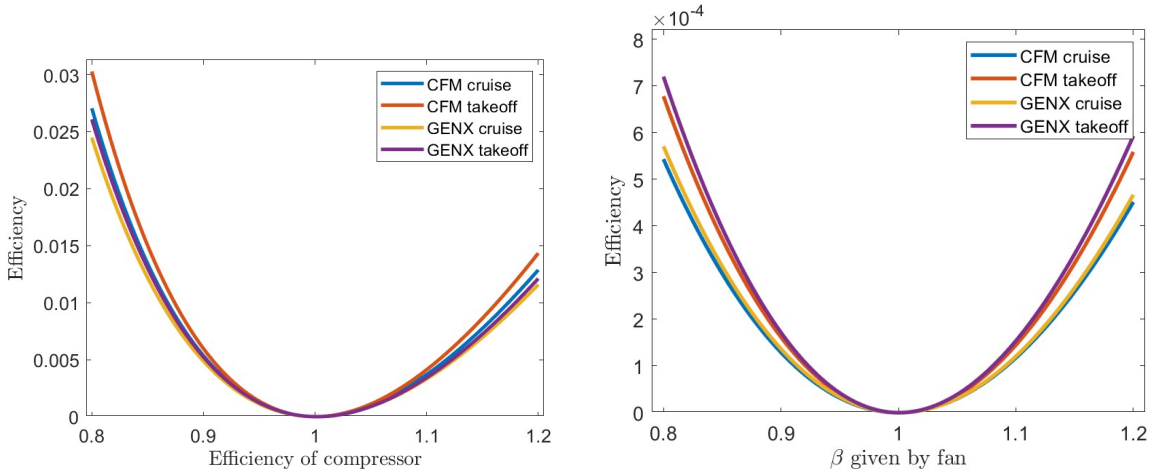

(a) CFM cruise

(b) CFM takeoff

(c) GENX cruise

(d) GENX takeoff

Figure 1.14: Discrepancy between the two interpolation

The most critical parameter is the correlation with the efficiency of the single compression process. This parameter has a small oscillation in the range analysed, but it is sufficient to obtain non practical results. The efficiency range, in the range ±20%, is between 0.7 and 1.056. An efficiency higher than 1 is unfeasible and an efficiency value of 0.7 is very low with the modern optimisation technique used during the design of a machine. The

β_{fan} affects the complete compression ratio request by the core. To analyse its effect on the efficiency, the cooling compressor is kept at the same percentage of the reference case. This choice is made to maintain the ratio between the compression process before and after cooling. In the range ±20% the solution is similar even if, instead of the pressure ratio, the fixed compression ratio before cooling is maintained. This second approach is rejected to avoid the extreme case in which the global compression ratio could overcome the imposed one.

1.3.3. Effect of different parameters on β of cooling

The correlations found for the optimal refrigerated stage are summarised in Table 1.9

		CFM cruise	CFM takeoff	GENX cruise	GENX takeoff
β fan	coefficient	-1.338	-1.2986	-1.2259	-1.189
	P-B value	-0.9967	-0.9969	-0.9968	-0.9970
β out turbine	coefficient	1.1518	1.1518	1.067	1.008
	P-B value	0.999	0.999	0.999	0.999
T_t inlet	coefficient	0.8246	0.8246	0.6827	0.6365
	P-B value	0.9977	0.9973	0.997	0.9967
$\eta_{compression}$	coefficient	-1.128	-1.227	-0.943	-0.967
	P-B value	-0,9985	-0.9972	-0.9979	-0.9984

Table 1.9: Results of numerical code for optimal βcooling

The single parameter effect on the optimal cooling position is completely opposite compared to the efficiency one. The parameters with a direct relationship show an indirect one and vice versa.

- The β_{fan} increase causes a decrease of the optimal cooling position. This trend confirms that the optimal cooling position is related to a percentage of the global compression ratio as assumed in the efficiency study.
- Increasing the pressure ratio at the turbine outlet section, causes an increase of the cooling compression ratio too. This behaviour is not so understandable since the compression and the expansion process are completely decouple by the imposition of a total temperature at the turbine inlet. A possible reason can be the requirement

of decreasing the compression work and the amount of fuel injected. This is just an hypothesis and further investigation are required on this parameter.

- An increase of the *inlet total temperature* increases also the entry entropy moving the cycle in the upper-right region where the divergence of the isobaric line is higher. This trend can probably explain the increase of the optimal cooling position to counter-balance the higher increase of entropy in the high-pressure compression.
- A decrease of the η of the compressor increases the entropy generation and the temperature at inlet of second compression stage. To decrease the second compression stage temperature, the cooling should be anticipate.

This hypothesis should explain the numerical results. They are the beginning of a creation of a Joule Brayton cycle meta-model. This is not the topic of this work and it could be a further step in the optimisation of a Joule Brayton cycle. The matches of these correlation with numerical results are shown in Figure 1.15:

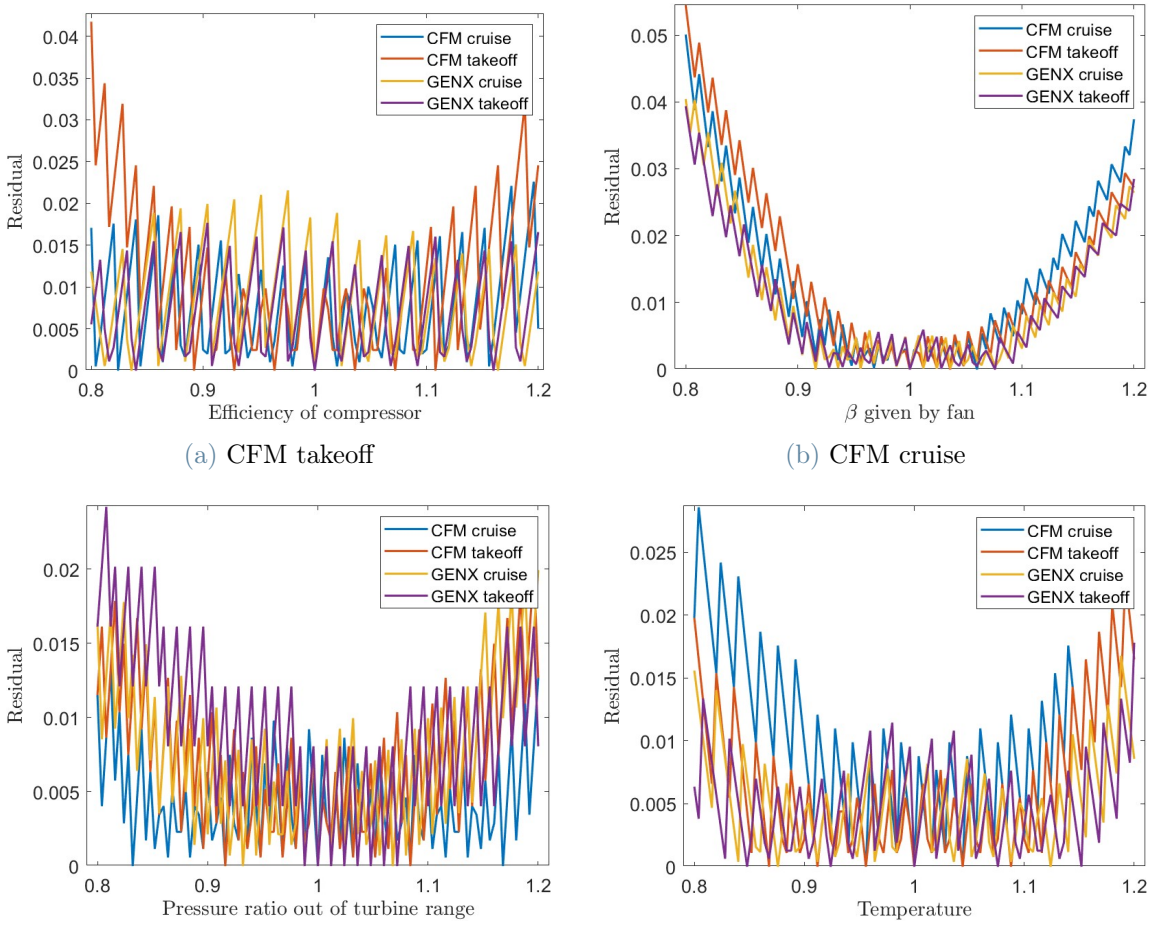

(a) CFM takeoff

(b) CFM cruise

(c) GENX cruise

(d) GENX takeoff

Figure 1.15: Discrepancy between the two interpolations

The absolute errors show for all the machines and the parameters a zigzagging trend. This trend is caused by the numerical discretisation of the compression ratio. The interpolation has a linear and continuous trend while the numerical code gives finite values of optimal compression depending on the discretisation adopted. This results are acceptable because it is just a rougher estimation of possible trends. In Figure 1.16 the zigzagging trend of the numerical results can be seen clearly.

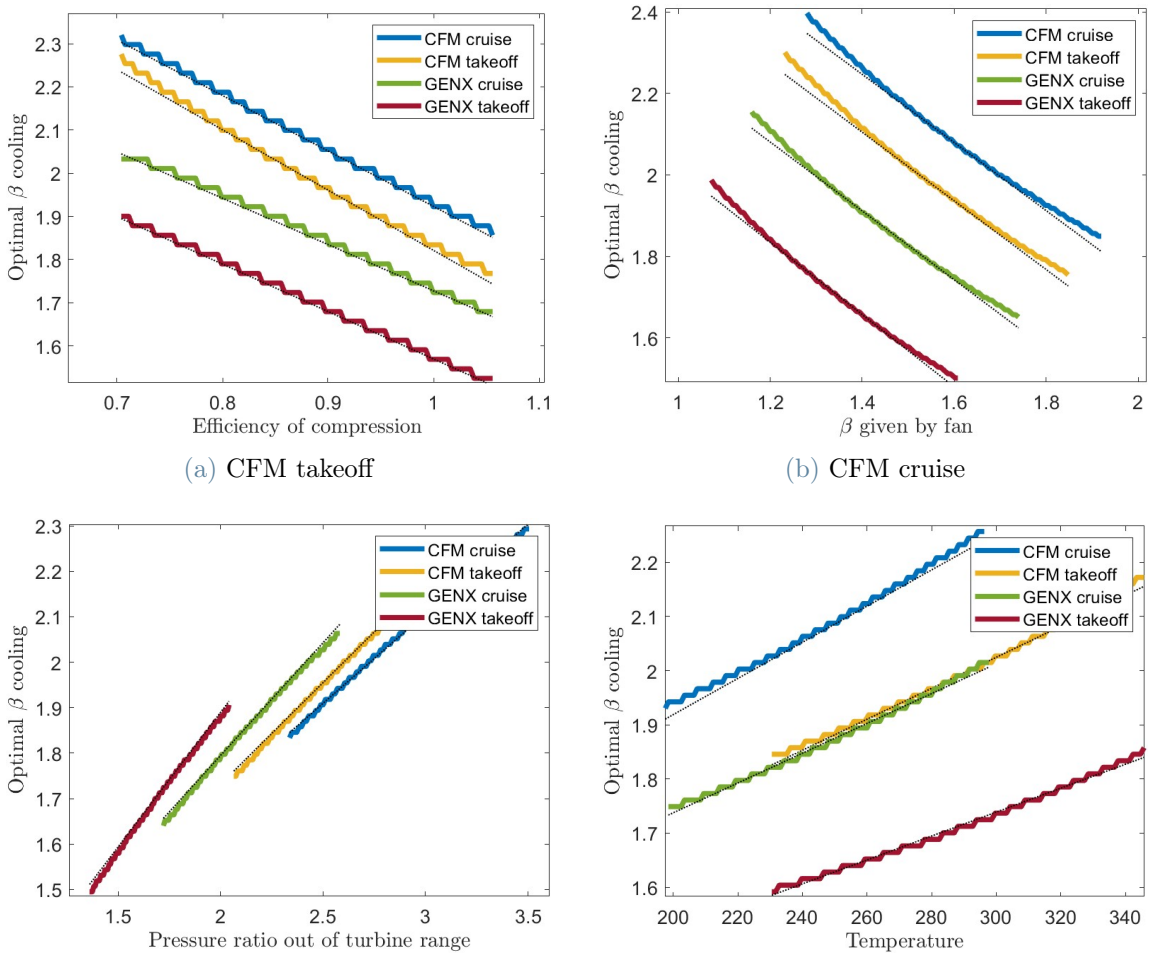

(a) CFM takeoff

(b) CFM cruise

(c) GENX cruise

(d) GENX takeoff

Figure 1.16: Discrepancy between numerical code and correlations

The single effect parameter is not investigated deeper since the aim of the work is to focus on the effect of the refrigeration of a compressor stage in an aeroengine. These results could be a starting point for another project.

2 | CFD study of inter-refrigerated compression

In this chapter it is explained the numerical investigation of a booster stage with a cooled stator blade. The selection of a booster blade instead of an high-pressure compressor comes from the results of chapter 1. The numerical simulations are done with the *CFD* solver *Numeca fine turbo 16.1* on the public Linux machine of Von Karman institute: a 32 threads workstation. In this chapter the mesh description, the setup of the simulation and the result obtained are reported. Then the results are processed to extract the amount of cooling that can be extracted by imposing a fixed temperature on the stator blade. In addition to the base line configuration, two other layouts are analysed, increasing the solidity through the number of blade (from 100 to 144) and imposing a fixing temperature to the stator casing too. The numerical results are intended to explain the flow field in the stage to understand cooling benefit and effect in the flow channel.

2.1. Layout of CFD calculation

This section explains the setup chosen for the numerical analysis. The booster stage investigated, called *"DREAM"* due to an European project on new engine architecture[7], is mounted in the high speed compressor facility R-4: Figure 2.1.

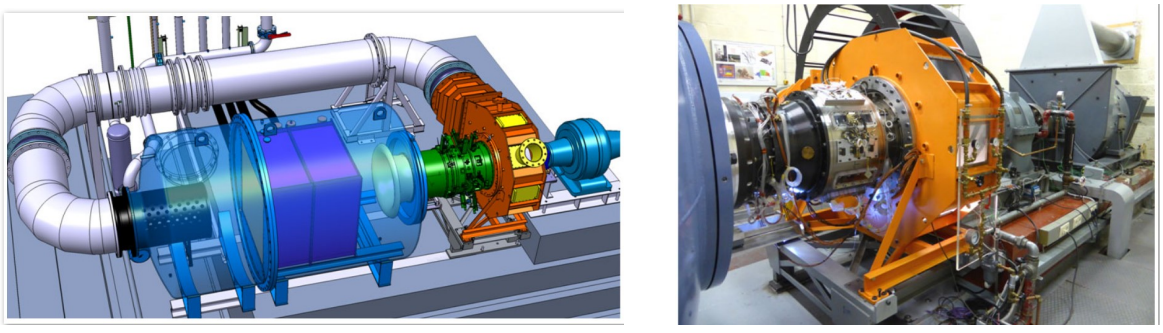

(a) Facility model (b) Real facility

Figure 2.1: Facility for experiments on DREAM compressor

The facility is an high speed compressor test bench with a closed loop system that can be pressurized form vacuum to 3 bars. The *DC MOTOR* driving the compressor has a power of 500 KW and, thanks to the gear box, it can reach the maximum shaft speed of 25000 revolution per minutes [13]. The *DREAM* compressor runs at a speed velocity of 8748.71 revolution per minutes. The characteristic of this compressor stage is its capability in reducing distortions in the flow field. The DREAM compressor is part of an European project, led by Rolls Royce,which has the aim to identify the technologies with which is possible to achieve a reduction of the CO_2 and the noise of the engines while maintaining a good efficiency. The parameters characterizing the real engine have to be respected in the facility, therefore the stage considered had to be adapted for the test rig, since:

- its diameter is smaller than the one of the engine
- the power available with the motor of the facility is lower than the one of the engine

therefore the diameter, the mass flow, the inlet conditions and all the parameters have been changed respecting the similitude. The characteristic parameter of DREAM compressor are: load (ψ) between 0.5 and 0.75 at hub, flow coefficient (ϕ) of 0.85-0.95 at hub and a pressure ratio (β) of 1.25 [11].

The turbomachinery department of Von Karman institute has already produced some publications, as reported in the paper [34]. In this paper an overview of the impact of the turbulence model on the evolution of critical flow structure in a highly-loaded is presented and the results are compared to the experimental one. The results of this thesis project are purely numerical since a cooled stator blade does not exist yet.

2.1.1. Generation of the mesh

The mesh layout is generated from the one used in the ASME publication [34]: it is a 56 millions cells mesh solved with 3 level of multi grid. The mesh used for this work is a coarse one due to the limited resources available. Furthermore this project is a principle work and, without experiments or DNS simulation to validate the results, this coarse mesh is considered sufficient to have a roughly estimation of the process. The mesh sensitivity analysis was performed for the original mesh and it is assumed still valid for the one used. This assumption is wrong but the results reported are always considered respect the adiabatic case and the error due to space discretisation should be the same between the simulation.

The mesh is generated with the Numeca grid generator *IGG 16.1* (Interactive Grid Generator) in the module *AutoGrid*. The grid is generated in cylindrical coordinate with a unit

of measurement of "*mm*". The *DREAM* compressor has one stage of IGV (inlet guide vane), the rotor stage and a stator one. The final stator stage will be investigated as the possible cooled one. AutoGrid software allows to create a structured mesh imposing some parameter as number of stream line at boundary layer and at main stream, the number of cell in every region. To reduce the computational effort is analysed just one channel imposing periodic condition on the main flow. Final mesh has the following parameters: Table 2.1

	IGV	ROTOR	STATOR
Number of flow path	81	97	81
Cell width at Hub	0.0005	0.0005	0.0005
Cell width at Shroud	0.0005	0.0005	0.0005
Percentage of MId-flow cells	20	20	20
Blade to blade topology	default	default	default
Number of point in boundary layer	37	37	37
Number of point in Clearance O-mesh	37	37	37
Expansion ratio	1.1	1.1	1.1

Table 2.1: Mesh input parameter

The "default" topology in *Autogrid5* is *O4H*, a 5 block topology composed by [25]:

- O block around the blade
- H block upstream the leading edge
- H block downstream the trailing edge
- H block in the pressure side
- H block in the suction side

The algorithm implement in *AutoGrid* allow an automatic creation of the structured mesh. The main mesh parameter are summarise in Table 2.2.

	IGV	ROTOR	STATOR	FULL MESH
Number of points	658935	883945	704295	2247175
Negative cells	0	0	0	0
Number of levels	3	3	3	3
Min. Skewness	23.819	22.217	22.139	22.139
Max Aspect Ratio	2924.8	2984.6	5114.7	5114.7
Max Expansion ratio	2.544	3.1212	2.555	3.1212
CPU time	31 sec	28 sec	27 sec	1min 38 sec

Table 2.2: Results of the mesh generated with AutoGrid5

The final graphical result is reported in Figure 2.3 and Figure 2.2. The blade to blade plane image shows the three structured mesh applied to the different stage: the number of blade rotor(76) is less than the IGV and stator one(100). The different number of blade is a common design choice in turbomachinery to avoid periodic stress and decrease fatigue effect. The lager pitch in the rotor stage does not affect the continuity of the flow: it is guaranteed by the mixing plane approach which is applied between stage.

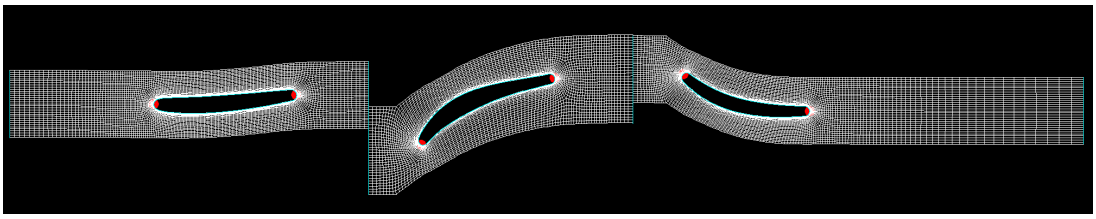

Figure 2.2: Blade to blade mesh

The meridional view of Figure 2.3 shows the different streamlines in which the span is divided. As reported in Table 2.1 the number of lines is different between rotating and fixing part with the same percentage of mid-flow cells: this increase the accuracy in the transition between boundary layer and free stream, especially in the rotor blade.

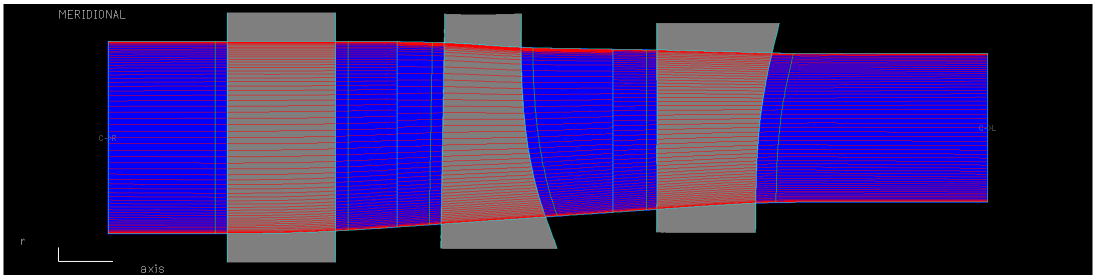

Figure 2.3: Mesh streamlines

In the stream lines picture are visible some green and light blue vertical lines: the blue one represent the change between the stages and the green one the intersection between the O-type mesh around the blade and the hexahedral one of the flow far from the blade.

The hybrid type structured mesh is visible in the mesh details in Figure 2.4a and 2.4b: the figures show the O-type mesh around the blade and the hexahedral one in the other domain region. The Figure 2.4b shows the finest discretisation of stator trailing edge. The properly simulation of the boundary layer around the stator blade is fundamental in this work to simulate properly the heat exchange process through the solid surface.

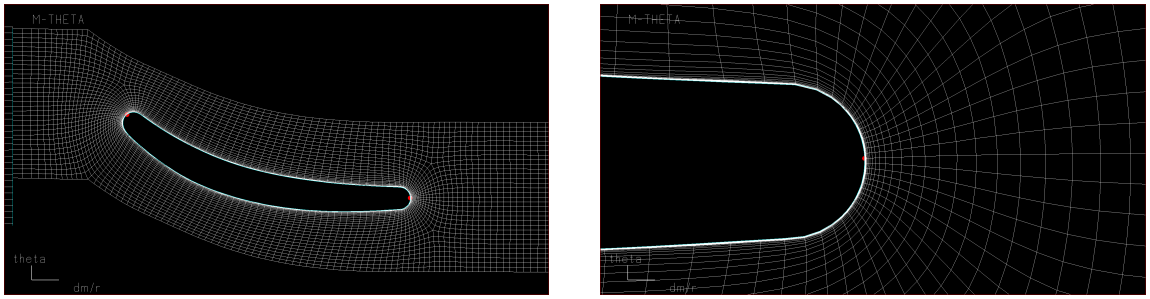

(a) Stator blade mesh (b) Trailing edge detail

Figure 2.4: Mesh details

2.1.2. Simulation Setting

The flow solver used is *Portland OMPI* (PGI), implemented in the *NUMECA* interface *fine*. *RANS* simulations are calculated to investigate the flow in the blade channel.The steady calculations are considered for multiple reasons:

- They require low computational time
- This work is just a principle analysis and a *RANS* simulation is considered sufficient to investigate the behaviour of the flow with a fixed blade temperature.

The real flow in a turbomachinery rotating at very high speed will never be completely steady and due to pressure waves, blade wake and other effects, it will never reach steadiness. The flow is simulated as perfect air, a built in configuration of *NUMECA*.The characteristic of this gas are:

- Constant Cp ($1006.0\frac{J}{Kg \cdot K}$) and γ (1.4)
- Prandtl heat conduction law with a Prandtl number of 0.708
- The Southerland Viscosity law

Turbulent Navier-Stokes equations are solved using the Shear Stress Transport (SST) turbulence model. The effects on the turbulence model are studied on the compressor map in the paper [34]; at design condition all the models predict the efficiency of the machine. To validate a turbulence model the numerical results should be compared with experiment [18] or DNS, on this technology there are none of them to use in the validation process. This lack of results is acceptable thrusting in the results already obtained on the same machine [34]. A comparison between turbulence model is done comparing the baseline SST result with the Spalart-Allmaras.

The Reynold number is estimated through the characteristic length (the blade chord), the characteristic density of air at inlet condition and the characteristic velocity of the problem assumed as the inlet velocity in the facility. The flow is completely turbulent and the Reynold number estimated is 414598.

Boundary conditions are required to perform the calculation: the compressor stage is subsonic, the 5 conditions required are assigned 4 at inlet and 1 at outlet section. The boundary conditions applied are a total pressure profile, a total temperature profile and a velocity direction normal to the surface that constrains two angles of the vector quantity. The total temperature profile and the total pressure one are estimated from experimental measurement (red dots) with a linear interpolation. The profiles are reported in Figure 2.5

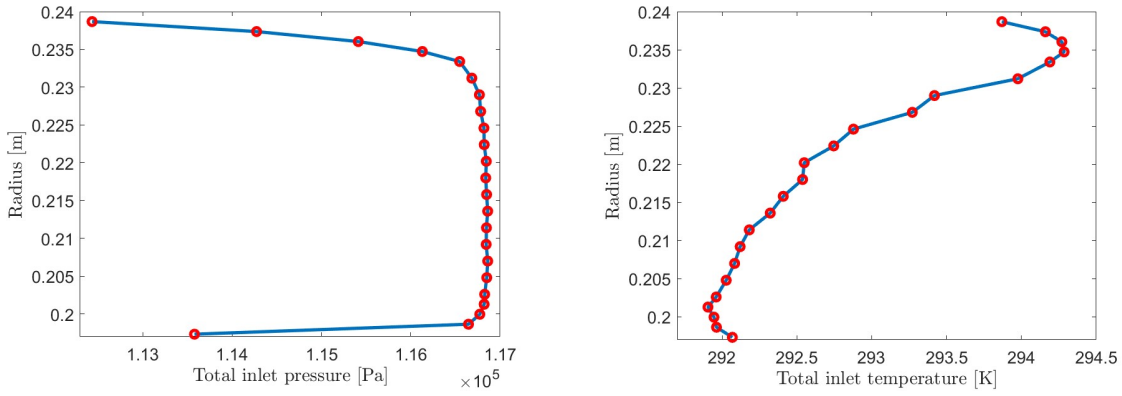

(a) Total Pressure profile

(b) Total T profile

Figure 2.5: Inlet boundary condition

The total pressure and temperature are measured in the Von Karman facility at ambient and ground condition. The result from chapter 1 shows a benefit in the thermodynamic cycle efficiency both at cruise and takeoff. There are no reason to simulate the booster compressor with specific inlet condition related to the aircraft operative point and this lead to the choice of the same boundary condition of the ASME publication [34]. At the

outlet section the mass flow rate is imposed to keep the machine at the design condition. The mass flow imposed is equal to $11.442\frac{Kg}{s}$ and a pressure adaptation condition is applied to stabilise the simulation. A rotational periodic condition is applied on the main stream blade channel surface. The boundary condition which will be most investigated is the blade stator temperature. A constant rotational speed of 0 rpm and a fixed temperature are imposed at the metal surface. The stator temperature is changed to simulate a cooling blade, three different temperature are studied and compared: $300K, 290K$ and $280K$. Other temperatures are simulated only to verify some trends. An adiabatic boundary condition with constant rotational speed is applied on all the other solid surface except for the hub of the rotor. The rotor hub surface contains both static and rotating surfaces; an area defined rotational speed is applied to split the static respect the moving one and imposing a rotational velocity respectively of 8748 rpm and 0 rpm. The adiabatic condition can introduce some uncertainty in the heat exchange process calculation. The fluid temperature may change in the different simulation due to the boundary condition on the cooled blade and affect due to the adiabatic condition, the metal temperature. The rotor and IGV (inlet guide vane) metal temperature should remain constant to not create a numerical heat sink on that blade and affect the calculation of the effective heat transfer coefficient of the stator blade. A check on the metal temperature is made: the blade temperature remains constant in all the simulation and doesn't affect the heat extraction process. This results can be seen both in *CFView* software image in Figure 2.6:

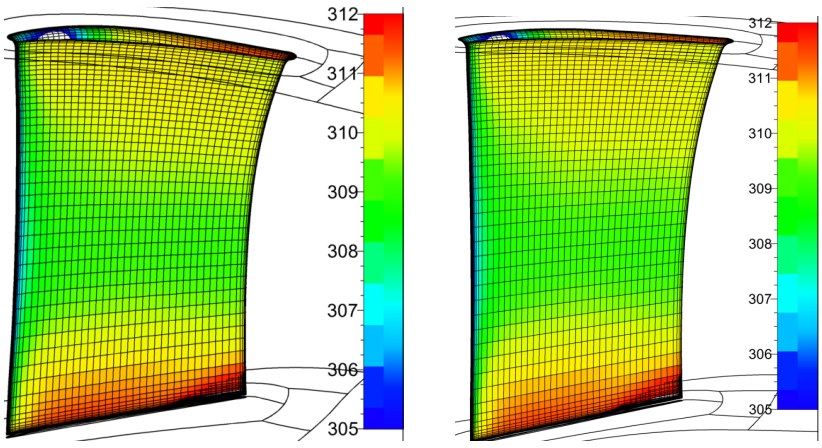

(a) Total relative adiabatic temperature

(b) $T_{stator} = 300K$

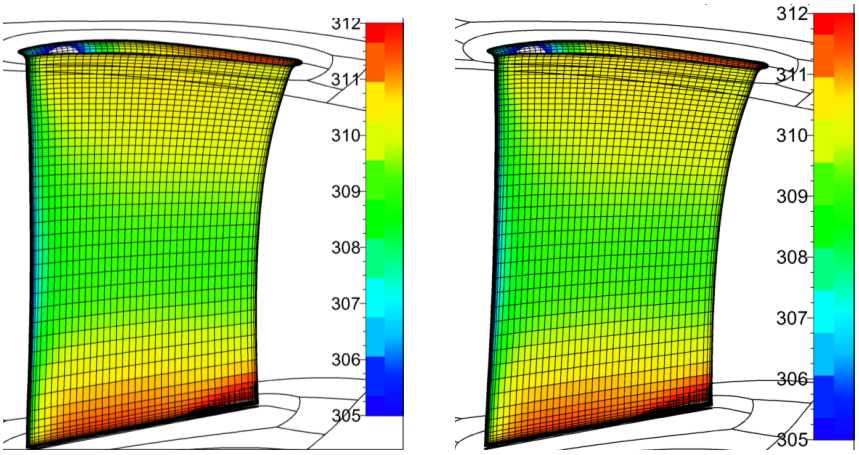

(c) $T_{stator} = 290K$ (d) $T_{stator} = 280K$

Figure 2.6: Total relative temperature on the rotor blade

Another check is made directly numerically, comparing the total relative temperature on the rotor in each grid point. The rotor total relative temperature can be seen in Figure 2.7.

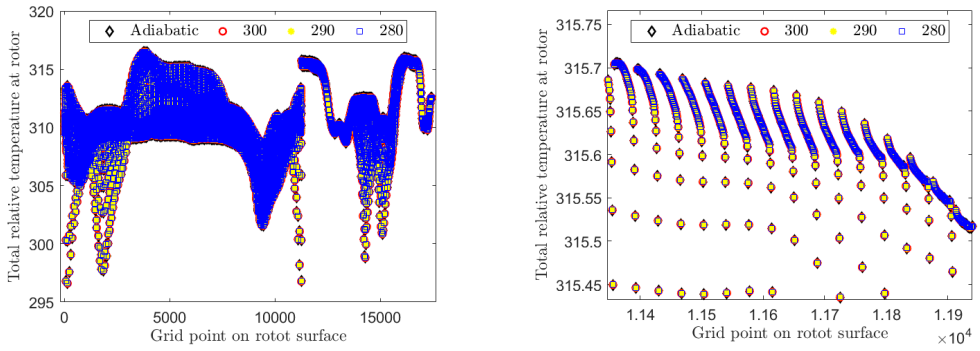

(a) Total relative temperature on the rotor (b) Check of coherence of point

Figure 2.7: Total relative temperature on the rotor blade

This result is obtained since the heat exchange process is performed in the downstream blade and it allows to run the upstream blade always adiabatic. In case of a cooling applied to an upstream blade, this condition is probably incorrect and a simulation with a fixing temperature applied to the downstream blade should be performed to guarantee a unique source of heat sink. The numerical model applied is a *multi-grid* with a 3 levels grid, the solution is first calculated on a 2 times coarsest level, then on an intermediate one and finally on the original mesh. The number of iterations is set to 2500 for each coarser level and to 10000 fir the final one with a convergence criteria set on the global residual equal to -10. The convergence map is reported in the next section subsection 2.1.3.

2.1.3. Results of simulation

The simulations reaches convergence before the number of iterations imposed but without the target global residual level. The global residual is reported in Figure 2.8.

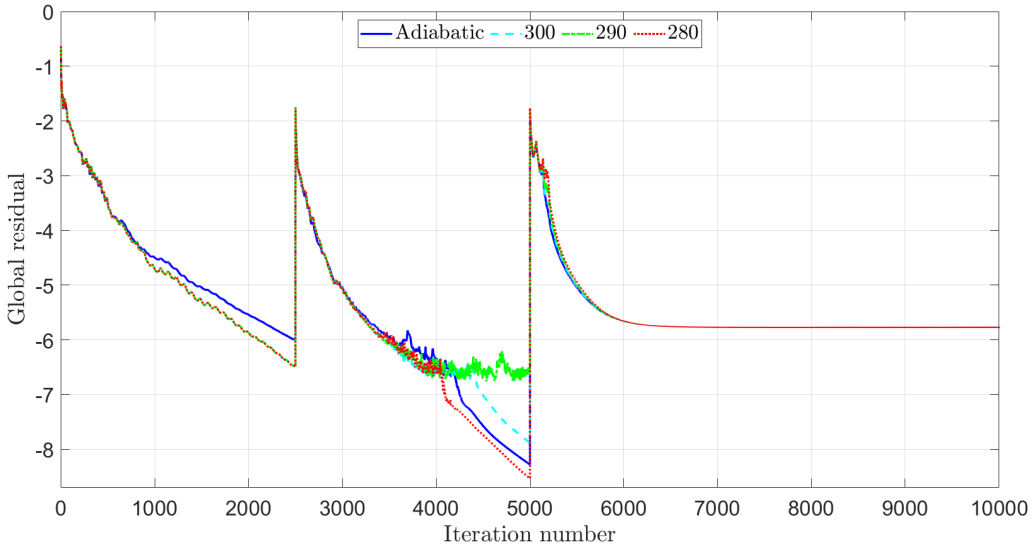

Figure 2.8: Residuals of different simulation

The global residual is calculated as the imbalance in the linearised system of the discrete equation (the sum of the imbalance of the discrete equation (residual R(U)) in each cell [26]:

$$RES = \sum R(U) \tag{2.1}$$

An oscillatory level of global residual between -5.75 and -5.78 is considered acceptable to thrust in the numerical simulation. The check on the convergence of mass flow is done to ensure the achievement of the target outlet boundary condition. The last variable considered to have confidence and thrust in the result is the y^+ value. Using the $k-\omega SST$ model this value should be less than 1 in the first cell close to the domain to guarantee a correct simulation of the boundary layer. The y^+ value on the stator blade is reported in Figure 2.9.

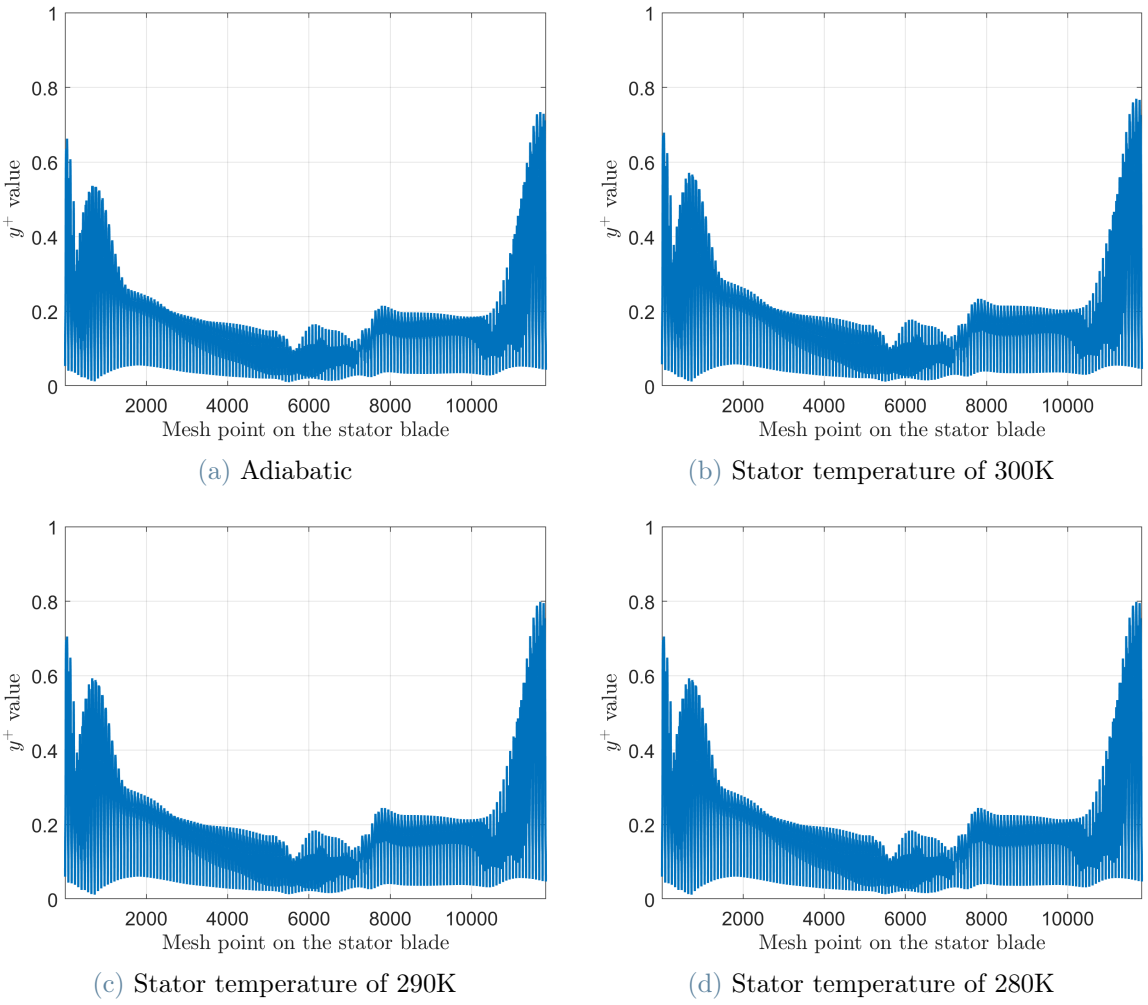

(a) Adiabatic

(b) Stator temperature of 300K

(c) Stator temperature of 290K

(d) Stator temperature of 280K

Figure 2.9: y^+ value on the stator blade

The y^+ value remain in all the first cell of the blade surface below 0.8 and so below the threshold level of 1. This check means that the boundary layer region is always solved and the wall function are never used in the simulation.The resolution of the boundary layer flow in case of a heat transfer increase the fidelity of the results: there are no study which compared and validate numerical results in case of a heat sink and wall function are set to simulate properly the turbulent kinematic quantities and not the thermodynamic one [18]. A fine resolution of the boundary layer increase the mesh refinement required and the computational effort, but is a crucial condition to simulate heat transfer process through a stator blade.

2.2. Post Processing

This section shows the results of the *CFD* calculation. These are obtained directly from *FINE* module of *NUMECA*, from the post processor (*CFView*) and through a post processing technique performed with Matlab. The results of the compressor efficiency and the effects of a fixed temperature blade on the fluid are explained completely in the next subsection 2.2.1 and subsection 2.2.2.

2.2.1. Efficiency of compressor

The efficiency of the *DREAM* compressor is computed automatically by *FINE* software. The results obtained are reported in the Table 2.3

	Adiabatic	$T_{stator} = 300K$	$T_{stator} = 290K$	$T_{stator} = 280K$
η_{stage}	0.8672	0.8739	0.8796	0.8856

Table 2.3: Efficiency of compressor

The stator blade temperature in the adiabatic simulation is not constant on the blade surface, it is calculated to have a reference value, as the average between the pressure side and the suction side temperature. The value obtained is $313.8707K$. The adiabatic efficiency is equal to 0.8672: this is the one used to estimate the real machine efficiency. It is lower than the efficiency applied in Joule Brayton numerical code (0.88). This value is due to the high pressure level required by DREAM compressor (compression ratio of 1.23); in Table 1.3 the effect of efficiency of stage is discussed and it will not affect the global result of chapter 1. The efficiency results show an increase of efficiency with a more severe cooling. The trend looks linear with a slope of $-5.64 \cdot 10^{-4}$: for each Kelvin grade cooled there is an increase of 0.056% of efficiency value. The linear trend catches also the efficiency value of other three simulations: one with an extreme cooled stator temperature of $270K$ and two with an heated stator with a blade temperature of $320K$ and $330K$. Figure 2.10 shows this trend:

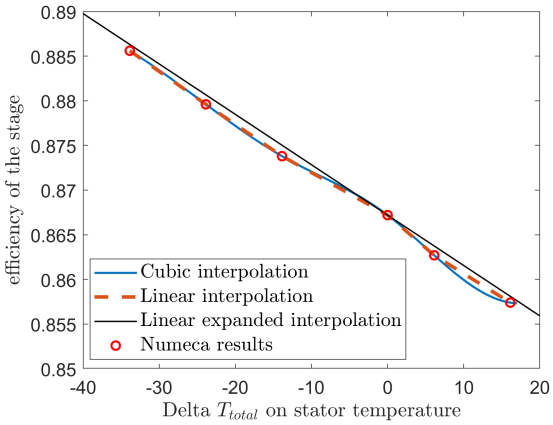

Figure 2.10: Numeca efficiency results

This results could lead to the conclusion that the cooling of the flow increase the aerodynamic stage efficiency. To check this results the span wise distribution of T_{total} Figure 2.11, P_{total} and P_{static} Figure 2.13 are plotted and compared in the difference application.

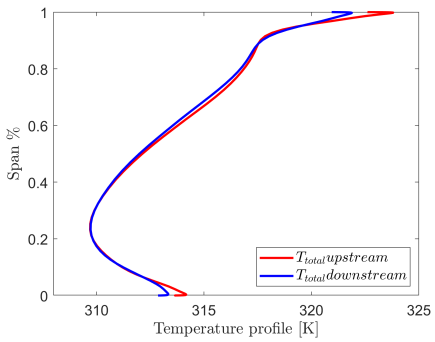

(a) T_{total} in adiabatic simulation

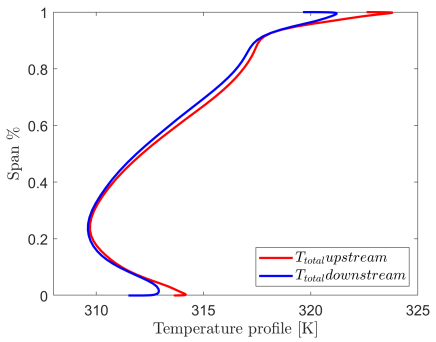

(b) T_{total} with stator temperature of 300K

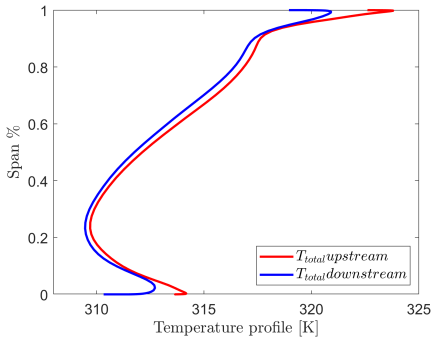

(c) T_{total} with stator temperature of 290K

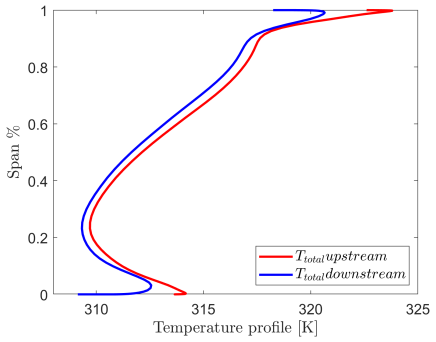

(d) T_{total} with stator temperature of 280K

Figure 2.11: T_{total} profiles, upstream and downstream stator blade, in the 4 cased analysed

The total temperature profiles show similar trends with a delta between the upstream and downstream conditions that increase with the severe of cooling. Through the stator blade the T_{total} remains constant [27], there is no work done by a fixed blade. The cooled surface introduces an heat sink and decreases the total temperature downstream the stator. Looking at the T_{total} losses Figure 2.12 the profiles are the same and shifted due to the heat sink. The quantity of heat shift is estimated in subsection 2.2.2. The total temperature losses in the four configurations show similar trends and increase with the severe of cooling. The graphically comparison can be seen in Figure 2.12.

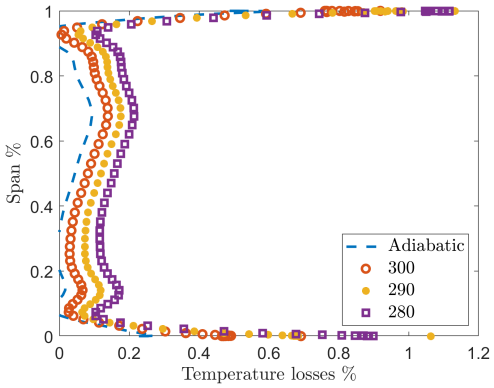

Figure 2.12: Total temperature losses in the 4 case studied

The Figure 2.12 shows an the higher capability of endwalls to extract heat: this result is related to the boundary layer behaviour. The boundary layer are more turbulent in the tip and hub region due to the higher flow angles (in the hub) and to tip flows (tip region). This effect increase the turbulence of the flow and the capability in exchanging heat.instead in the free stream the flow is more laminar and the heat extraction process is limited. The parameter which most shows the entropy generation and the losses in a turbomachinery row is the total pressure (P_{total}) [27]. The P_{total} profile and the P_{static} are reported in Figure 2.13.

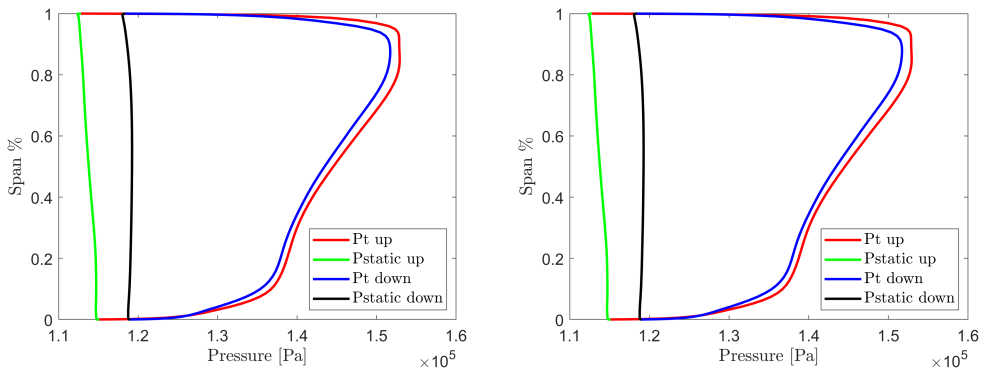

(a) Adiabatic (b) Pressure with T_{stator} of 300K

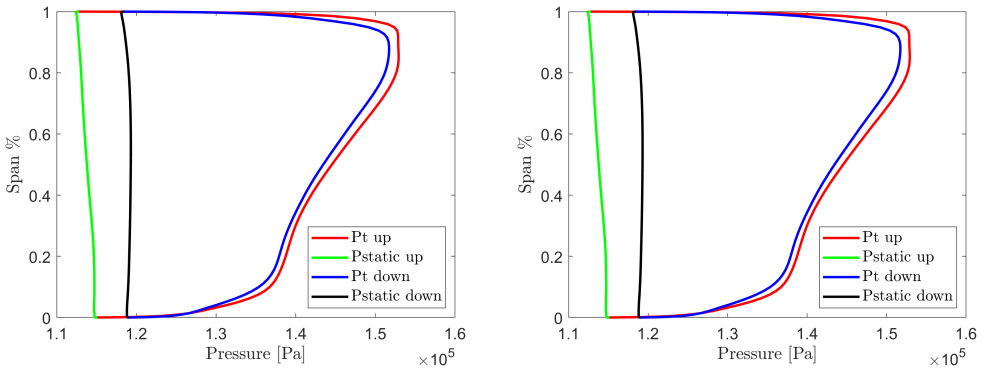

(c) [Pressure with T_{stator} of 200K (d) [Pressure with T_{stator} of 290K

Figure 2.13: P_{total} and P_{static} in the 4 cased analysed

The static pressure increases through the stator blade, this is correct because the blade is a compressor stator. The total pressure profile between the 4 configurations analysed are the same. This results can be better seen plotting the percentage pressure loss through the stator, Figure 2.14a, and a detailed view reported in Figure 2.14b.

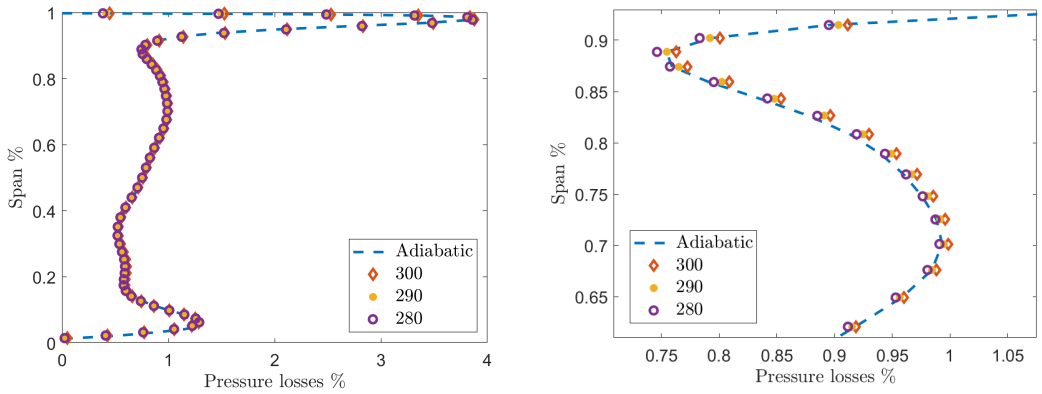

(a) All span (b) Details

Figure 2.14: P_{total} percentage loss

The values show no variation between the simulations. The same percentage of pressure drop is associated to the same entropy generation and the same efficiency. The results obtained with *NUMECA* are affected by the efficiency definition used. The user guide of *NUMECA* reports the efficiency definition implemented in the software NUMECA and applied to the perfect gas subject to compression.

$$\eta_{is} = \frac{\left(\frac{p_{t2}}{p_{t1}}\right)^{\frac{\gamma-1}{\gamma}} - 1}{\frac{T_{t2}}{T_{t1}} - 1} \tag{2.2}$$

In Equation 2.2 the denominator changes with the total temperature value after the stage. The value of T_{t2} is strongly affected by the boundary condition imposed: cooling the blade, the total temperature value decreases, the denominator decreases too and this is the reason why the final efficiency values increase with severity of cooling. This efficiency definition does not consider the heat losses and, as we can see from the total pressure loss graph Figure 2.14 the efficiency of the compressor remain the same. The thermodynamic quantity mostly related to efficiency is entropy: the entropy generated profiles through the stator are visible in Figure 2.15:

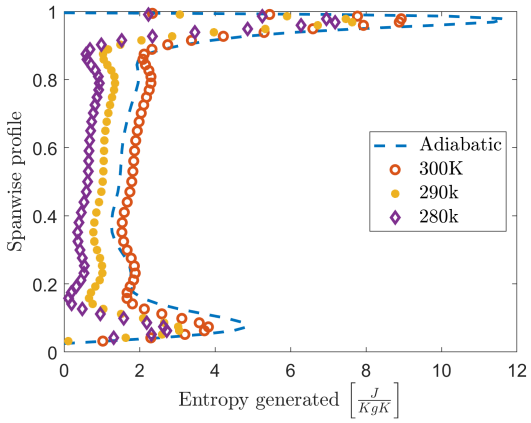

Figure 2.15: Spanwise entropy generation

The entropy profiles show higher losses at endwall and a constant value in the main stream. The P_{total} losses are the same (Figure 2.14b) so the entropy variation in the different cases is only due to the decrease of temperature across the stage. The entropy generated with a stator temperature of 300K is higher in the main flow respect the adiabatic one. The adiabatic entropy profile has a different shape, this is because the adiabatic condition depends on the flow temperature and it is different from an isothermal one; this results has been obtained also in other publication [5]. The sum of the entropy generated spanwise in adiabatic case is higher due to the high quantity in the endwall, the sum of entropy for the 4 cases is in Table 2.4:

Stator temperature	Adiabatic	300 K	290 K	280 K
Entropy generated $\left[\frac{J}{KgK}\right]$	168.51	151.88	97.84	74.54

Table 2.4: Entropy generated

The advantage of a lower level of entropy does not affect the efficiency of compressor stage upstream but will improve the performance of the downstream stage. This consideration is a further prove that the optimal cooling position is in the LPC.

2.2.2. Cooling effect

The efficiency result does not show an increase of performance and a decrease one neither. The real advantages of cooling the stator are mostly in the Joule-Brayton cycle. The stator blades are designed following the aerodynamics performance to obtain the required velocity triangle or to minimize the secondary losses due to secondary flow. The blade surface is also a source of losses due to friction that create a boundary layer. In a heat exchanger, instead, the surface is a key parameter to increase the efficiency of the process increasing the amount of heat exchanged. The consideration report will predict a non optimal behaviour of the stator blade as heat exchanger. To estimate the heat transfer coefficient of the *DREAM* compressor stator blade, the variation of *total enthalpy* from the adiabatic case is considered. In the *CFView* software the surface integral quantities can be extracted in each surface. The analysed surface is the outlet one, which stays 2 chords apart from the stator trailing edge. This surface is sufficiently far from the stator blade one and the heat flow can be considered fully mixed with the main stream one. The surface is represented in Figure 2.16

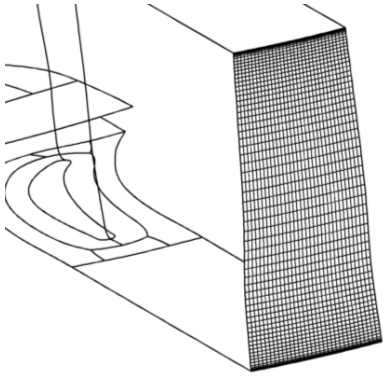

Figure 2.16: Image of outlet section

The results can be seen graphically in the picture

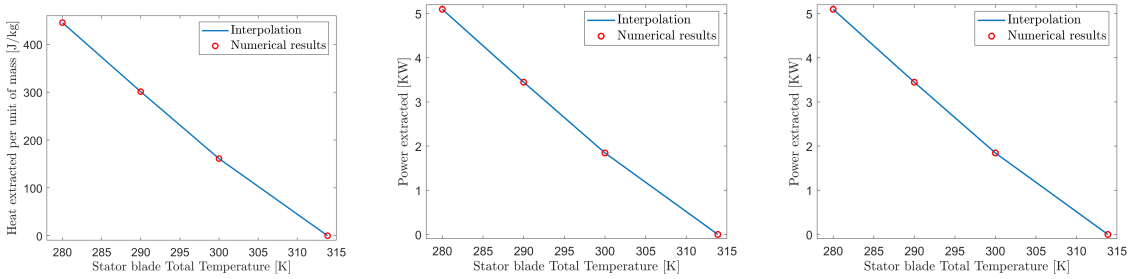

(a) Heat extracted per unit of mass

(b) Power extracted

(c) Power per unit of area

Figure 2.17: Cooling results

They can be also collected in the following Table 2.5:

	T_{stator} : 300K	T_{stator} : 290K	T_{stator} : 280K
Heat extracted per unit of mass $[\frac{J}{kg}]$	161.1891	301.1690	445.3908
Power extracted [KW]	1.844	3.4454	5.093
Power per unit of area $[\frac{MW}{m^2}]$	0.9911	1.8517	2.7384

Table 2.5: Cooling extraction with a fixed blade temperature

From this results it is possible to estimate the heat transfer coefficient of the stator blade. The mathematical steps and the value of area extracted are in Table 2.6:

	Adiabatic	T_{sator}:300K	T_{stator}:290K	T_{stator}:280K
Area outlet $[m^2]$		0.000471496		
Blade surface $[m^2]$		0.00186065		
$h_t[\frac{Jm^2}{Kg}]$ outlet section	148.618	148.542	148,476	148.408
Mass flow $[\frac{Kg}{s}]$		11.44		
h $[\frac{KW}{m^2K}]$		71.14	77.57	80.85

Table 2.6: Calculation of heat transfer parameter

The heat transfer coefficient is in the order of tens of kilowatt per unit of area and per unit of temperature gradient. To extract the optimal amount of heat found in the numerical modelling, some estimation of the temperature gradient with the dream stator blade area is done Table 2.7.

	CFM cruise	CFM takeoff	GENX cruise	GENX takeoff
ΔT required	90.69	233.7893	152.5	357.93

Table 2.7: ΔT required to extract optimal amount of cooling

Another roughly estimation is done to obtain the area required with a ΔT of *30* Table 2.8.

	CFM cruise	CFM takeoff	GENX cruise	GENX takeoff
Area m^2	0.5625	1.45	0.9458	2.22

Table 2.8: $Area[m^2]$ required to extract optimal amount of cooling

The temperature gradients are not feasible without a very complex cryogenic system; this system will be too much heavy and complex to be coupled in an aircraft engine. The area required, using just a stator blade with a cooled surface, is lots of times the dream compressor one ($18.61[cm^2]$) and reaching the area value of Table 2.8 is unfeasible to. The optimal amount of heat estimated in chapter 1 cannot be extracted with this technology.

2.2.3. Cooling penetration in the blade channel

To analyse how many flow streams are affected by cooling, a pitchwise representation of the total enthalpy variation is performed close to the stator trailing edge. The total enthalpy value in the blade channel is extracted in two sections which stay just *0.25* chord downstream the trailing edge. The difference is the theta angle coordinate: the larger one contains all the blade channel pitch while the second one contains a limited pitch range from 0.25 to 0.75. The results of the total enthalpy map for the full blade channel surface are in Figure 2.18.

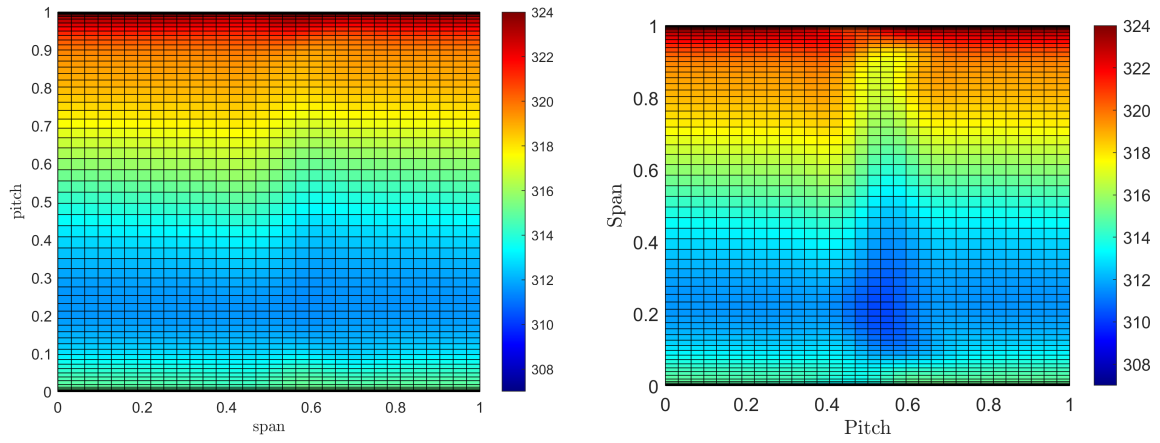

(a) Adiabatic (b) T_{stator} : $300K$

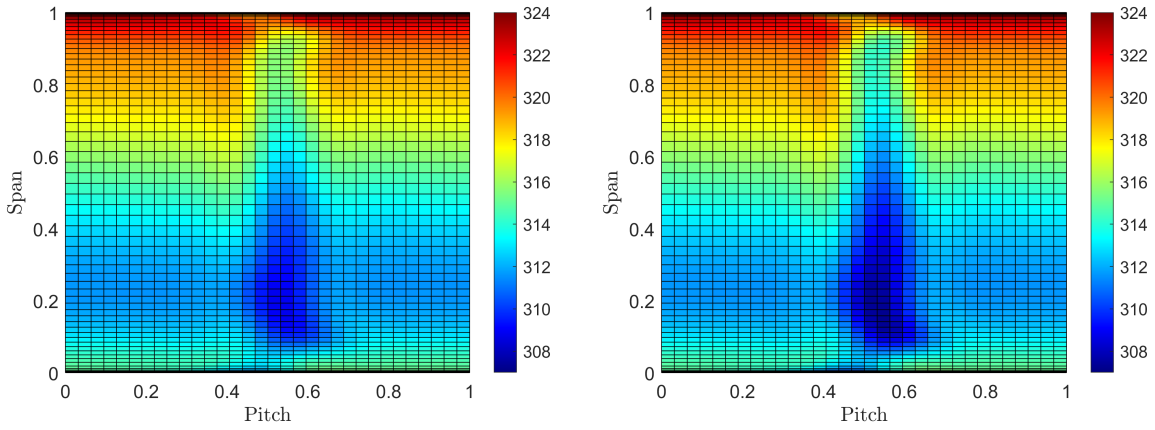

(c) T_{stator} : $290K$ (d) T_{stator} : $280K$

Figure 2.18: Enthalpy map in the blade channel $\frac{KJ}{Kg}$

The cooling penetration could be better appreciated in the smaller details Figure 2.19.

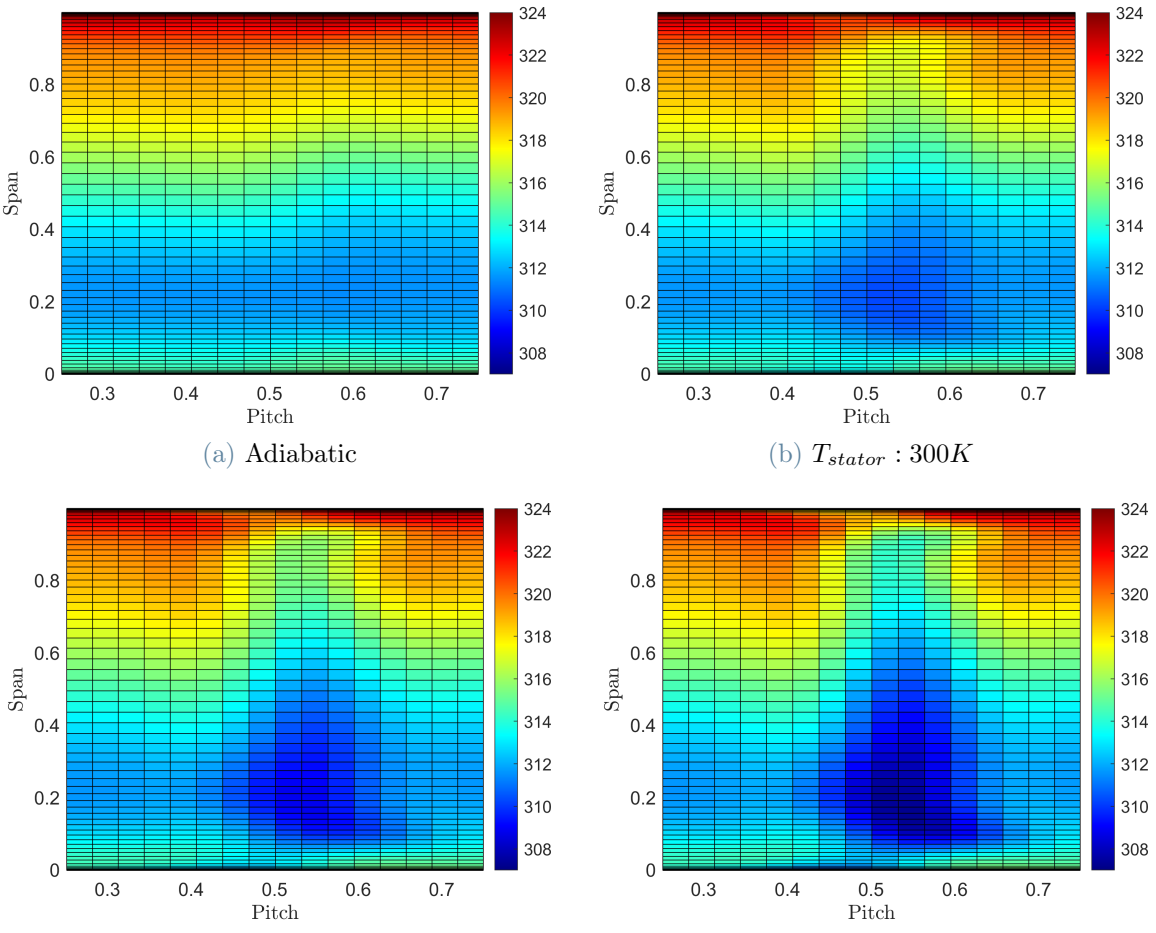

(a) Adiabatic (b) T_{stator} : $300K$

(c) T_{stator} : $290K$ (d) T_{stator} : $280K$

Figure 2.19: Detailed enthalpy map in the blade channel $\frac{KJ}{Kg}$

The cooling penetration is visible in the decrease of total enthalpy on the surface. To quantify it, the variation of enthalpy is summed spanwise, to estimate how cooling propagates in the blade channel and pitchwise to quantify the difference between endwall and main flow: Figure 2.20 and Figure 2.21.

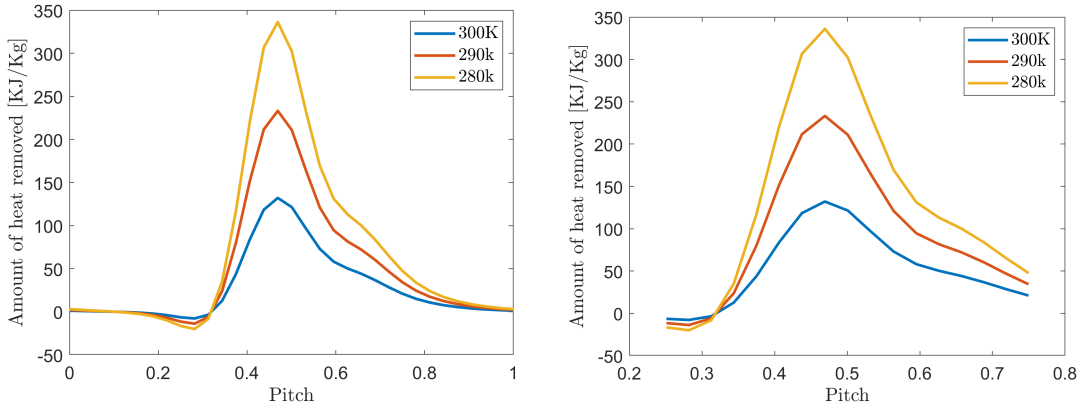

(a) Pitchwise all channel (b) Pitchwise details

Figure 2.20: Cooling effect in the blade channel: pitchwise profile

The sum of the total enthalpy variation spanwise shows a similar trend in the three different cases, The heat propagation is higher in the pressure side and affects the flow until the 0.8 of pitch coordinate.The stator temperature affects the amount of cooling and the profile becomes sharper in case of more severe cooling.

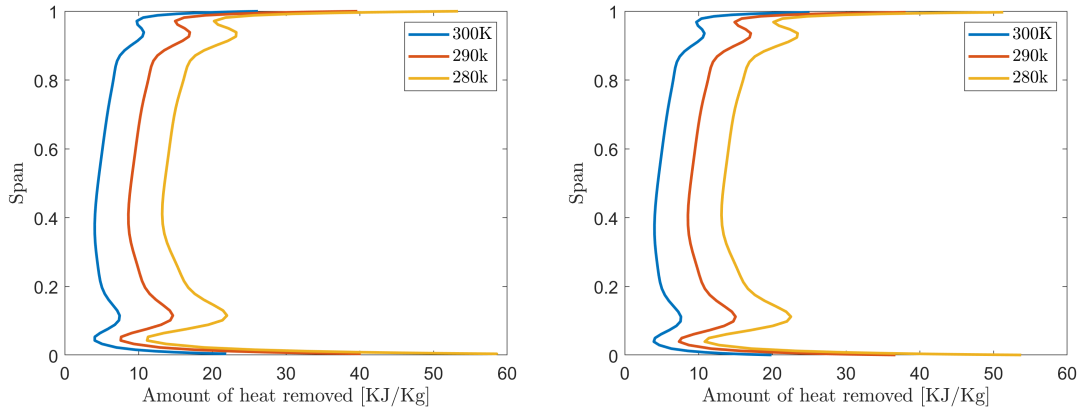

(a) Spanwise all channel (b) Spanwise details

Figure 2.21: Cooling effect in the blade channel: spanwise profile

The sum of heat pitchwise shows the same trend in both the surfaces. That means that the variation of heat is related only to the pitch range between 0.38 and 1. This graph shows that the heat exchange is higher at the end wall than the main flow.

These results lead to two difference layout variations to increase the heat exchange process:

- The increase of solidity. This solution can decrease the pitch between the two blades and allows a deeper penetration of the heat extraction in the blade channel.
- The introduction of cooling through the stator casing too. This layout can increase the heat exchange in the end wall where the process seems more effective.

This two results are analysed singularly in the next section section 2.3.

2.2.4. Comparison with Spalart Allmaras turbulence model

The effect of the turbulence model on the heat extraction process is investigated comparing the $k-\omega SST$ results to the Spalart Allmaras. The simulations with the SA models run with the $k-\omega SST$ results as initial solution. The results are compared in terms of amount of heat extracted and the effect on a cooled stator blade in the flow. The results will be different from the previous one since the heat transfer process is performed through a solid blade and the turbulence model affects the calculation of the flow quantities in the boundary layer region. The heat transfer coefficient h, calculated with the new turbulence model, is in Table 2.9:

	Adiabatic	T_{sator}:300K	T_{stator}:290K	T_{stator}:280K
Area outlet $[m^2]$		0.000471496		
Blade surface $[m^2]$		0.00186065		
h_t outlet section $[\frac{Jm^2}{Kg}]$	148.653	148.567	148,495	148.422
Mass flow $[\frac{Kg}{s}]$		11.44		
h $[\frac{KW}{m^2K}]$		80.95	85.83	88.90

Table 2.9: Calculation of the heat transfer parameter with SA turbulence model

The heat transfer parameter, calculated with Spalart-Allmaras turbulence model, is higher than the $k-\omega SST$ one; however, they have the same order of magnitude and the same trend, that increases with the decrease of stator temperature. The differences in the results are purely due to the numerical discretisation.

	$T_{stator}: 300K$	$T_{stator}: 290K$	$T_{stator}: 280K$
Heat extracted per unit of mass $[\frac{J}{kg}]$	182.40	332.98	489.93
Power extracted [KW]	2.09	3.81	5.60
Power per unit of area $[\frac{MW}{m^2}]$	1.1215	2.0473	3.0123

Table 2.10: Cooling extraction with a fixed blade temperature: SA turbulence model

This value comes from the integral of the total enthalpy in the outlet section (Figure 2.16). A graphical comparison between SA and $k-\omega SST$ is reported in Figure 2.22:

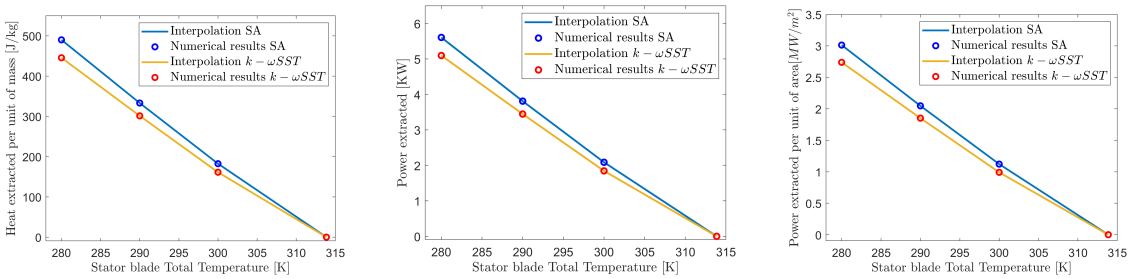

(a) Heat extracted per unit of mass (b) Power extracted (c) Power per unit of area

Figure 2.22: Comparison between turbulence models

The blue line, the SA one, has an higher value of heat extracted, coherently with the results of heat transfer coefficient. The effects on the blade channel are visible in the spanwise and pitchwise heat extraction profile of Figure 2.23:

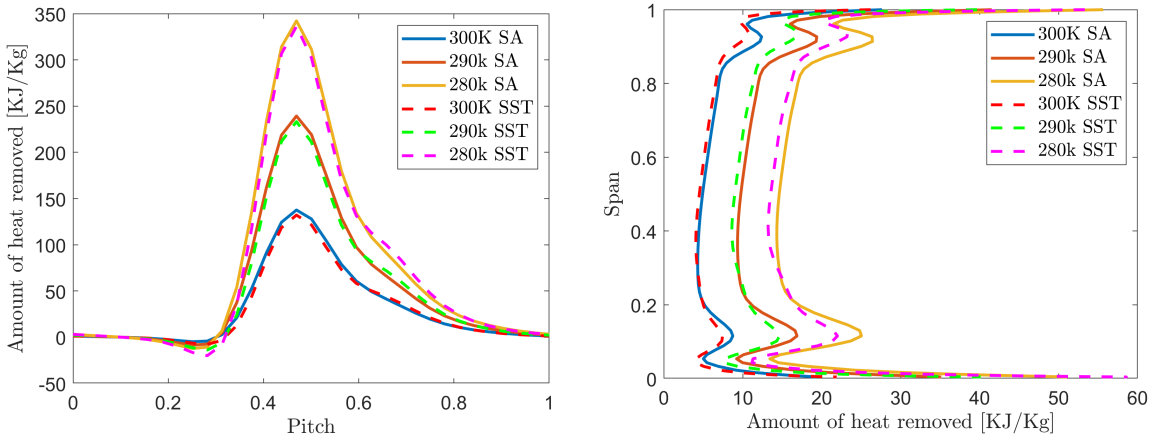

(a) Pitchwise profile SA and $k-\omega SST$ (b) Spanwise profile SA and $k-\omega SST$

Figure 2.23: Cooling extraction profiles comparison

Pitchwise the two profile are almost identical and the lines overlap themself. In the spanwise profile,instead, the effect of the turbulence model is more visible: the endwall losses and the tip flow are more severe in the SA and they enhance the heat transfer process too.

The Spalart Allmaras results confirm the order of magnitude of the heat transfer coefficient and the heat transfer profile obtained with the $k-\omega SST$. The match of the results is a further confirmation that at design condition many turbulence models show similar results as obtained in the publication done by VKI turbine and propulsion department [34]: in that case numerical results match the experimental ones and can be considered for sure reliable. In this work the same conclusion cannot be done because it is a preliminary turbulence model sensitivity analysis. The following results are all extracted with the $k-\omega SST$ turbulence model and no variations are expected using the Spalart-Allmaras.

2.3. Layout variation to increase the cooling process

This section shows two possible strategies to increase the amount of cooling extracted from the dream compressor. The increase of solidity increases the stage weight too, but it can lead to an higher load and decrease the stage number in the cascade. This trade off requires a re-design of the machine and could be evaluated in a future work. The cooling of the casing instead can be straightforward in the real application since the cooling system pipes has to enter from the casing. The design of the possible real layout is not part of this thesis and will be a future work.

2.3.1. Cooling of the casing

The CFD solid boundary conditions are changed to simulate the casing cooling. The solid wall temperature of the stator hub is fixed to a unique value equal to the stator blade one. This layout is unfeasible since the cooler temperature cannot remain constant moving from the casing to the blade. The new metal boundary conditions are visible in Figure 2.24.

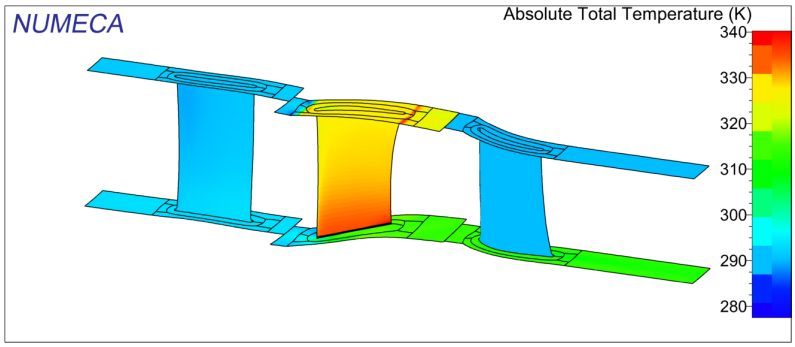

Figure 2.24: Constant total temperature applied to both blade and casing surfaces

The casing surface calculated by *CFView* is $10.41cm^2$ and it is lower than the blade one that is $18.6cm^2$. The calculation of the heat extracted is performed as in the base case and it is already explained in subsection 2.2.2.

The results can be seen graphically in the picture Figure 2.25:

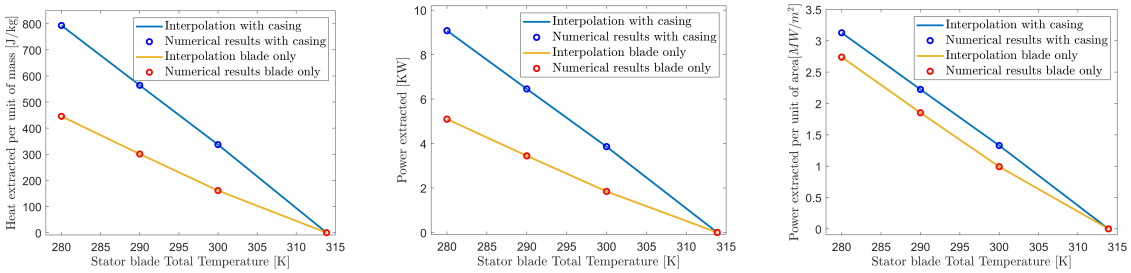

(a) Heat extracted per unit of mass

(b) Power extracted

(c) Power per unit of area

Figure 2.25: Comparison between blade only and blade+casing cooling

Or in the Table 2.11

	$T_{stator}: 300K$	$T_{stator}: 290K$	$T_{stator}: 280K$
Heat extracted per unit of mass $[\frac{J}{kg}]$	161.19	301.17	445.39
Power extracted [KW]	1.844	3.4454	5.093
Power per unit of area $[\frac{MW}{m^2}]$	0.9911	1.8517	2.7384
Heat extracted per unit of mass with casing$[\frac{J}{kg}]$	337.22	564.16	793.22
Power extracted with casing [KW]	3.8578	6.4540	9.0744
Power per unit of area with casing $[\frac{MW}{m^2}]$	1.3292	2.2237	3.1266

Table 2.11: Results comparison: blade only and blade+casing cooling

The results show an increase of machine capability in extracting heat: the most interesting value is the power extracted per unit of area. The heat removed is normalized respect of the solid area to which a constant temperature boundary condition is applied. The increases of the megawatt extracted per unit of area mean an higher capability of casing in heat exchange process respect of the stator blade. A possible reason of this trend could be explained with the high velocity and so higher Re number, turbulence and mixing capacity of cooled and warmed flow. This effect can be seen also in the pitchwise and in the spanwise profile. The pitchwise heat extraction profile shows the presence of a heat sink in all the blade channel.The spanwise integral value of heat extracted is shifted upstream of 200 $\left[\frac{KJ}{Kg}\right]$ compared to the blade only cooled case of Figure 2.20. The pitchwise profile of total enthalpy variation in the casing and blade surface cooling design is reported in Figure 2.26.

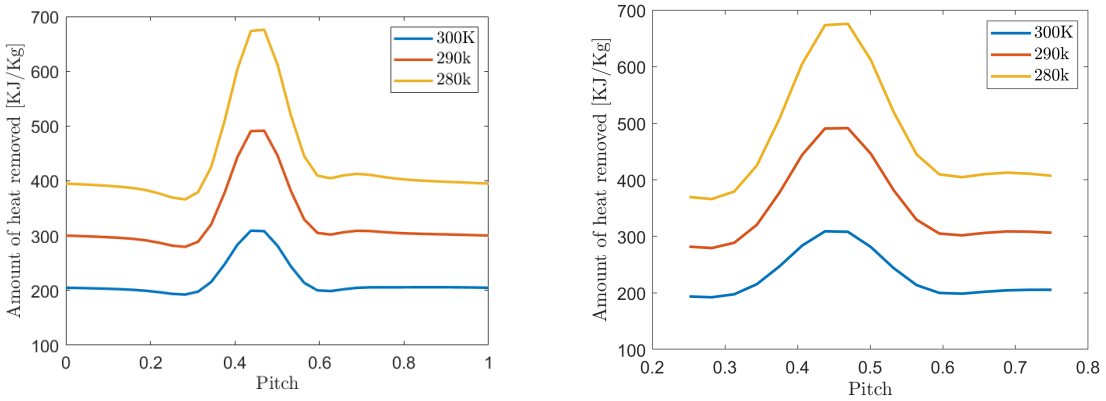

(a) Pitchwise all span

(b) Pitchwise details

Figure 2.26: Casing and blade stator cooling: pitchwise heat extracted profile

The spanwise plot of heat penetration shows that the additional heat removed is concentrated in the tip region Figure 2.27.

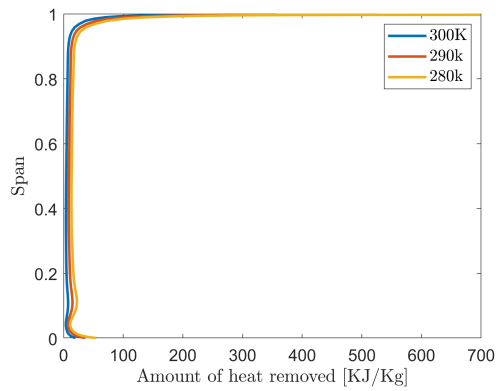

(a) Pitchwise all channel

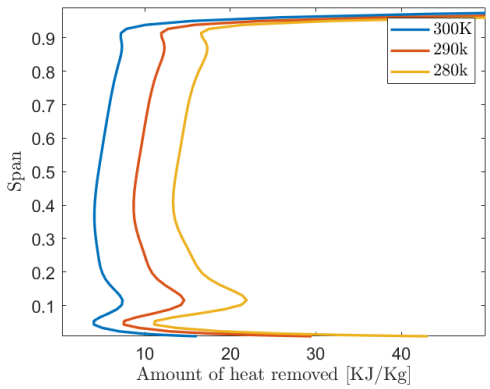

(b) Pitchwise details

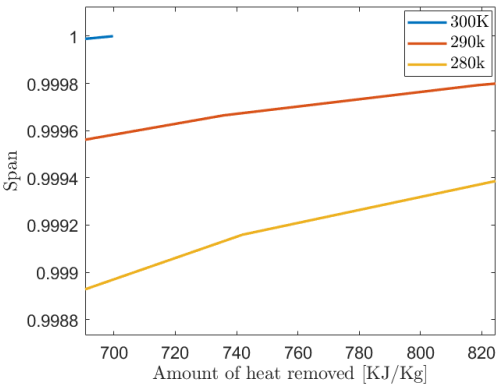

(c) Pitchwise details

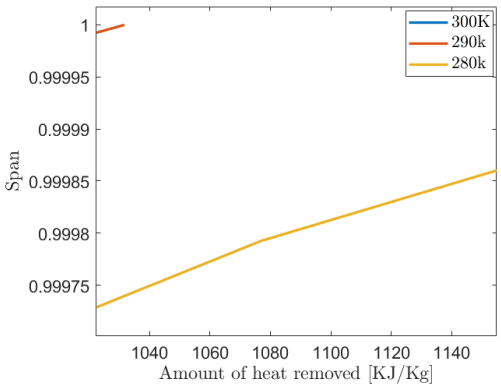

(d) Pitchwise details

Figure 2.27: Casing and blade stator cooling: spanwise heat extracted profile

The spanwise profile shows an high increase of heat removed in the casing region: in the case with T_{stator} equal to $280K$ the amount of heat removed is $1364\frac{kJ}{KG}$. The limit of the casing cooling is the low amount of flow rate affected by the cooling. From figures 2.27c and 2.27d the span-wise flow affected by cooling is limited in less than 10% of all the radial coordinate. Figure 2.27b shows the same trend and the same values of cooling penetration as the base case: the casing cooling does not change the heat flow condition at a span wise coordinate below 0.9.

2.3.2. Cooling of casing only

A possible layout variation is cooling only the casing. This layout is less efficient than the cooling of the stator blade but it can be easily achieved from the mechanical point of view. The thickness of the casing allows the presence of internal pipes for cooling with an high pressure fluid as refrigerator. The results of cooling the casing only are compared to

the cooling of the blade only in Table 2.12.

	$T_{stator}: 300K$	$T_{stator}: 290K$	$T_{stator}: 280K$
Heat extracted per unit of mass $[\frac{J}{kg}]$	161.19	301.17	445.39
Power extracted [KW]	1.844	3.4454	5.093
Power per unit of area $[\frac{MW}{m^2}]$	0.9911	1.8517	2.7384
Heat extracted per unit of mass only casing$[\frac{J}{kg}]$	182.40	271.48	358.43
Power extracted only casing [KW]	2.0866	3.1057	4.1005
Power per unit of area only casing $[\frac{MW}{m^2}]$	2.003	2.9813	3.9462

Table 2.12: Results of heat extraction: comparison between blade only and casing only

The same results are reported graphically in Figure 2.28

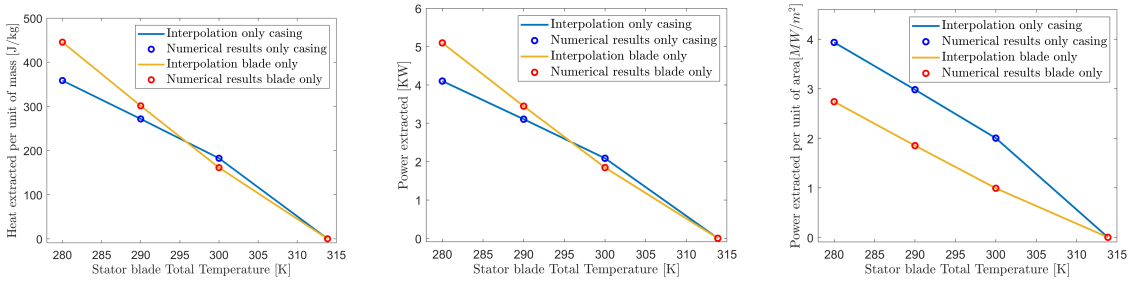

(a) Heat extracted per unit of mass

(b) Power extracted

(c) Power per unit of area

Figure 2.28: Comparison between blade only and blade only cooling

In the simulation with only the casing cooled the difference between the adiabatic case and the isothermal simulation is more relevant. The linear trend of the isothermal does not match the adiabatic results. Another interesting result is that the two lines cross each other close to a stator temperature of 295K: further investigation is needed to explain these CFD results. The cooling of casing can exploit the high turbulent flow close to endwall that increases the heat transfer process Figure 2.21 and Figure 2.27 in that streamlines. The main problem of this solution is the high temperature gradient in the channel that will probably enhance the secondary flow intensity and so the losses.

2.3.3. Increase of solidity

To simulate an higher solidity cascade the number of stator blade is increased from 100 to 144. This number is obtained looking at the pitchwise cooling penetration graph. The

results of Figure 2.20 show that cooling affect the range between $0,38$ and 1 of the pitch region: that range correspond almost to an angle of 2.5°. To create a stator blade channel with that angle the value of 144 is imposed to the periodicity of stator blade. This change of the mesh is performed in *AutoGrid* increasing the periodicity number. To check the correct shape of the mesh and the curvature imposed to casing and hub, the number of blade shown in *CFView* is increased and the result is reported in Figure 2.29.

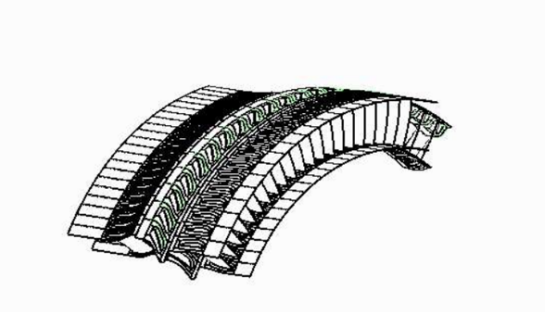

Figure 2.29: Representation of mesh periodicity

The results of cooling penetration are computed spanwise in Figure 2.31 and pitchwise in Figure 2.30.

Pitchwise result shows the same trend of the base case. The increase of solidity does not affect the amount of stream flow which are subjected to cooling. This trend could be explained with the boundary layer development. In all the simulations the design mass flow and the flow angle are fixed: these conditions create the same boundary layer development in the baseline and an higher solidity cascade. The similitude between the fluid dynamics of the boundary layer causes the same cooling penetration trend. This result is true only at design conditions where a variation in the solidity does not affect significantly the flow motion in the blade to blade channel. The fluid flow and consequently the heat flow are driven by the pressure gradient blade to blade that remains the same in the optimised design point; in off design conditions the variation due to an increase of solidity will probably be more significant. The effect of higher solidity is visible in the amount of heat removed that increases with the number of blade due to the increase of surface.

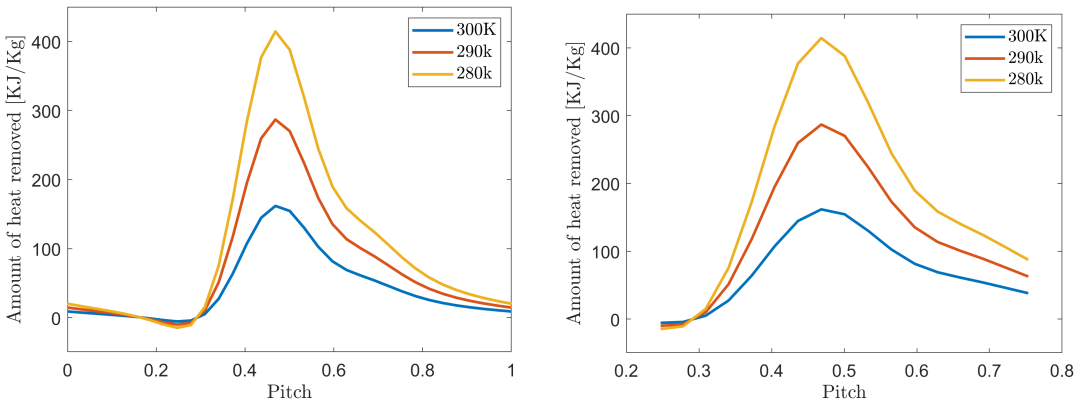

(a) Pitchwise all channel (b) Pitchwise details

Figure 2.30: Cooling effect in the blade channel with 144 blade: pitchwise profile

The spanwise trend is similar to the base line case too: higher in the endwall and constant in the main stream. The only difference is in the $0.3 - 0.4$ region where there is a second oscillatory trend of amount of heat extracted. A possible explanation is that the solidity is not constant along the spanwise direction due to the increase of pitch with the radius. In the lower part the absolute increase of metal is higher than at the casing one Figure 2.31.

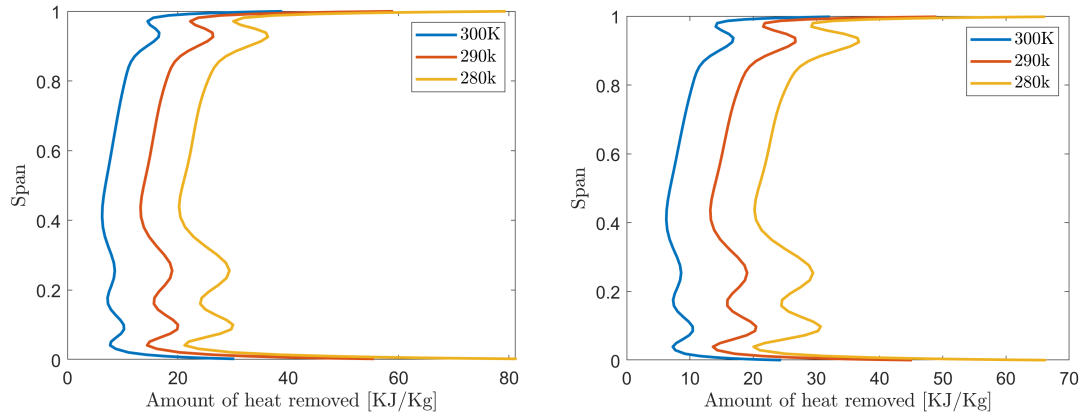

(a) Spanwise all channel (b) Spanwise details

Figure 2.31: Cooling effect in the blade channel: spanwise profile

3 | Coupling of the cycle analysis with the CFD results

This chapter couples the optimal thermodynamic condition of chapter 1 with the heat transfer capacity computed in chapter 2. The optimal amount of heat cannot be extracted cooling one single stator blade and this will change the optimal cooling position and the increase of efficiency due to inter-refrigerated compression. The numerical code is modified to analyse the Joule Brayton cycle: instead of variable q^*, a fixed amount of heat extracted is imposed and the number of stages cooled, from 1 to 5,is the new variable.

3.1. Joule-Brayton cycle with a cooled stator

The CFD results show a limited capacity of a stator blade to extract heat from the flow. The heat extracted per unit of mass is reported in Table 2.5, in case of a cooling system applied only to the stator blade, and in Table 2.11, with a fixed temperature imposed at the casing too. In this code the maximum amount of heat is imposed and the optimal value of efficiency is evaluated as function of the compression ratio position and the number of cooled stage. The single stage is simulated with a compression ratio (β_{stage}) of 1.23, equal to the *DREAM* compressor one, and with an efficiency value of 0.88 as the compressor in chapter 1. Figure 3.1 shows the Joule Brayton cycle of the GENX engine at cruise condition. In the Figure 3.1a the 5 cooling steps are applied to the HPC just for example. The detailed picture Figure 3.1b shows that even with a stator temperature of $280K$ the amount variation on thermodynamic cycle is very low.

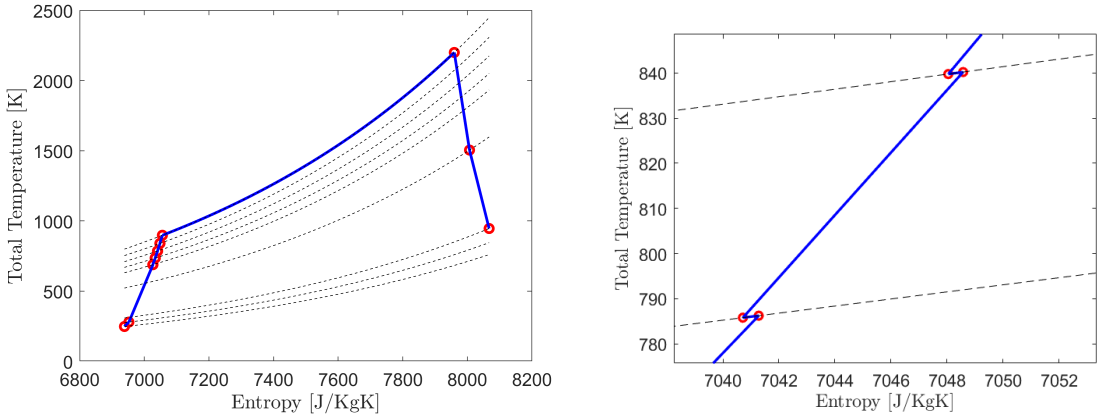

(a) Full Joule-Brayton cycle

(b) Details of 2 inter-refrigeration

Figure 3.1: GENX cycle with 5 inter-refrigeration, $T_{stator} = 280K$

The final optimal position and the number of stage cooled confirm the results of chapter 1. The results for the three stator temperature are similar, they are summarised in the following Table 3.1, Table 3.2 and Table 3.3 for the stator temperature of $300K$, $290K$, $280K$.

	CFM cruise	CFM takeoff	GENX cruise	GENX takeoff
Efficiency	0.4719	0.4452	0.5237	0.5203
Efficiency variation	0.0206%	0.02098%	0.019336%	0.01910%
Number of cooled stages	1	1	1	1
Cooling pressure ratio	1	1	1	1

Table 3.1: Results with a stator temperature of $300K$: $161\frac{J}{Kg}$ removed per stage

The parameter "cooling pressure ratio" is the pressure ratio level at which the first cooling happens.

	CFM cruise	CFM takeoff	GENX cruise	GENX takeoff
Efficiency	0.4721	0.4454	0.5239	0.5205
Efficiency variation	0.03850%	0.03921%	0.03614 %	0.03569%
Number of cooled stages	1	1	1	1
Cooling pressure ratio	1	1	1	1

Table 3.2: Results with a stator temperature of $290K$: $301\frac{J}{Kg}$ removed per stage

	CFM cruise	CFM takeoff	GENX cruise	GENX takeoff
Efficiency	0.4722	0.4456	0.5240	0.5206
Efficiency variation	0.05690%	0.05796%	0.05341%	0.05275%
Number of cooled stages	1	1	1	1
Cooling pressure ratio	1	1	1	1

Table 3.3: Results with a stator temperature of $280K$: $405\frac{J}{Kg}$ removed per stage

The results confirm that the optimal cooling position is in the booster; with a very low amount of cooling the optimal pressure ratio becomes equal to 1, that means after the fan. The comparison of adiabatic and inter-refrigerated cycle efficiency shows for all the machines a limited region in which cooling can increase efficiency. The efficiency surfaces are reported individually for the 4 applications coupled with the contour of efficiency variation. The colorful graph is the efficiency surface of the efficiency of the inter refrigerated Joule Brayton cycle compared with the light blue one which is the adiabatic reference case. The $\Delta\eta$ between the two configuration can be seen in the contour graph. The CFM curve at cruise condition is visible in Figure 3.2.

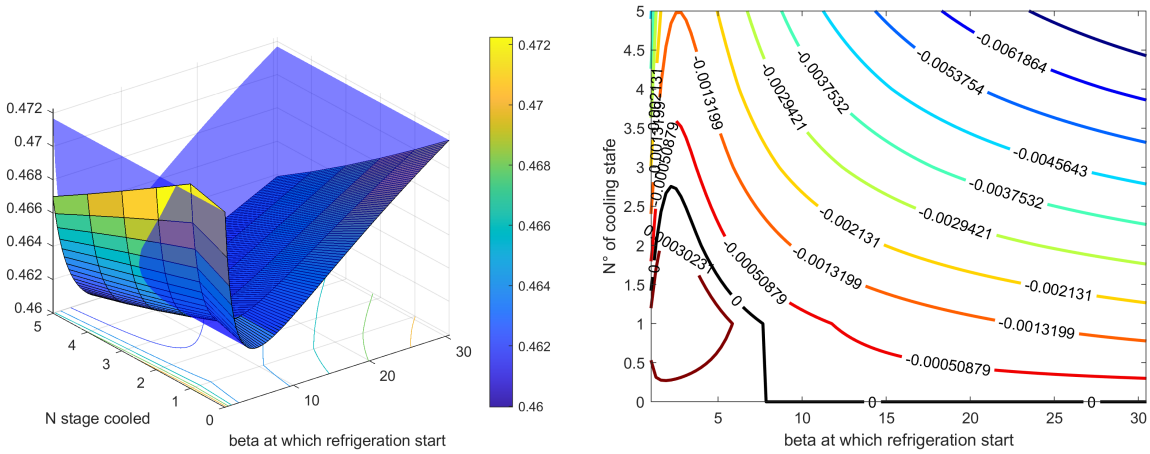

(a) 3D efficiency map (b) Efficiency variation

Figure 3.2: CFM cruise feasible cycle

From the CFM graph the position of cooling which generate an increase of efficiency is restricted in the booster area and the zero value line of Figure 3.5b goes to a no cooling stages number very quickly. This trend never appear in chapter 1 due to the high amount of heat extraction simulated. These considerations are applicable also to the other applications analysed; the efficiency maps and the efficiency variation contours are visible in: Figure 3.3 Figure 3.4 Figure 3.5.

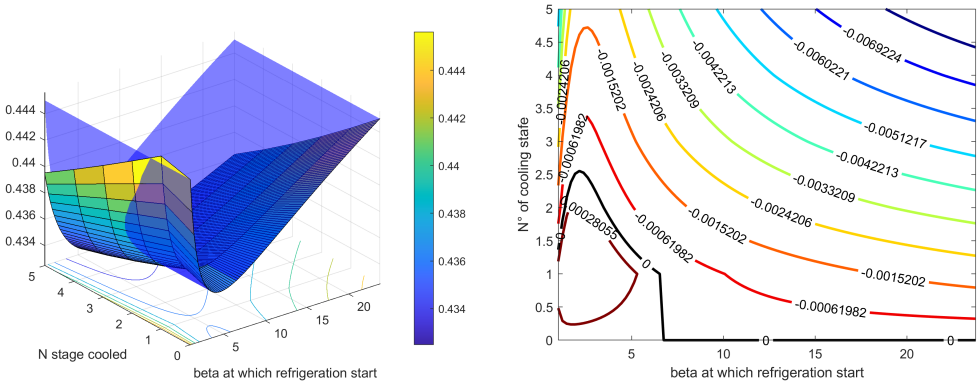

(a) 3D efficiency map (b) Efficiency variation

Figure 3.3: CFM takeoff feasible cycle

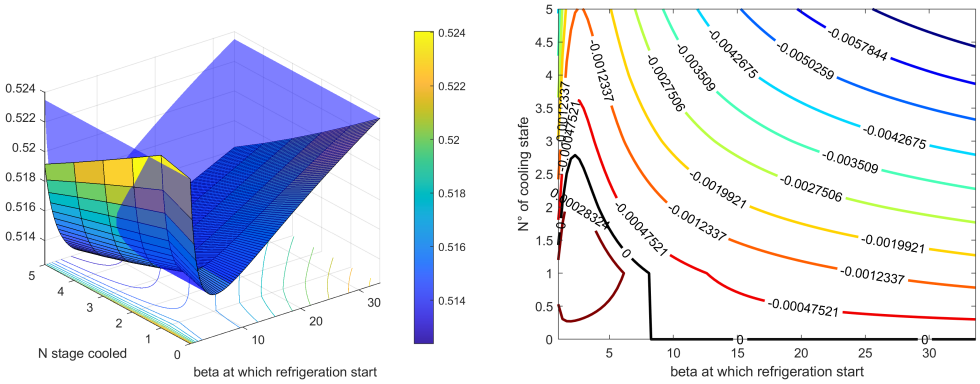

(a) 3D efficiency map (b) Efficiency variation

Figure 3.4: GENX cruise feasible cycle

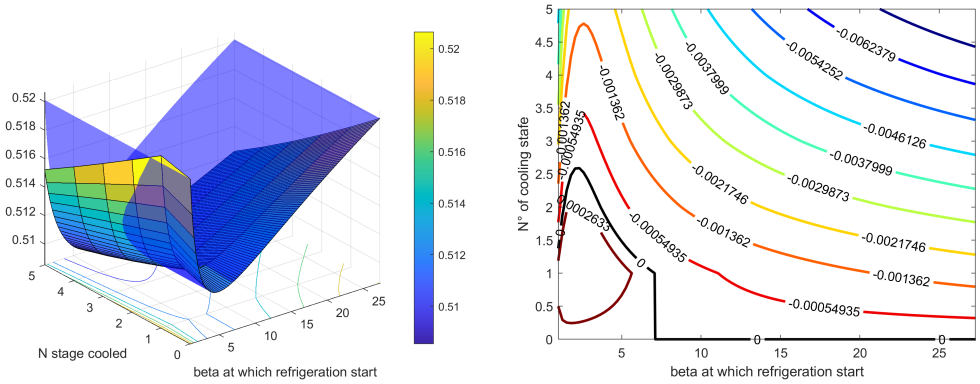

(a) 3D efficiency map (b) Efficiency variation

Figure 3.5: GENX takeoff feasible cycle

The real cycle with cooling applied both on stator blade and on stator casing gives higher results in efficiency and efficiency variation, but this configuration does not change the optimal cooling position. The amount of heat increase but it is not sufficient to apply it at higher compression ratio. Table 3.4, Table 3.5, Table 3.6 collect the results obtained with the three different isothermal temperatures applied at both the blade and the casing.

	CFM cruise	CFM takeoff	GENX cruise	GENX takeoff
Efficiency	0.4721	0.4455	0.5239	0.5205
Efficiency variation	0.0431%	0.04393%	0.04048%	0.03999%
Number of cooled stages	1	1	1	1
Cooling pressure ratio	1	1	1	1

Table 3.4: Results with a stator and casing temperature of $300K$: $337.2245\frac{J}{Kg}$ removed per stage

	CFM cruise	CFM takeoff	GENX cruise	GENX takeoff
Efficiency	0.4724	0.4458	0.5242	0.5208
Efficiency variation	0.0721%	0.07346%	0.06769 %	0.06686%
Number of cooled stages	1	1	1	1
Cooling pressure ratio	1	1	1	1

Table 3.5: Results with a stator and casing temperature of $290K$: $564.16\frac{J}{Kg}$ removed per stage

	CFM cruise	CFM takeoff	GENX cruise	GENX takeoff
Efficiency	0.4727	0.4461	0.5244	0.5211
Efficiency variation	0.101%	0.103%	0.0951%	0.0939%
Number of cooled stages	1	1	1	1
Cooling pressure ratio	1	1	1	1

Table 3.6: Results with a stator and casing temperature of $280K$: $793.22\frac{J}{Kg}$ removed per stage

The results with the cooling of casing only are not reported since are very similar to the stator blade only being the amount of heat removed almost identical. The interesting result is the increase of efficiency of the 0.1% reached with the cooling of both stator blade and casing at a temperature of $280K$.

3.2. Inter cooled and regenerated cycle

The thesis work focuses only on the increase of efficiency due to the reduction of work required by the compression process. The heat extracted during the compression is lost in the metal casing or in the cooled system. The final application uses the liquid hydrogen, the fuel that will be injected in the combustion chamber, as a cooler. In the Appendix C the combustion energy balance is performed. The energy insert by the fuel increases with the fuel temperature since its chemical energy increases too: to exploit it in some cycle, the heat is taken by the outlet of turbine to warm up the fuel before combustion. This layout variation is named *preheating* or *regeneration*. This positive effect does not appear if the heating process extracts air from the oxidizer: the ΔQ generated by the combustion is null if compared to the process with fuel and oxidizer at the reference temperature. This is because the energy plus available in a warmer fuel is required to heat up the oxidizer at the reaction temperature.

The heat extraction from the compressor moves energy from the compression process directly to the combustion one and creates the same positive effect of a *preheating*. The Figure 3.6 shows the different efficiency in the 4 real machines analysed. These values are obtained with the ideal thermodynamic analysis in which the heat can be completely extracted from the oxidizer.

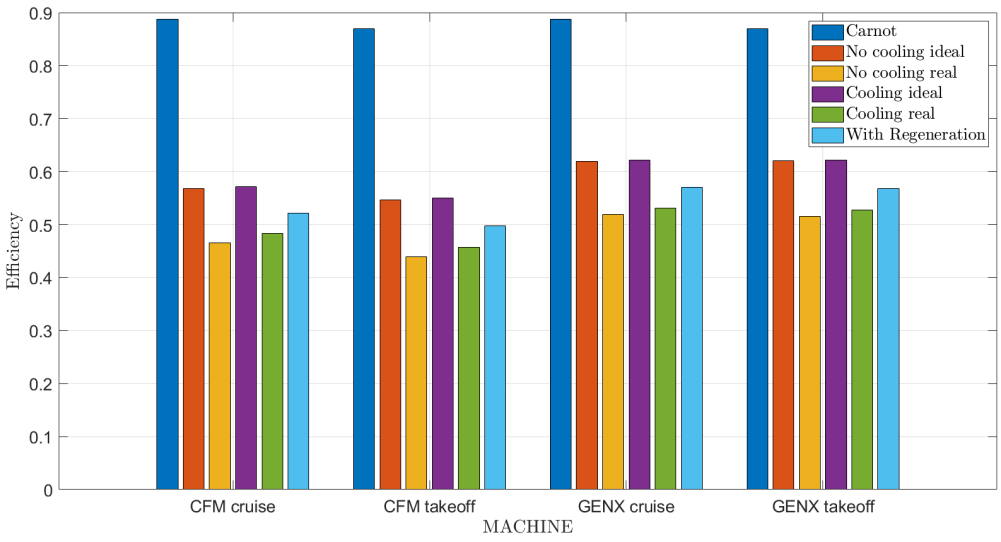

Figure 3.6: Efficiency results

The efficiency values are reported in tabular form to be more readable: Table 3.7.

	CFM_{cruise}	$CFM_{takeoff}$	$GENX_{cruise}$	$GENX_{takeoff}$
Carnot	0.8878	0.8690	0.8872	0.8690
Ideal adi	0.5683	0.5462	0.6196	0.6204
Real adi	0.4659	0.4395	0.5190	0.5159
Ideal cooled	0.5720	0.5499	0.6213	0.6212
Real cooled	0.4833	0.45719	0.5315	0.5269
Real cooled with reg	0.5214	0.4975	0.5706	0.5684

Table 3.7: Efficiency values

The cooled real case is closer to the ideal one compared to the adiabatic. This result is reasonable since with cooling the entropy generation is compensated. In the ideal case the addition of cooling does not change significantly the efficiency of the cycle. The most interesting graph is the light blue one: the capability of fuel of removing heat from compression and adding it directly in the combustion chamber could increase the efficiency up to 4% point. The contribution of the two different layouts configuration compared to the adiabatic real case can be better represented in terms of $\Delta\eta$, as shown in Figure 3.7

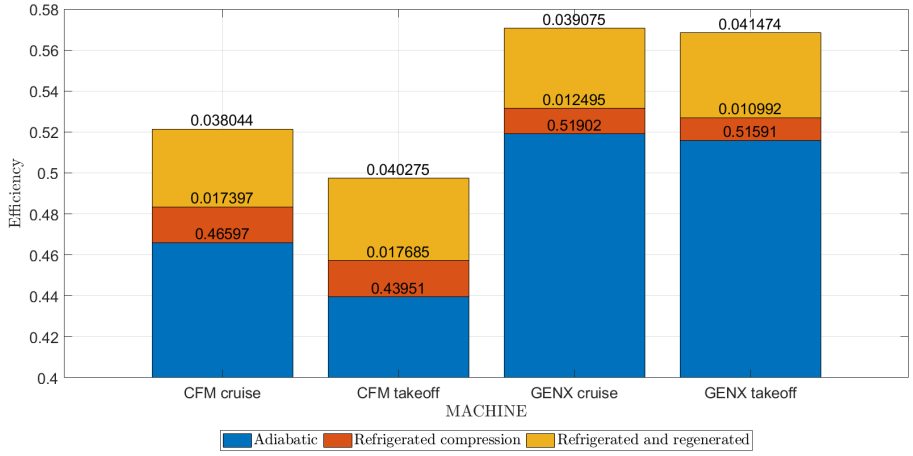

Figure 3.7: Delta efficiency in real application

The reduction of compression work is more evident in the CFM engine, an engine that is used since the 80s, than in GENX, that was introduced in 2011. The efficiency advantages of preheating are higher during the take off condition for both engines. The analysis of this trend requires a meta model development as done in subsection 1.3.2. Some rough considerations are done to understand why preheating causes so important advantages in the cycle efficiency. The amount of preheating injected in the combustion chamber can

be estimated as a percentage of the global amount of heat added in the cycle by the fuel, with only inter cooling effects. The percentage of heat removed compared to the heat injected by fuel is reported in Table 3.8.

	CFM cruise	CFM takeoff	GENX cruise	GENX takeoff
$\frac{Heat_{removed}}{Heat_{injectedfuel}}$	5.54%	5.79%	5.16%	5.24%

Table 3.8: Percentage of heat removed respect heat injected

This value could explain the high increase of efficiency respect the only cooled layout.

In all the machine the $\Delta\eta$ due to preheating is more than doubled compared to the advantages obtained only decreasing the compression work. The effect of preheating configuration could probably change the layout of the machine and the optimal cooling position, moving the pressure ratio of cooling at an higher level to increase the removed heat. This solution will be strongly affected by the effectiveness of heat transfer process and by heat losses, but it could give an higher advantage to perform an inter cooling compression. In the numerical simulated cycle with fuel preheating, the heat removed from compression is directly injected in the combustion chamber. The optimal preheated and inter-refrigerated cycle with an ideal effectiveness ($\epsilon = 1$) for the four application is reported in Figure 3.8 and Figure 3.9:

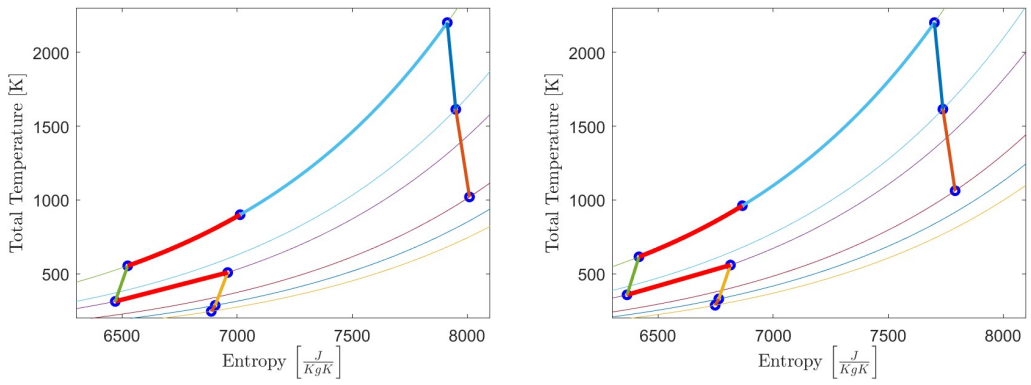

(a) CFM cruise (b) CFM takeoff

Figure 3.8: Optimal JB cycle with preheating and inter cooling for CFM engine

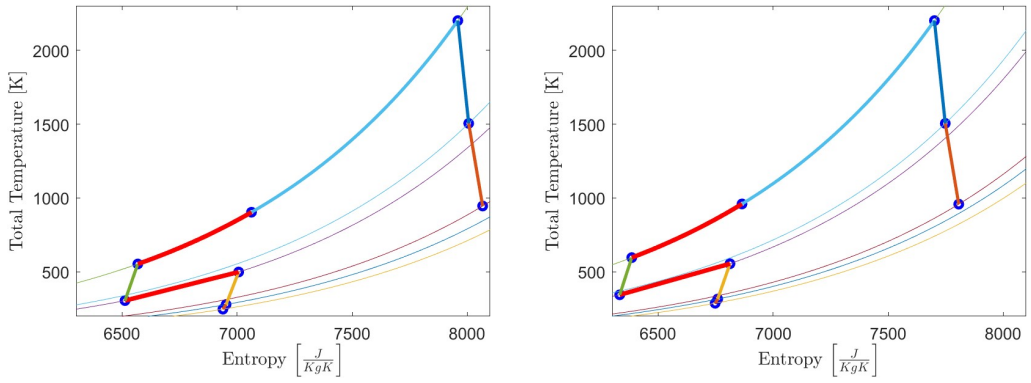

(a) GENX cruise (b) GENX takeoff

Figure 3.9: Optimal JB cycle with preheating and inter-cooling for GENX engine

The red segment represents the heating removed by the compressor which is directly injected in the combustion chamber. These graphs show the same optimal ideal cycle as the ones in chapter 1 with the capability of removing an amount of heat (Q) equal to the total enthalpy (h_t) given by compression process. The optimal cycles with a turbine entry temperature of $2200K$ are in Table 3.9:

	CFM cruise	CFM takeoff	GENX cruise	GENX takeoff
η_{max}	0.5214	0.4975	0.5706	0.5684
$\beta_{optimum}$	6.1616	5.2759	6.3023	5.9367
Q extracted [MW]	3.975	9.839	8.095	22.391
Power [MW]	9.825	19.428	20.801	52.422
$\Delta\eta$	5.85%	6.17%	5.54%	5.68%

Table 3.9: Optimal inter refrigerated and regenerated cycle

The optimal inter cooled compression ratio is increased respect the base case without preheating effect. These results could change completely the optimal position moving the refrigerated stage from the booster to the high pressure compression. The amount of heat that could be extracted by a cooled stator blade is really low compared to the optimal one of Table 3.9. The effects of heat losses are more relevant in case of low quantity of heat exchanged as in case of a refrigeration through a stator blade: for these reasons an accurate analysis of heat losses and heat flow in the machine has to be performed before moving the optimal cooling position from the booster to the HPC (high pressure compressor).

4 | Conclusions and future developments

This thesis work is a principle analysis of a future possible layout for an aeroengine. The new design analysed is strongly related to the possibility of using hydrogen as fuel, following the European trend of Alliance for zero-emission aviation [8] and the WINGS(Wallon INnovations for Green Skies) program of Belgium government [16]. The results of this thesis give further reasons to follow and continue the development of the technologies to exploit hydrogen as fuel. The emission advantages are globally known, but the high investment required and the liquid hydrogen cost brakes often its application to commercial machines. The possibility of performing an inter refrigeration compression increases the efficiency of the all Joule Brayton cycle in different flight conditions and in different machines.The results of chapter 1 quantify these advantages between $1-2$ points percentage. An increase of the cycle efficiency could bring investment from engine suppliers to keep developing this technology. The actual design of blades does not allow such an extreme cooling in just one stage and the heat transfer coefficient is estimated in chapter 2 to the value of 80 $\left[\frac{KW}{m^2K}\right]$. The possibility of cooling the casing too increases the amount of heat that can be extracted, without reaching the optimal value for the thermodynamic cycle. Coupling the CFD results in the thermodynamic cycle, the high potentiality of cooling decreases but it is still present, as described in chapter 3. The aeroengine technology has reached a very high level of optimisation and an increase of efficiency of some ten percent is positive evaluated by the market. The future developments of this project are a lot and the final results could lead to a new technology for civil aviation. The main future work can be listed as:

- A new optimal condition in the thermodynamic cycle between turbine entry temperature and the stoichiometric combustion ratio should be found. The efficiency increases both decreasing the total turbine entry temperature (subsection 1.2.1), with a fixed stoichiometric ratio and increasing the amount of fuel (subsection 1.2.2), keeping constant the combination between compression ratio and turbine entry temperature.

- The full machine should be re-designed to fit the new layout and exploit all the advantages of cooling: the volume of air changes through cooling and this could lead to a variation of geometry or velocity triangle to optimise the compression ratio of each stage.
- The effect of cooling on the flow angle after a cooled blade will be the topic of a future PhD project at Von Karman Institute to investigate the variation on the deviation angle.
- The increase of solidity, as reported in subsection 2.3.3, lead to an increase of heat extraction process; and a trade off between the higher load and the high advantages of solidity should also be performed.

One of the most relevant point that has to be developed is how to realise cooling: liquid hydrogen requires an high pressure level [32] to keep its state, but this pressure level is too much for the combustion chamber. An expansion process should be performed during the passage from the fuel tank to the combustor. Further analyses should regards:

- The quantification and estimation of pressure drops in the coolant high pressure liquid fluid due to its passage in bended pipes.
- The technology to create such small pipes in a stator blade and a structural analysis to verify the feasibility of a blade subjected both to internal pressure and external load.

The possible layout variation with the cooling of the casing could help in solving the problem, but it will create another local source of high density flow and so a pressure gradient in the flow channel. The last point of the project will analyse again the effectiveness of heat transfer process through a stator blade with a real cooled system:

- The heat extraction capacity of a stator blade with a reliable cooling system has to be re-estimated and, in case of an internal cooling through the stator, a finite element analysis (FEM) of the blade is necessary to understand the maximum allowable internal pressure of the structure.

The future developments of this working thesis are a lot and they represent a real challenge for engineers. The 2050 zero emission aviation target fixed by European commission is not so far and the possibility of having more efficient and zero emission engines in the future of aviation will stimulate the research on this topic to continuously improve this high potentiality technology.

Bibliography

[1] A.Kiss and Z.Spakovsxky. Effect of transient heat transfer on compressor stability. *Journal of turbomachinery*, 2018. URL `https://link.springer.com/article/10.1007/s00231-014-1392-3`.

[2] G. Aviation. Ge9x engine, 2022. URL `https://www.geaviation.com/propulsion/commercial/ge9x`.

[3] Bagatti, Corradi, Desco, and Ropa. *Immagini della chimica*, chapter 11. Zanichelli, arancione edition, 2014.

[4] M. Baldassarri. Counter rotating electric fan, mission analysis and preliminary sizing. Master's thesis, Politecnico di Milano, 2022.

[5] B. Cernat, J. Pinho, M. Okada, and S. Lavagnoli. Experimental investigation of a high-speed turbine with rainbow rotor and rim seal purge flow. *ASME*, 2022.

[6] CFM. Cfm rise program, 2021. URL `https://www.cfmaeroengines.com/wp-content/uploads/2021/07/CFM_RISE_Whitepaper_Media.pdf`.

[7] E. Commission. validation of radical engine architecture systems, 2019. URL `https://cordis.europa.eu/project/id/211861`.

[8] E. Commission. Alliance for zero-emission aviation, 2022. URL `https://defence-industry-space.ec.europa.eu/eu-aeronautics-industry/alliance-zero-emission-aviation_en`.

[9] F. Cozzi. Combustion: Fundamentals and applications energy engineering aa. 2020-2021: Thermochemistry.

[10] G. Dassù and F.Inzoli. Lezioni di fisica tecnica.

[11] G. dell'Era. Unsteady measurements in a high speed axial compressor. Master's thesis, Politecnico di Milano, 2012.

[12] D.Exposito, S.L.Gal, and A.LNeely. Wall temperature and bluntness effects on hyper-

sonic laminar separation at a compression corner. *Journal of Fluid Mechanics 922,A1*, 2021. URL https://doi.org/10.1017/jfm.2021.474.

[13] V. K. I. for fluid dynamic. High speed compressor facility r-4. URL https://www.vki.ac.be/index.php/facilities-other-menu-148/turbomachinery/57-research-and-consulting/facilities/turbomachinery-facilities/95-high-speed-compressor-facility-r-4.

[14] GE, 2022. URL https://lnkd.in/ezdsqfBY.

[15] G.E.Gadd and W.F.Cope. Heat-transfer and skin-friction measurements at a mach number of z.44 for a turbulent boundary layer on a flat surface and in regions of separated flow;. 1958.

[16] W. government. Wings, 2022. URL www.wingspartnership.be.

[17] N. III. Quantifyng heat transfer effects of a high speed, multi stage, axial research compressor, 12 2021. URL https://hammer.purdue.edu/articles/thesis/QUANTIFYING_HEAT_TRANSFER_EFFECTS_OF_A_HIGH-SPEED_MULTI-STAGE_AXIAL_RESEARCH_COMPRESSOR/17005816.

[18] J.E.Bardiina, P.G.Huang, and T.J.Coakley. Turbulence modelling validation. 1997.

[19] J.Pacio, L.Marocco, and Th.Wetzel. Review of data and correlations for turbulent forced convective heat transfer of liquid metals in pipes. 2014. URL https://link.springer.com/article/10.1007/s00231-014-1392-3.

[20] D. J. Kurzke. Aero-engine design: From state of the art turbofans towards innovative architectures: Preliminary design. 2013. VKI lecture series April 9-12,2013.

[21] L.Marocco and A.Franco. Direct numerical simulation and rans comparison of turbulent convective heat transfer in a staggered ribbed channel with high blockage. *Journal of heat transfer*, 2017. URL https://asmedigitalcollection.asme.org/GT/proceedings-abstract/GT2015/56635/V02AT37A039/236924.

[22] M.G.Turner, A.J.Gannon, and W.Sanz. Measured heat transfer in a transonic fan rig at casing with implications on performance. *ASME Turbo expo*, 2015. URL https://asmedigitalcollection.asme.org/GT/proceedings-abstract/GT2015/56635/V02AT37A039/236924.

[23] T. Morgan, A. J.Gannon, G. V. Hobson, and W. C. Smith. Using blade surface heat transfer for partial intercooling and thrust augmentation. *ASME*, 2022.

[24] N.R.L.Maccallum and A.D.Grant. The effect of boundary layer changes due to tran-

sient heat transfer on the performance of an axial-flow air compressor. *SAE International*, pages 1357–1364, 2022. URL https://www.jstor.org/stable/44648156.

[25] NUMECA. *USER MANUAl, AutoGrid5 v8: $FINE^{TM}$/Turbo*13.2. 2010.

[26] NUMECA. *USER GUIDE: $FINE^{TM}$ Turbo 13.2*. 2013.

[27] C. Osnaghi. *Teoria delle Turbomacchine*. September 2013.

[28] P.N.Shah and C.S.Tan. Effect of blade passage surface heat extraction on axial compressor performance. *Journal of Turbomachinery*, pages 457–467, 2007. URL https://asmedigitalcollection.asme.org/turbomachinery/article-abstract/129/3/457/477965/Effect-of-Blade-Passage-Surface-Heat-Extraction-on?redirectedFrom=PDF.

[29] prof:Dossena, Osnaghi, and P.Ferrari. Corso di macchine e sistemi energetici per allievi meccanici: Raccolta di esercizi con soluzione, 4 2004.

[30] R.A.Crawford and A.E.Burwell. Quantitative evaluation of transfer heat on axial flow compressor stability. *21st Join Porpulsion Conference*, 1985. URL https://doi.org/10.2514/6.1985-1352.

[31] Safran-Propulsion, 2022. URL https://www.linkedin.com/posts/safran-propulsion_hydrogen-startup-hydrogen-activity-6949965142835003393-UDsz?utm_source=linkedin_share&utm_medium=ios_app.

[32] S. Suttil. Idrogeno: proprietà. Master's thesis, Master Alta Form "Energie Rinnovabili AGIRE-UNI MN, The address of the publisher, 5 2007. slide 76.

[33] C. team. Pearson function, calculates the pearson product-moment correlation coefficient for two sets of values, 7 2022. URL https://corporatefinanceinstitute.com.

[34] R. Toracchio, F. Fontaneto, and K. Hillewaert. On the impact of the turbulence model on the secondary flow structure of a highly-loaded compressor stage. 2022.

[35] T.Schumam, F.Magagnato, M.Niemann, and L.Marocco. Numerical prediction of heat transfer in liquid metal application. *Conference paper*, 2015. URL https://www.researchgate.net/publication/282657484.

[36] C. Wood. *Analysis of the effect of transient heat transfer on axial flow compressor blade boundary layer*. PhD thesis, Aerospace Engineer department, University of Tennessee, 1985.

A | Appendix A

This appendix reports the full mathematical analysis of the efficiency definition that leads to the results of Equation 1.2 in section 1.1. The efficiency, since it is a compressor, is defined as the ratio between the isentropic work required (numerator) and the real work applied: the total enthalpy variation plus the heat extracted with inter-refrigeration.

$$\eta = \frac{c_p \cdot T_{T0} \cdot ((\beta_1 \cdot \beta_2)^{\frac{\gamma-1}{\gamma}} - 1)}{h_{T2} - h_{T1} + Q}$$

$$\eta = \frac{c_p \cdot T_{T0} \cdot ((\beta_1 \cdot \beta_2)^{\frac{\gamma-1}{\gamma}} - 1)}{T_{T0} \cdot c_p (\frac{T_{T2}}{T_{T0}} - 1) + c_p \cdot T_{T0} \cdot (\beta^{\frac{\gamma-1}{\gamma}} - 1) \cdot q}$$

$$T_{T2} = \frac{h_{T2}}{c_p} = \frac{1}{c_p \cdot \eta} \cdot (h_{T2is} - h_{T1c}) + h_{T1c}$$

$$T_{T2} = \frac{1}{c_p \cdot \eta} \cdot [c_p \cdot (\beta_2^{\frac{\gamma-1}{\gamma}} - 1) \cdot T_{T1c} - h_{T1c}] + h_{T1c}$$

$$T_{T2} = \frac{1}{c_p \cdot \eta} \cdot [c_p \cdot (\beta_2^{\frac{\gamma-1}{\gamma}} - 1) - c_p + \eta)] \cdot T_{T1c}$$

$$T_{T1c} = T_{T1} - \frac{Q}{c_p}$$

$$T_{T1c} = T_{T1} - q \cdot \frac{T_{T0} \cdot (\beta_1^{\frac{\gamma-1}{\gamma}} - 1)}{c_p}$$

$$T_{T1c} = T_{T0} + \frac{h_{T1} - h_{T0}}{c_p} - q \cdot \frac{T_{T0} \cdot (\beta_1^{\frac{\gamma-1}{\gamma}} - 1)}{c_p}$$

$$h_{T1} - h_{T0} = \frac{h_{T1is} - h_{T0}}{\eta} + h_{T0} - h_{T0} = \frac{T_{T0}}{c_p \cdot \eta} \cdot (\beta_1^{\frac{\gamma-1}{\gamma}} - 1)$$

$$T_{T1c} = T_{T0} \cdot [1 + (\frac{1}{c_p \cdot \eta} + q) \cdot (\beta_1^{\frac{\gamma-1}{\gamma}} - 1)]$$

$$a = \frac{1}{c_p \cdot \eta} c_p \cdot [(\beta_2^{\frac{\gamma-1}{\gamma}} - 1) - c_p + \eta]$$

$$b = 1 + (\frac{1}{c_p \cdot \eta} + q) \cdot (\beta_1^{\frac{\gamma-1}{\gamma}} - 1)$$

$$\eta = \frac{(\beta_1 \cdot \beta_2)^{\frac{\gamma-1}{\gamma}} - 1}{(a \cdot b - 1) + (\beta_1^{\frac{\gamma-1}{\gamma}} - 1) \cdot q}$$

B | Appendix B

This appendix complete the results of Table 1.5 with the results of the cycle with a total temperature at turbine inlet of $1600K$ and $2000K$. These results are in agreement with the consideration done in subsection 1.2.2.

T_t turbine	CFM		GENX	
	Cruise	Takeoff	Cruise	Takeoff
1600	$\eta_{max} = 0.4216$ $\beta = 2.475$ Q:1.72 [MW] W:2.2 [MW] $\Delta\eta$: 4.78%	$\eta_{max} = 0.38776$ $\beta = 2.425$ Q:4.65 [MW] W:1.93[MW] $\Delta\eta$: 5.57%	$\eta_{max} = 0.47645$ $\beta = 2.22$ Q:3.00[MW] W:3.69 [MW] $\Delta\eta$: 3.61%	$\eta_{max} = 0.46913$ $\beta = 1.9873$ Q:7.32 [MW] W:8.71[MW] $\Delta\eta$: 3.51%
2000	$\eta_{max} = 0.46825$ $\beta = 2.1061$ Q:1.38[MW] W:6.58[MW] $\Delta\eta$: 2.24%	$\eta_{max} = 0.44068$ $\beta = 2.1402$ Q:3.93 [MW] W:12.22 [MW] $\Delta\eta$: 2.46%	$\eta_{max} = 0.51793$ $\beta = 1.8157$ Q:2.17 [MW] W:13.06 [MW] $\Delta\eta$: 1.61%	$\eta_{max} = 0.5129$ $\beta = 1.6582$ Q:5.25 [MW] W:32.33 [MW] $\Delta\eta$: 1.44%

Table B.1: Results of numerical code

C | Appendix C

The energy balance of a combustion process is reported following the analysis shown in the slide of combustion course of Politecnico di Milano [9].

$$\mathrm{CH_4} + 2\,\mathrm{O_2} \longrightarrow \mathrm{CO_2} + 2\,\mathrm{H_2O}\ h_{f\mathrm{CH_4}} + 2 \cdot h_{f\mathrm{O_2}} - [h_{f\mathrm{CH_4}} + 2 \cdot h_{f\mathrm{O_2}}] = LHV$$

$$\left(h_{f\mathrm{CH_4}} + \int_{T_{ref}}^{T} c_{p\mathrm{CH_4}}\, dT\right) + 2 \cdot \left(h_{f\mathrm{O_2}} + \int_{T_{ref}}^{T} c_{p\mathrm{O_2}}\, dT\right) =$$
$$\left(h_{f\mathrm{CO_2}} + \int_{T_{ref}}^{T} c_{p\mathrm{CO_2}}\, dT\right) + 2 \cdot \left(h_{f\mathrm{H_2O}} + \int_{T_{ref}}^{T} c_{p\mathrm{H_2O}}\, dT\right) + Q$$

In the combustion process studied the temperature of fuel increases (T^+), due to heat exchange process, and the one of air (oxidizer) decreases (T^-).

$$\left(h_{f\mathrm{CH_4}} + \int_{T_{ref}}^{T^+} c_{p\mathrm{CH_4}}\, dT\right) + 2 \cdot \int_{T_{ref}}^{T^-} c_{p\mathrm{O_2}}\, dT - \left(h_{f\mathrm{CO_2}} + \int_{T_{ref}}^{T} c_{p\mathrm{CO_2}}\, dT\right) - 2 \cdot \left(h_{f\mathrm{H_2O}} + \int_{T_{ref}}^{T} c_{p\mathrm{H_2O}}\, dT\right) = Q$$
$$(h_{f\mathrm{CH_4}} - h_{f\mathrm{CO_2}} - 2 \cdot h_{f\mathrm{H_2O}}) + \left(\int_{T_{ref}}^{T^+} c_{p\mathrm{CH_4}}\, dT + 2 \cdot \int_{T_{ref}}^{T^-} c_{p\mathrm{O_2}}\, dT - \int_{T_{ref}}^{T} c_{p\mathrm{CO_2}}\, dT - \int_{T_{ref}}^{T} c_{p\mathrm{H_2O}}\, dT\right) = Q$$

Assuming no variation on the exhaust gas temperature, the sum of the enthalpy of formation of the substance is equal to the LHV and depends only by the chemistry. The variation of heat introduced in the combustion is:

$$\left(\int_{T_{ref}}^{T^+} c_{p\mathrm{CH_4}}\, dT + 2 \cdot \int_{T_{ref}}^{T^-} c_{p\mathrm{O_2}}\, dT\right) = \Delta Q$$

The ΔQ value is equal to "0" if the heat exchange process is done between the two fuels needed for combustion. The energy provided by the fuel during combustion is only its chemical one described by the low heating value.

List of Figures

List of Tables

List of Symbols

Variable	Description	SI unit
CFM	CFM56-7824 engine	
GENX	GENX-1864 engine	
Re	Reynolds number	
η	efficiency	
N_c	Reduced thermodynamic speed	rpm
HPC	High pressure compressor	
LPC	Low pressure compressor	
HPT	High pressure turbine	
LPT	Low pressure turbine	
SFC	Specific fuel consumption	$\frac{Kg}{s}$
γ	adiabatic coefficient	
T_t	Total temperature	K
h_t	Total enthalpy	$\frac{J}{kg}$
Q	Heat extracted	W
q^*	non dimensional amount of heat extracted	
P-B	Pearson-Bravais parameter	
$m_{\beta fan}$	linear coefficient β_{fan} and $\eta_{cycle} and \beta_{cooling}$	
R	residual	
RES	global residual	
h	heat transfer coefficient	$\frac{J}{m^2 K}$
SA	Spalart Allmaras turbulence model	
k-ωSST	Shear stress transport turbulence model	
JB	Joule Brayton	
VKI	Von Karman Institute	

Acknowledgements

This thesis work is the end of a very intense university track at Politecnico di Milano. The results obtained in this years were possible only thank my family support: both economically that leave me the possibility of focus myself on the studies than psychological when the exams results does not correspond to the expected one. The schetzch friend first and later the CALDAIA family helps me in living every university day with happiness and the seriousness required by the course of study. Emanuele, Matteo, Simone, Federico, Aurora, Andrea, Irene, Raffaele, Alessandro, Chiara (and all the other who I forgetting in this list) this work has only my name but it comes from a real team work in the last five years. Another great contribution come from the Geg friends, that help me both in preparing some exam than in chilling out when it was necessary. Thank you Sara for supporting me always and been my right hand during the last two years, Our relationship let me feel always loved and help me in thrust in my capacity. The final lines are for the people who make it possible: professor Paolo Gaetani for sharing the possibility of developing the thesis at the Von Karman Institute, professor Fabrizio Fontaneto and the research engineers Bogdan Cernat for advising and following me during all the project.